University of Alberta

Maintaining Chromophore Alignment in Nonlinear Optical Materials via Non-covalent Interactions

by

Colin Ronald Vitols

A thesis submitted to the Faculty of Graduate Studies and Research in partial fulfillment of the requirements for the degree of Master of Science

Department of Chemistry

Edmonton, Alberta

Spring 2003

National Library of Canada
Acquisitions and Bibliographic Services
395 Wellington Street
Ottawa ON K1A 0N4
Canada

Bibliothèque nationale du Canada
Acquisitions et services bibliographiques
395, rue Wellington
Ottawa ON K1A 0N4
Canada

Your file Votre référence

Our file Notre référence

The author has granted a non-exclusive licence allowing the National Library of Canada to reproduce, loan, distribute or sell copies of this thesis in microform, paper or electronic formats.

The author retains ownership of the copyright in this thesis. Neither the thesis nor substantial extracts from it may be printed or otherwise reproduced without the author's permission.

L'auteur a accordé une licence non exclusive permettant à la Bibliothèque nationale du Canada de reproduire, prêter, distribuer ou vendre des copies de cette thèse sous la forme de microfiche/film, de reproduction sur papier ou sur format électronique.

L'auteur conserve la propriété du droit d'auteur qui protège cette thèse. Ni la thèse ni des extraits substantiels de celle-ci ne doivent être imprimés ou autrement reproduits sans son autorisation.

0-612-82359-8

Canada

University of Alberta

Library Release Form

Name of Author: *Colin Ronald Vitols*

Title of Thesis: *Maintaining Chromophore Alignment in Nonlinear Optical Materials via Non-covalent Interactions*

Degree: *Master of Science*

Year this Degree Granted: 2003

Permission is hereby granted to the University of Alberta Library to reproduce single copies of this thesis and to lend or sell such copies for private, scholarly or scientific research purposes only.

The author reserves all other publication and other rights in association with the copyright in the thesis, and except as herein before provided, neither the thesis nor any substantial portion thereof may be printed or otherwise reproduced in any material form whatever without the author's prior written permission.

Colin Vitols
6 - 10731 85 Ave NW
Edmonton, AB
T6E 2K9

January 20, 2003

University of Alberta

Faculty of Graduate Studies and Research

The undersigned certify that they have read, and recommend to the Faculty of Graduate Studies and Research for acceptance, a thesis entitled *Maintaining Chromophore Alignment in Nonlinear Optical Materials via Non-covalent Interactions* submitted by *Colin Ronald Vitols* in partial fulfillment of the requirements for the degree of *Master of Science*.

Dr. Rik R. Tykwinski, Supervisor

Dr. David R. Bundle

Dr. Ray DeCorby

January 20, 2003

Dedicated to my dad,
for teaching me to ask "Why?"
And to my mom,
for teaching me how to tell people
what I found out.

ABSTRACT

Recent developments in the field of nonlinear optics have led to demand for second-order NLO materials and devices with designed properties, both of the NLO response itself and of the physical properties of the device or material. Among the more elusive characteristics targeted in this field is that of temporal stability of the NLO response in organic and, especially, polymeric materials. Hydrogen bonding has long been used as a method of generating or stabilizing nanoscale molecular architectures. The work presented herein seeks to integrate these ideas by incorporating second-order NLO chromophores into a polymeric material in which long-term stability of the NLO response might be enhanced by intramolecular hydrogen bonding. A synthetic pathway has been developed, leading to the synthesis of a series of azobenzene-based chromophores, some of which exhibit a number of interesting properties. One of these chromophores has been incorporated into a polymeric material via metathesis polymerization using Grubbs-type catalysis. The resulting polymer has been characterized via spectroscopic and physical analysis, and attempts have been made to prepare high-quality thin films through a variety of casting techniques, in order to study the NLO properties of the material.

Acknowledgments

As with any extended project, the credit (or blame) for the completion of this degree lies at the feet of more people than I could conveniently name here, so I'll have to settle for the short list. First and foremost, of course, is my supervisor, Dr. Rik Tykwinski, and my lab coordinator, under whom I taught Chem 10X labs, Dr. Norman Gee. Also, members of my research group(s), past and present, for various technical discussions, feedback on seminars, and comic relief.

Thanks also to Hue Nguyen from TR Labs, for her tireless efforts to obtain NLO measurements of my oligomers.

A huge thank you is also due to all of the fantastic support staff in the Department of Chemistry, including Spectral and Microanalytical Services, NMR Spectral Services, Mass Spectrometry, as well as the general office, storeroom, machine shop and glass shop people, all of whom helped make the whole painful process just a little easier.

Emotional support and stress relief is a much, much longer list, and as a result, one that could never quite be complete. But here's a shot at it, in more or less random order: Chantelle, Kathryn, Kris, Cory, Kathy, Karmon, Anthony, Warren, Christopher Robin, Michelle, Carolyn, Robin, Tracy, Ross, Bryan, Pankaj, James, Lara, Reshma, Julia, Véronic, Nadine, Jamal, Katherine, Lorna, Devon, Shandie, Shannon, Shaylen, Veronica, the entire UADC TA Corps and assorted other UADC people (all wonderful, but far too

numerous to list). You may not all realize how much you helped, but I couldn't have done it without each and every one of you.

To all that I've listed here, and all the others that I didn't, thank you. It has been said that the best measure of wealth is in the quality of one's friends; if that is true, then Bill Gates has got nothing on me. Especially since I wrote this in WordPerfect®...

Table of Contents

I. INTRODUCTION 1

1. Nonlinear Optics 1

A. Polarization and NLO Effects 1

A.1 Second Harmonic Generation (SHG) 2

A.2 Linear Electro-Optic (LEO) or Pockels Effect 3

B. Nonlinear Optical Materials 4

B.1 Organic Crystals 5

B.2 Organic Dopants 8

B.3 Poled Polymeric Thin Films 9

(a) High-T_g Polymer Matrix 10

(b) Cross-Linking Strategies 11

(c) Secondary Bonding Interactions 16

(d) Polymeric Chromophore 17

2. Non-Covalent Interactions 19

A. Hydrogen Bonding 19

B. Secondary Interactions and Schneider's Rule 21

C. Hydrogen Bonding Complexes and Cooperativity 23

C.1 Complexes Involving 1 H-Bond 23

C.2 Complexes Involving 2 H-Bonds 24

C.3 Complexes Involving 3 H-Bonds 25

C.4 Complexes Involving 4 H-Bonds 26

D. Hydrogen Bonding in NLO Materials 27

3. Thesis Proposal 31

II. RESULTS AND DISCUSSION 34

1. Chromophore Synthesis 34

A. Nitro Terminus 34

B. Amino Terminus 38

B.1 Amine Series 39

B.2 Acid Series 41

C. Azo Coupling 43

2. Metathesis Oligomerization 45

3. Properties of the Azobenzene Chromophore Series 48

A. UV-Vis Spectroscopy and pH 48

B. Nuclear Magnetic Resonance Spectroscopy 53

B.1 ^{13}C NMR Chemical Shifts 53

B.2 ^{1}H NMR Chemical Shifts 57

C. Infrared Spectroscopy 60

4. Properties of the Metathesis Monomer (**45b**) 61

5. Properties of the Metathesis Oligomers 64

A. Nuclear Magnetic Resonance Spectroscopy 64

B. Mass Spectrometry 66

B.1 Cooperativity Effects and MS Analysis 68

C. Solvatochromism 70

D. Thermal Analysis 71

D.1 Differential Scanning Calorimetry 71

D.2 Thermal Gravimetric Analysis 73

E. Thin Films 74

E.1 Electronic Properties 74

E.2 Nonlinear Optical Effects - The Electro-Optic Effect 75

III. CONCLUSIONS 78

IV. EXPERIMENTAL 81

Bibliography 110

Appendix A – Nuclear Magnetic Resonance Spectra 116

List of Tables

Table I - Absorption Characteristics of the Azobenzene Series in Methanol at r.t. 48

Table II - ^{13}C Chemical Shifts of the Chromophore Series As Measured at r.t. 54

Table III - Comparison of ^{13}C Chemical Shifts of New Chromophores, Azobenzene Reference Compounds, and Key Structural Fragments 56

Table IV - ^{1}H Chemical Shifts of the Chromophore Series As Measured at r.t. 58

Table V - Solvatochromism of Compound **45b** at r.t. 61

Table VI - Solvatochromism of **45b** and Its Oligomers 70

Table VII - Solvatochromism of Oligomers in Solution and Thin Film Casts 75

List of Figures

Figure 1. Typical organic materials for second order nonlinear optical effects. These are donor-acceptor (D–A) substituted molecules with π-electron ring systems. Also shown are the charge-transfer first excited states [5] 6

Figure 2. Schematic illustrating centrosymmetric (a,b) and noncentrosymmetric (c) arrangements of molecular dipoles, and the resulting bulk polarization, **P** 7

Figure 3. 2-methyl-4-nitroaniline (MNA) and *trans*-4′-dimethylamino-*N*-methylstilbazolium methyl sulfate (DSMS) are examples of organic crystals in polar space groups [3] 8

Figure 4. The NLO chromophore at left, 4-dimethylamino-4′-nitrostilbene (DANS), was doped into the liquid crystalline polymer at right and poled to obtain a novel second order NLO material [5] 9

Figure 5. A dicyanoethylene-based chromophore is incorporated into a high-T_g polymer matrix [8] 10

Figure 6. Disperse Red 19 is embedded in a high-T_g poly(urethane imide) in one synthetic step [9] 11

Figure 7. The photopolymerization of the bis(acrylate) chromophore, at top, yields the network polymer below [10] 12

Figure 8. Reaction of a partially cross-linked prepolymer with a trilink chromophore leads to a 3D network [11] 13

Figure 9. An acrylate-functionalized copolymer allows simultaneous cross-linking, via photopolymerization, and photoinduced orientation of the chromophore [12] 14

Figure 10. Photopolymerization of an acrylate copolymer yields this network polymer [10] 14

Figure 11. Pendant epoxides on this maleimide copolymer allow both thermal and photochemical cross-linking [13] 15

Figure 12. Oxidative coupling of terminal bis(acetylene)s yields thermally cross-linked poly(diacetylene)s [14] 15

Figure 13. A 3D polyurethane network, resulting from reaction between a multifunctional prepolymer and an α,ω-diol chromophore [15] 16

Figure 14. Dipole-dipole interactions between the host polymer and the chromophore dopant help stabilize the resulting material [16] 17

Figure 15. Another variation on the host-guest system, incorporating a novel 2D NLO chromophore [17] 18

Figure 16. Complexation of Ru(II) with a poly(bipyridine) chain creates an NLO chromophore on a σ-π alternating polymer backbone [18] 18

Figure 17. Azo coupling to a polymer with an aromatic system in the backbone provides another path to main-chain chromophore materials [19] 19

Figure 18. Interactions between proton donors (XH,D) and proton acceptors (Y,A) yield hydrogen bonds 20

Figure 19. Attractive and repulsive secondary interactions account for the 10.7 kcal mol^{-1} difference in thermodynamic stability for the 1-methylcytosine·9-methylguanine (C·G) dimer and the 1-methyluracil·2,6-diaminopyridine (U·DAP) dimer [20] 22

Figure 20. Multidentate zipper complexes reported by Hunter and co-workers ($\mathbf{1}_2$) and Gong and co-workers ($\mathbf{2}_2$) [31-34] 24

Figure 21. Examples of a DDD·AA dimer (**3**) stabilized by a bifurcated H-bond, and various 3-H-bonded dimers (**4**, **5** and **6**) with their corresponding stability constants [35] 25

Figure 22. Self-assembly behavior of the self-complementary (C_{2v}) and non-self-complementary (C_s) dipyridone modules **7** and **8** [36] 26

Figure 23. Equilibria between tautomeric forms and between monomer and dimer of 2-ureido-4(1*H*)-pyrimidone derivatives [39] 27

Figure 24. Co-crystallization of these pairs of compounds yields NLO materials with high mechanical and thermal stability [40a-c] 28

Figure 25. Strong hydrogen bonding between the urethane-urea carbonyls and the rigidity of the Si-O bonds are credited with the high thermal stability of these copolymers [41] 29

Figure 26. Schematic illustration of the anisotropic structure of the mixture of a smectic liquid crystal and the hydrogen-bonded complexes shown above [42] 30

Figure 27. Schematic of primary research goal. Hydrogen-bonding interactions resist electrostatically-driven relaxation to a centrosymmetric arrangement 31

Figure 28. Specific synthetic target **9** 32

Figure 29. Key intermediate, used to optimize metathesis conditions and generate oligomeric material for NLO studies 33

Figure 30. Titration of **43a** with ~ 5 M aqueous hydrochloric acid, pH 10–2. Isosbestic points indicated by (*) 50

Figure 31. Titration of **43a** with ~ 5 M hydrochloric acid, pH 12-10. Isosbestic point indicated by (*) 50

Figure 32. Three distinct absorption bands between 300 and 400 nm can be seen as a function of pH 51

Figure 33. Proposed protonation states of **43a** from pH 2–12. 52

Figure 34. Structures of the azobenzene derivatives (top row) and monocyclic fragments (bottom row) 55

Figure 35. Representative Beer's Law curve for **45b** in carbon tetrachloride 62

Figure 36. Solvatochromism of **45b** in selected solvents, at r.t. 63

Figure 37. The ^{1}H NMR integral ratios of the alkene resonances of **45b** develop over time, as shown at (a) 0h00, (b) 3h00, (c) 5h20, (d) 22h30 and (e) 56h00, as measured in $(CD_3)_2CO$, at r.t. 65

Figure 38. Negative mode ESIMS of an oligomer sample, indicating about 5 repeat units 67

Figure 39. MALDI-TOF of the oligomer sample, indicating up to 11 repeat units 67

Figure 40. Schematic representation of the expected shape of the mass spectrum of a polymer sample, where *n* is the degree of polymerization of the specific oligomer, and M_w is the average molecular weight of the sample 68

Figure 41. Schematic representation of the observed shape of the mass spectra obtained, where *n* is again the degree of polymerization of the specific oligomer 69

Figure 42. Differential scanning calorimetry (DSC) analysis of **45b**, showing a melting point at 157 °C and two exotherms, at 200 °C and 260 °C 72

Figure 43. DSC analysis of the oligomeric material, showing two exotherms, at 200 °C and 250 °C 72

Figure 44. Thermal gravimetric analysis (TGA) of **45b**, showing 5% mass loss at 200 °C and substantial mass loss above 220 °C 73

Figure 45. TGA of oligomeric material, showing 5% mass loss at 160 °C, and substantial mass loss above 220 °C 74

Figure 46. 0.49 in^2 ITO plates coated with polymer films cast from tetrahydrofuran (THF, top left), *N,N*-dimethylformamide (DMF, top center), *N,N*-dimethylacetamide (DMAc, top and bottom right), pyridine (bottom left) and 2,6-lutidine (bottom center). A gold electrode has been deposited on the bottom right film, cast from DMAc, visible as a pale circular area 76

Figure 47. Micrographs of the films cast from *N,N*-dimethylacetamide, at low magnification (a), medium magnification (b), and high magnification (c) and (d). The average diameter of the surface defects is approximately 15 μm, and the average depth is approximately 0.4 μm, as measured by profilometry studies 76

Figure A.1 ^{13}C and ^{1}H NMR spectra of compound **31a** 116

Figure A.2 ^{13}C and ^{1}H NMR spectra of compound **31b** 117

Figure A.3 ^{13}C and ^{1}H NMR spectra of compound **31c** 118

Figure A.4 ^{13}C and ^{1}H NMR spectra of compound **33a** 119

Figure A.5 ^{13}C and ^{1}H NMR spectra of compound **40a** 120

Figure A.6 ^{13}C and ^{1}H NMR spectra of compound **40b** 121

Figure A.7 ^{13}C and ^{1}H NMR spectra of compound **41a** 122

Figure A.8 ^{13}C and ^{1}H NMR spectra of compound **41b** 123

Figure A.9 ^{13}C and ^{1}H NMR spectra of compound **43a** 124

Figure A.10 ^{13}C and ^{1}H NMR spectra of compound **43b** 125

Figure A.11 ^{13}C and ^{1}H NMR spectra of compound **44** 126

Figure A.12 ^{13}C and ^{1}H NMR spectra of compound **45a** 127

Figure A.13 ^{13}C and ^{1}H NMR spectra of compound **45b** 128

Figure A.14 ^{13}C and ^{1}H NMR spectra of compound **46a** 129

Figure A.15 ^{13}C and ^{1}H NMR spectra of compound **46b** 130

Figure A.16 ^{13}C and ^{1}H NMR spectra of compound **poly(45b)**, the oligomeric material derived from compound **45b** 131

List of Reaction Schemes

Scheme 1. Key synthons for the chromophore synthesis arise from disconnection of the N=N double bond 34

Scheme 2. Friedel-Crafts alkylation to obtain lactam **12** was unsuccessful 35

Scheme 3. The attempted double Curtius rearrangement/Schmidt reaction of **16** led to an anomalous product 36

Scheme 4. Identification of the anomalous product resulted in a new route to lactam **12** 37

Scheme 5. Aryl bromide **20** proved unreactive to substitution 38

Scheme 6. Attempts at benzylic bromination of toluidine **23** did not yield useful products 39

Scheme 7. Synthesis of the amine series for the amino terminus of the chromophore 40

Scheme 8. Preparation of *N,N*-diallyl-3-toluidine (**34**) 41

Scheme 9. Synthesis of the carboxylic acid series for the amino terminus of the chromophore 42

Scheme 10. Synthesis of the chromophores via azo coupling reactions 44

Scheme 11. Synthesis of related chromophores, lacking one functionalized alkyl chain 45

Scheme 12. Structures of the ruthenium catalysts used for ADMET oligomerization 46

Scheme 13. ADMET oligomerization yielded chain lengths of 10-12 repeat units, suitable for preparation of thin films 47

List of Symbols, Nomenclature and Abbreviations

β	second-order molecular (hyper)polarizability
γ	third-order molecular (hyper)polarizability
δ	chemical shift in ppm
ε	molar absorptivity
λ_{max}	wavelength of maximum absorption
$\chi^{(2)}$	second-order bulk susceptibility
ω	frequency
^{13}C NMR	^{13}C nuclear magnetic resonance
^{1}H NMR	^{1}H nuclear magnetic resonance
A	acceptor; may refer to hydrogen-bonding or electron distribution
AAB	4-aminoazobenzene
acetone-d_6	deuterated acetone, $(CD_3)_2CO$
ADMET	acyclic diene metathesis
AIBN	2,2′-azo-bis-isobutyrylnitrile
An	aniline
ANAB	4-amino-4′-nitroazobenzene
APT	attached proton test; ^{13}C NMR experiment
aq	aqueous
b	broad, as in peak shape
BB	broadband proton decoupling; ^{13}C NMR experiment
conc	concentrated
cm	centimeter
cm^{-1}	unit of frequency in FTIR
D	donor; may refer to hydrogen-bonding or electron distribution
d	doublet
DANAB	4-dimethylamino-4′-nitroazobenzene
DANS	4-dimethylamino-4′-nitrostilbene

DC	direct current
DCNP	dicyanoethenyl pyrazole
dec.	decomposition point
DMAc	*N,N*-dimethylacetamide
DMF	*N,N*-dimethylformamide
DMSO	dimethyl sulfoxide
DMSO-d_6	deuterated dimethyl sulfoxide, $(CD_3)_2SO$
DP	degree of polymerization
DR1	Disperse Red 1
DSC	differential scanning calorimetry
DSMS	*trans*-4′-dimethylamino-*N*-methylstilbazolium sulfate
e.g.	for example
EIMS	electron impact ionization mass spectrometry
ESIMS	electrospray ionization mass spectrometry
Et_2O	diethyl ether
EtOH	ethyl alcohol
FTIR	Fourier transform infrared spectroscopy
h	hour(s)
H-bond	hydrogen bond
HEMA	2-hydroxyethylmethacrylate
HRMS	high resolution mass spectrometry
Hz	hertz
in^2	square inches
ITO	indium tin oxide; coating used as a transparent electrode material
J	coupling constant in Hz
LEO	linear electro-optic effect (Pockels effect)
m	multiplet
m/z	mass-to-charge ratio

M	concentration in $mol \cdot L^{-1}$
M^+	molecular ion
MALDI MS	matrix-assisted laser desorption ionization mass spectrometry
MALDI-TOF	matrix-assisted laser desorption ionization with time-of-flight detection
MeOH	methyl alcohol
mg	milligram(s)
MHz	megahertz
mmol	millimole(s)
mol	mole(s)
MNA	2-methyl-4-nitroaniline
Mp	melting point
MS	mass spectrometry
M_w	molecular weight, especially of a polymer sample
NAB	4-nitroazobenzene
NB	nitrobenzene
NLO	nonlinear optics or nonlinear optical
nm	nanometers
PEK	poly(ether ketone)
*p*NAn	*p*-nitroaniline
*p*PDA	*p*-phenylenediamine
ppm	parts per million
r.t.	room temperature
R_f	retention factor
s	singlet
sh	shoulder peak; incompletely resolved subsidiary peak in UV-Vis
SHG	second harmonic generation
t	triplet

T_g	glass transition temperature
TGA	thermal gravimetric analysis
THF	tetrahydrofuran
TLC	thin layer chromatography
TMEDA	tetramethylethylenediamine
UV-Vis	ultraviolet/visible (spectroscopy)

I. INTRODUCTION

1. Nonlinear Optics

The nonabsorptive interaction of light with a medium generally results from polarization of the medium by incident light and is of particular interest for visible to near infrared wavelengths (~300-1800 nm).[1] This polarization can be linear, as in the case of simple optical effects, such as refraction and birefringence, or nonlinear, as in the electro-optic effect and second harmonic generation (SHG).[1] Nonlinear optical (NLO) effects result from nonlinear polarization. This occurs when the polarization of a material as a function of an applied electric field (such as that of a light beam) generates an internal electric field that modifies both the applied field and the subsequent polarization. This polarization is dependent on the frequency (ω) of the applied field and can be symmetric or asymmetric with respect to the molecule. Asymmetric polarization can be decomposed via Fourier analysis into components at zero frequency (DC), at the fundamental frequency (ω), and at harmonic frequencies ($n\omega$, where $n = 2, 3\ldots$). Only asymmetric polarization leads to second-order NLO effects, and these effects can thus only be observed in noncentrosymmetric materials, since centrosymmetric materials yield symmetric polarization.

A. Polarization and NLO Effects

At the molecular level, optical effects are due to the polarization of electrons, and are thus subject to the polarizability of the associated molecules, which has both linear as well as nonlinear components. A detailed description of the underlying mathematical and physical concepts of molecular polarizability is well beyond the scope of this document, however, the reader is directed to a number of treatises on these subjects for

further background.[2] Although the precise mathematical description of the nonlinear polarization is not known, this polarization can be approximated as a Taylor series expansion:[1]

$$\vec{\mu}_i = \mu_i^0 + \alpha_{ij}\vec{E}_j + \tfrac{1}{2}\beta_{ijk}\vec{E}_j\vec{E}_k + \tfrac{1}{6}\gamma_{ijkl}\vec{E}_j\vec{E}_k\vec{E}_l + \ldots \quad (1)$$

In this expression, μ_i^0 is the static dipole in the absence of an electric field, α is the linear polarizability, relating to linear optical effects, β and γ are the first and second hyperpolarizabilities, relating to second- and third-order nonlinear optical effects, respectively, the subscripts *i*, *j*, *k*, *l* refer to the molecular coordinate system, and E_j, E_k, E_l denote components of the applied electric field along the coordinate axes.[1,3] Molecular hyperpolarizabilities can give an estimate of the NLO activity of a compound. However, more important for materials applications is the bulk susceptibility, which correlates to the bulk polarization.

The observed bulk polarization of a material is given by the expression:

$$\vec{P} = P_0 + \chi^{(1)}\vec{E} + \chi^{(2)}\vec{E}\vec{E} + \chi^{(3)}\vec{E}\vec{E}\vec{E} + \ldots \quad (2)$$

where P_0 is the static dipole of the sample, E is the applied electric field, $\chi^{(1)}$ is the linear susceptibility, and $\chi^{(2)}$, $\chi^{(3)}$, etc. are the second-, third- and higher-order bulk susceptibilities, respectively. A number of second-order NLO effects can be described by simple mathematical derivations of this expression; two of these effects are described in the following sections.

A.1 Second Harmonic Generation (SHG)

If an intense light beam of frequency ω passes through a second-order NLO material, light at 2ω will be generated (second harmonic), as well as a static electric field (optical rectification). Mathematically, the electric field of a plane light wave is given by:

$$\vec{E} = E_0 \cos(\omega t) \quad (3)$$

Thus, for an arbitrary point in space, substituting equation (3) into equation (2), the polarization may be rewritten as:

$$\vec{P} = P_0 + \chi^{(1)} E_0 \cos(\omega t) + \chi^{(2)} E_0^2 \cos^2(\omega t) + \chi^{(3)} E_0^3 \cos^3(\omega t) + \ldots \quad (4)$$

and, since $\cos^2(\omega t) = \frac{1}{2} + \frac{1}{2}\cos(2\omega t)$, equation (4) may be rewritten:

$$\vec{P} = [P_0 + \tfrac{1}{2}\chi^{(2)} E_0^2] + \chi^{(1)} E_0 \cos(\omega t) + \tfrac{1}{2}\chi^{(2)} E_0^2 \cos(2\omega t) + \chi^{(3)} E_0^3 \cos^3(\omega t) \quad (5)$$

where the first term, in brackets, represents the static electric field, consisting of the static dipole of the material P_0 plus a second-order DC field component (related to optical rectification). The second term refers to a standard linear interaction with the incident light, while the third term contains the frequency-doubled (2ω) component, which results in the observed SHG effect. Subsequent, higher-order, terms are unchanged from the original series, expressed in equation (4).

A.2 Linear Electro-Optic (LEO) or Pockels Effect

When a static DC electric field is used to polarize NLO materials, the refractive index can be modified as a function of the static field. In the presence of two electric fields E_1 and E_2, equation (4) for an arbitrary point in space becomes:

$$\vec{P} = P_0 + \chi^{(1)}[E_1 \cos(\omega_1 t) + E_2 \cos(\omega_2 t)] + \chi^{(2)}[E_1 \cos(\omega_1 t) + E_2 \cos(\omega_2 t)]^2 + \chi^{(3)}[E_1 \cos(\omega_1 t) + E_2 \cos(\omega_2 t)]^3 + \ldots \quad (6)$$

If one of the fields is a static DC electric field, then $\omega_2 = 0$, E_2 is the magnitude of the voltage applied to the material, and equation (6) becomes:

$$\vec{P} = P_0 + \chi^{(1)}[E_1 \cos(\omega_1 t) + E_2] + \chi^{(2)}[E_1 \cos(\omega_1 t) + E_2]^2 + \chi^{(3)}[E_1 \cos(\omega_1 t) + E_2]^3 \quad (7)$$

The second-order term of equation (7) can be expanded to give:

$$\chi^{(2)}[E_1 \cos^2(\omega_1 t) + 2E_1 E_2 \cos(\omega_1 t) + E_2^2] \quad (8)$$

So, neglecting third-order terms, the optical frequency polarization (i.e., that relating to ω) may be expressed:

$$\vec{P}_{opt} = [\chi^{(1)} + \chi^{(2)} E_1 \cos(\omega_1 t) + 2E_2]E_1 \cos(\omega_1 t) \quad (9)$$

The refractive index is related to the linear susceptibility of the material and thus to the first-order term of equation (4):

$$\chi^{(1)} E_1 \cos(\omega_1 t) \quad (10)$$

In effect, the applied voltage changes the linear susceptibility $\chi^{(1)}$ to $[\chi^{(1)} + \chi^{(2)}E_1\cos(\omega_1 t) + 2E_2]$, and thus alters the refractive index η, since

$$\eta^2(\omega) = 1 + 4\pi\chi^{(1)}(\omega) \quad (11)$$

This effect leads to devices such as electro-optic modulators, which can be of use for non-mechanical switching in fiber-optic networks, among other applications.

B. Nonlinear Optical Materials

Nonlinear optical materials, by definition, are materials that exhibit nonlinear optical effects. These materials can take a variety of specific forms, ranging from inorganic semiconductors, from which the field of nonlinear optics emerged,[2b] to the current area of interest, the molecular and polymeric organic materials.[2c] Also, within this last category, a wide range of materials has arisen designed to address applications, as well as to further elucidate the structure-property relationships at work in this still-evolving field.

B.1 Organic Crystals

As the field of nonlinear optics emerged from solid-state physics, which is typically dominated by inorganic semiconductors, insulators, and crystals, many of the early experimental and theoretical investigations into the field focused on these classes of materials. More recently, however, it was recognized that organic polymeric materials containing large delocalized π-electron systems can also exhibit very large nonlinear responses.[4] Additionally, organic synthesis offers enormous flexibility in optimizing not only nonlinear optical characteristics but also other necessary attributes such as mechanical and thermal stability, and resistance to laser damage. As a result, interest in the nonlinear responses of organic compounds began to grow.

The polarizability of a crystal can be seen as arising from contributions from the lattice components (atoms and molecules) and the interactions among these components.[5] The latter contribution is dominant in inorganic materials, due to their weakly polarizable atoms and complexes, but the former is dominant in organic materials, due to relatively weak intermolecular bonding (Van der Waals forces, dipole-dipole interactions, and hydrogen-bonding).[5] In organic molecules, polarizability can generally be correlated with the presence of extended conjugated π-systems. This can be translated to second order nonlinear optical effects when these π-systems link electron-donating groups (such as amines, ethers, and alcohols) with electron-accepting groups (such as nitrosyl or nitro groups, aldehydes, and nitriles).[5] The result is an enhanced asymmetric electronic distribution in either or both the ground state and excited state configurations of the molecule.[5] Some simple generalized examples are shown in Figure 1, where electron-donating groups are denoted D and electron-accepting groups A.

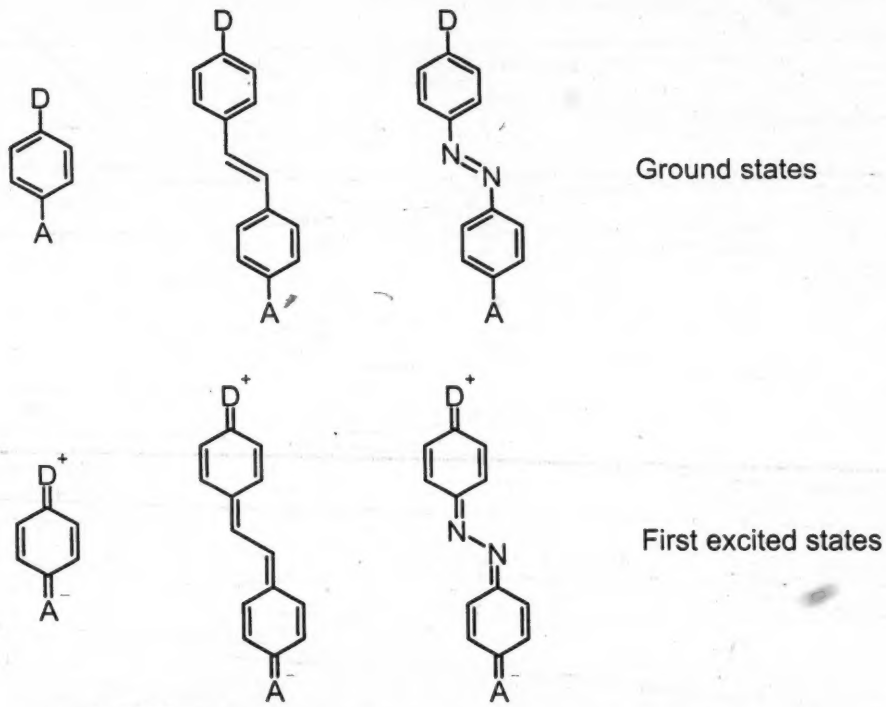

Figure 1. Typical organic materials for second order nonlinear optical effects. These are donor-acceptor (D–A) substituted molecules with π-electron ring systems. Also shown are the charge-transfer first excited states [5]

It is apparent that a large number of organic compounds meet these general criteria for second order *molecular* (hyper)polarizability (β). It is, however, *bulk* effects that lead to useful materials. The second order bulk susceptibility of a material, $\chi^{(2)}$, is the macroscopic analog of β, and to a first approximation corresponds to the same molecular characteristics. An additional requirement for translating a molecule with a high β value into a crystalline material with a high $\chi^{(2)}$ value is that the molecule must crystallize into

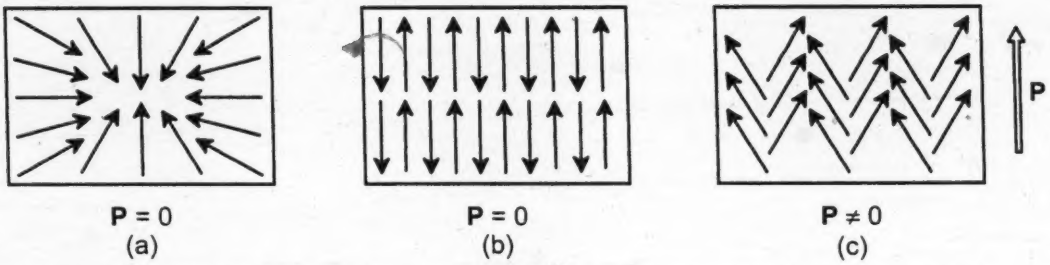

Figure 2. Schematic illustrating centrosymmetric (a,b) and noncentrosymmetric (c) arrangements of molecular dipoles, and the resulting bulk polarization, **P**

a polar, or noncentrosymmetric space group.[3] Figure 2 illustrates this distinction in schematic form, in which the generic D-π-A systems shown previously in Figure 1 are represented as arrows. Arrangements (a) and (b) are centrosymmetric, so that although the individual components of the system possess internal dipoles, the bulk polarization is zero. Arrangement (c) is noncentrosymmetric, resulting in a bulk polarization **P** as shown. Most organic compounds tend to crystallize centrosymmetrically, in which case the bulk polarization, and therefore the second order susceptibility, of the material is zero. Some organic compounds, however, are known to crystallize in noncentrosymmetric, polar space groups, for example, 2-methyl-4-nitroaniline (MNA, space group Cc), or *trans*-4′-dimethylamino-*N*-methylstilbazolium methyl sulfate (DSMS, point group mm2) (Figure 3).[3] These crystals do show large second order susceptibilities, rivaling those of the best inorganic crystals, such as $LiNbO_3$ or InSb.[3] Despite these results, attention has more recently shifted toward polymeric and thin film materials, favored for their increased technological utility, especially for the fabrication of wave-guided nonlinear optical devices.

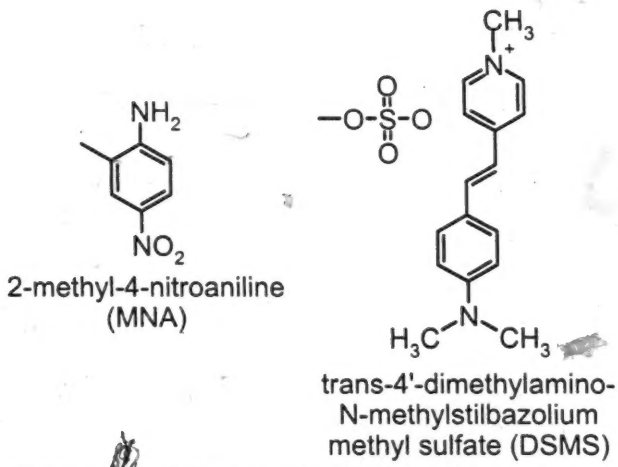

Figure 3. 2-methyl-4-nitroaniline (MNA) and *trans*-4′-dimethylamino-*N*-methylstilbazolium methyl sulfate (DSMS) are examples of organic crystals in polar space groups [3]

B.2 Organic Dopants

It was known that many organic compounds, specifically those with high molecular hyperpolarizabilities (β), could exhibit bulk nonlinear optical responses if appropriately oriented in the bulk material.[3] This could be achieved in a polymeric film doped with a molecule possessing a strong static dipole by applying an external DC electric field to a film softened by heating the host polymer above its glass transition temperature, T_g, then cooling the film below T_g in the presence of the external electric field. The effect of this process, called "poling," was to remove the orientational averaging of the dopant molecules within the polymer matrix, resulting in a noncentrosymmetric arrangement of the dopant dipoles, and a bulk nonlinear response. As anticipated, the poling of doped polymers yielded many novel nonlinear optical materials with large second-order nonlinear coefficients (Figure 4).[6] Although the materials thus obtained possessed useful

second-order properties, they also showed a significant limitation, in that the nonlinear responses were thermodynamically unstable. Over time, the NLO responses of these

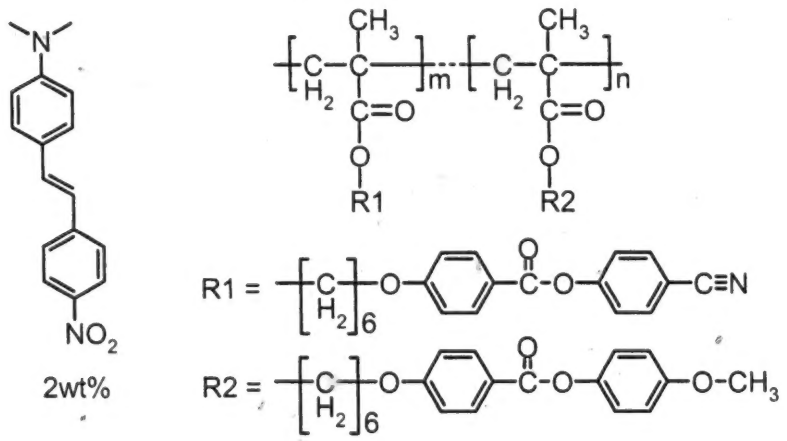

Figure 4. The NLO chromophore at left, 4-dimethylamino-4′-nitrostilbene (DANS), was doped into the liquid crystalline polymer at right and poled to obtain a novel second order NLO material [5]

materials degraded, due to an electrostatically-driven randomization of the dipole orientation.[7] This limitation still prevents the development of NLO materials today. While many approaches have been attempted, most still focus on refining the concept of a poled polymeric thin film and, specifically, on restricting the orientational freedom of the NLO chromophore after poling.

B.3 Poled Polymeric Thin Films

Although the poling of organic dopants within a polymer matrix has yielded some promising results, the issue of *maintaining* bulk dipole orientation poses a significant barrier to device applications. As a result, several different approaches to restricting chromophore orientation after poling have been developed. Among these are (a) the use

of a high-T_g polymer matrix, (b) the introduction of assorted cross-linking strategies, (c) the use of secondary bonding interactions as non-covalent stabilizing influences, and (d) the attachment or incorporation of an NLO chromophore into the polymer backbone to give a side or main chain polymer, respectively.

(a) High-T_g Polymer Matrix

Given the goal of restricting the orientational freedom of the NLO chromophores within the polymer matrix, one of the most straightforward approaches is to rigidify the matrix itself. Polymers with high glass transition temperatures (T_g ~ 150 °C or higher) are known to possess very rigid matrix structures, and thus a number of systems have been developed to exploit this property. Among these is the system shown in Figure 5, in which a dicyanoethylene-based NLO chromophore is incorporated into a high-T_g

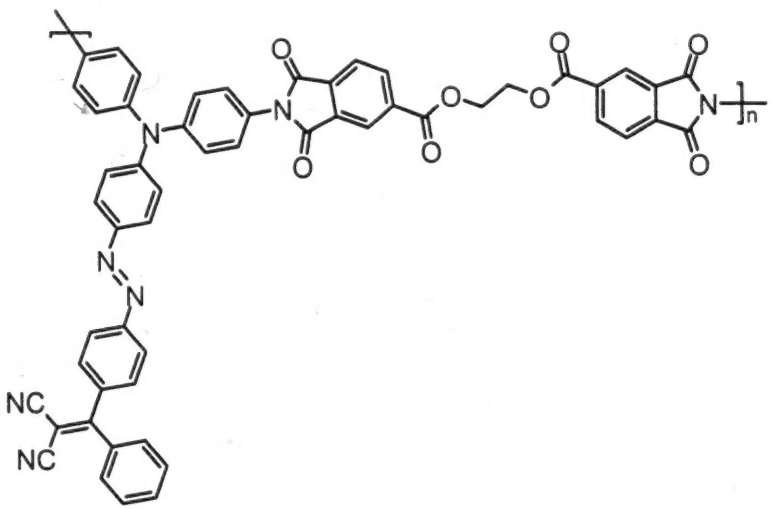

Figure 5. A dicyanoethylene-based chromophore is incorporated into a high-T_g polymer matrix [8]

polyimide chain.[8] Another system (Figure 6) uses a poly(urethane imide) chain generated from Disperse Red 19, pyromellitic anhydride, and tolylene diisocyanate.[9]

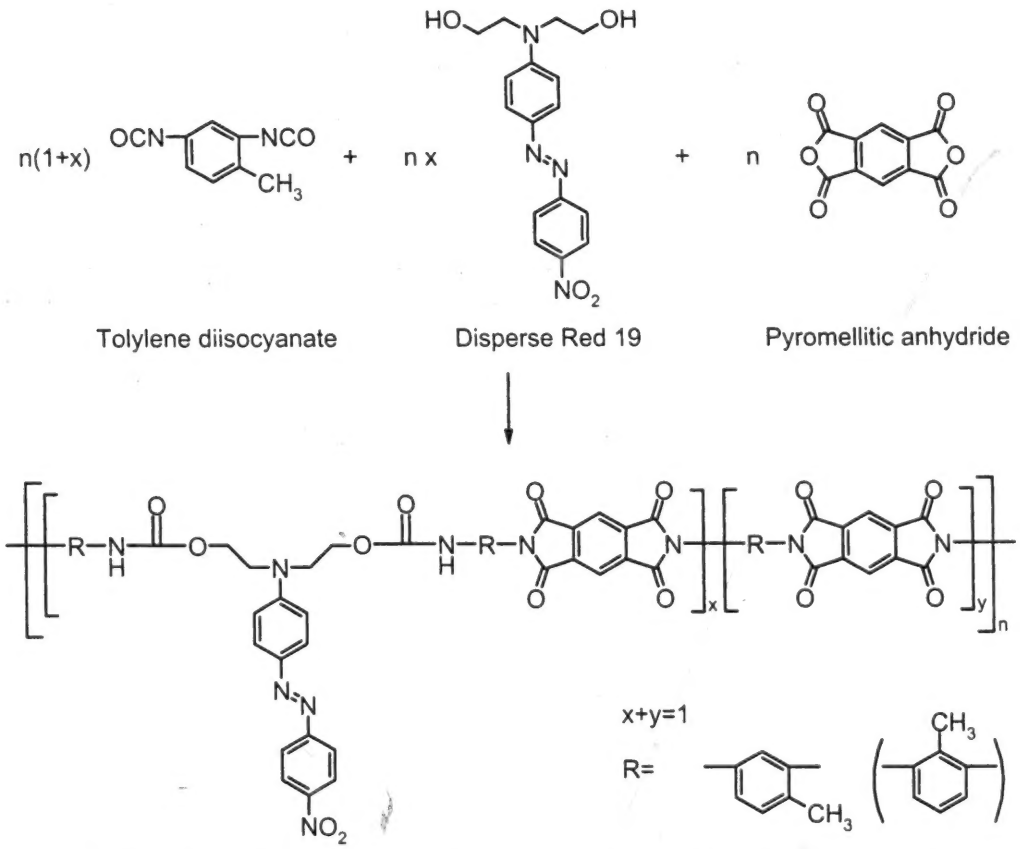

Figure 6. Disperse Red 19 is embedded in a high-T_g poly(urethane imide) in one synthetic step [9]

(b) Cross-Linking Strategies

Rather than pre-selecting a polymer matrix with a high T_g, such a matrix can also be generated around the chromophore. This is commonly achieved with cross-linking reactions, through which additional bonds are formed, either among the repeat units of the polymer, or among different portions of the polymer backbone.

Via Functionality on the Chromophore

Conceptually, one of the simplest cross-linking strategies is to start with a multiply-functionalized monomer unit, and, under appropriate conditions, these functional groups form a combination of three or more covalent links to other monomers. With certain types of systems, these processes are simultaneous, as in the system shown in Figure 7, where a ferroelectric liquid-crystalline bis(acrylate) is photopolymerized to generate a network polymer.[10]

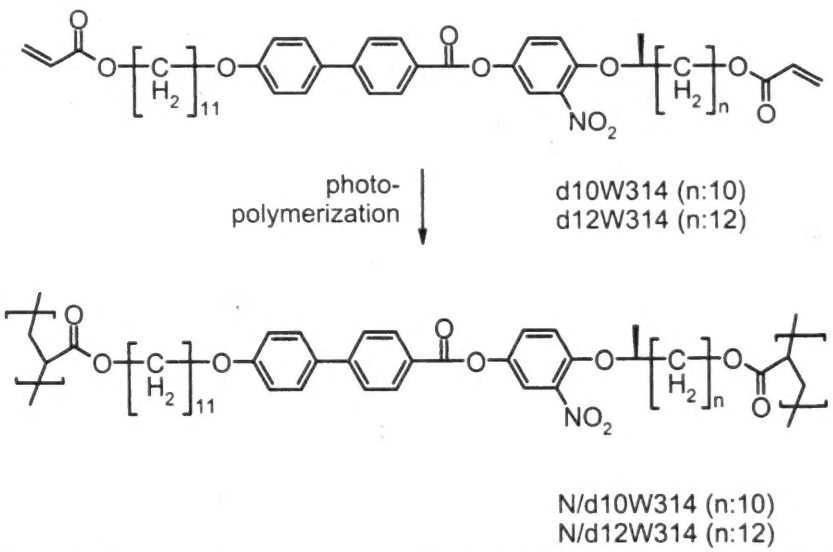

Figure 7. The photopolymerization of the bis(acrylate) chromophore, at top, yields the network polymer below [10]

In other cases, a mixture of cross-linking agents is allowed to partially react, and the monomer unit is added to this prepolymer mixture and cured to generate the fully cross-linked polymer (Figure 8).[11]

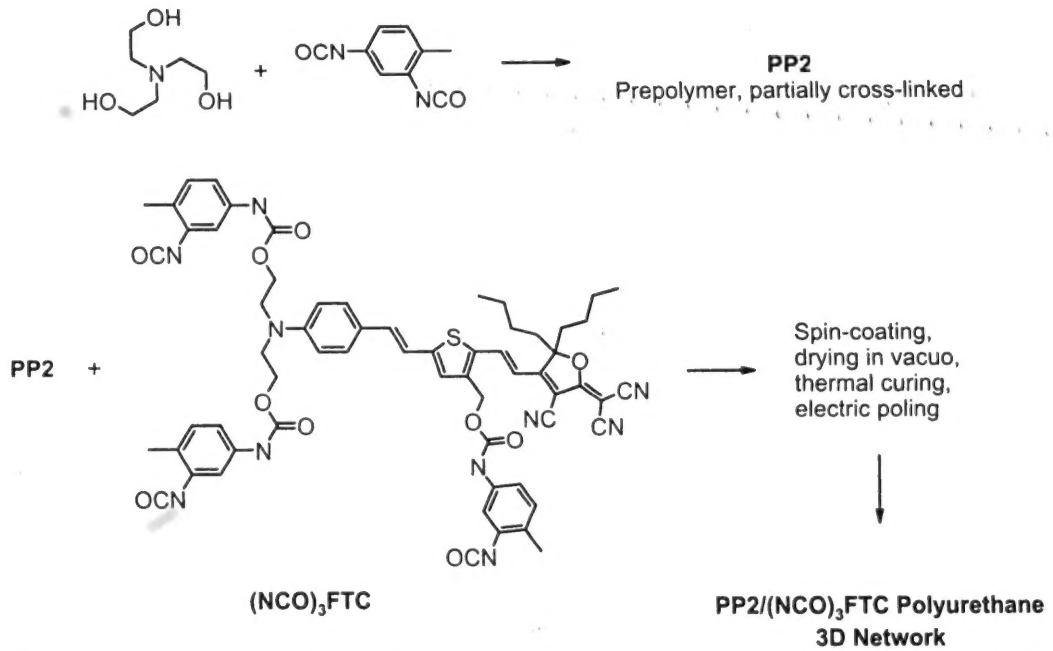

Figure 8. Reaction of a partially cross-linked prepolymer with a trilink chromophore leads to a 3D network [11]

Via an Alternating Copolymer

In a concept related to the multiply-functionalized monomer, the NLO chromophore and cross-linking moiety can be integrated into two types of monomer units, which can then be polymerized into an alternating copolymer. A common method of accessing these co-monomer pairs is via acrylate esters. For example, in recent work the methacrylate ester of Disperse Red 1 (DR1M) was copolymerized with 2-hydroxyethylmethacrylate (HEMA) to generate a copolymer.[12] The pendant hydroxyl group was then used to generate another acrylate ester, which allowed for thermal cross-linking by polymerization of the acrylic groups (Figure 9). A similar system

incorporating a different NLO chromophore simply used a bis(acrylate) as the non-chromophore co-monomer (Figure 10), but used photopolymerization of the acrylic

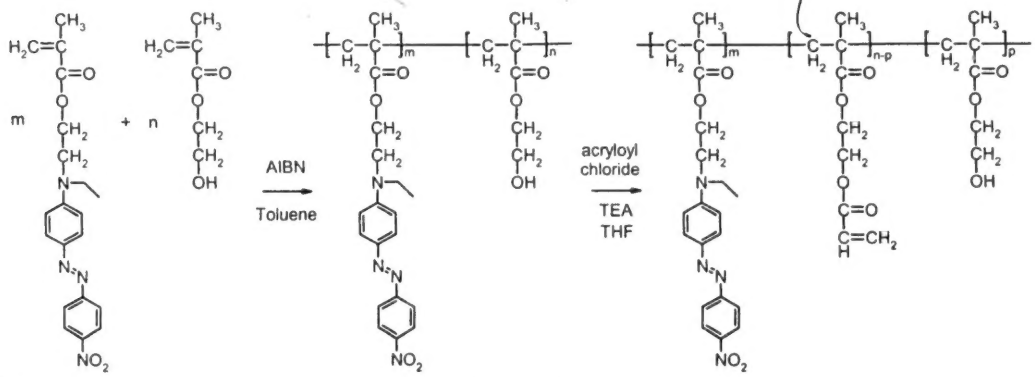

Figure 9. An acrylate-functionalized copolymer allows simultaneous cross-linking, via photopolymerization, and photoinduced orientation of the chromophore [12]

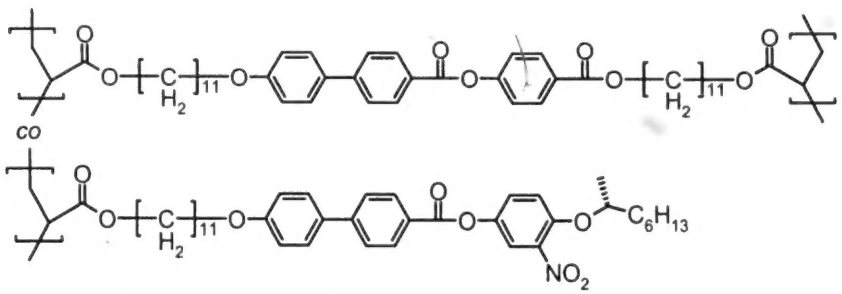

Figure 10. Photopolymerization of an acrylate copolymer yields this network polymer [10]

groups to cross-link the polymer.[10] Another system uses *N*-phenyl maleimides and epoxy-substituted methylvinylisocyanates to generate the necessary co-monomer pairs (Figure 11), which are cross-linked via epoxide photopolymerization or thermal polymerization.[13]

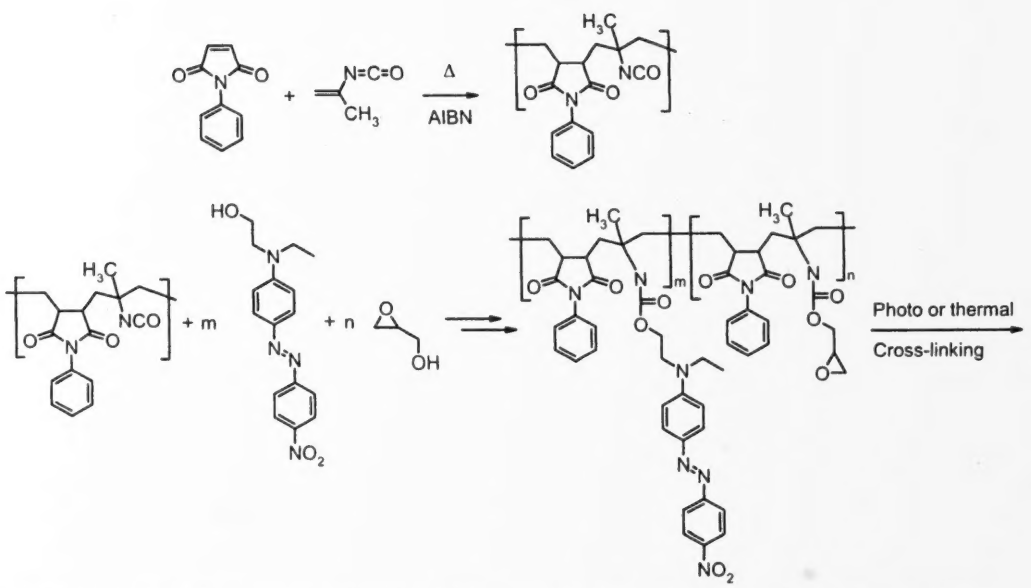

Figure 11. Pendant epoxides on this maleimide copolymer allow both thermal and photochemical cross-linking [13]

Via Functionality on the Polymer Backbone

An appropriate choice of polymerization method can yield a functionalized polymer chain that can further react to generate the desired cross-linked polymer matrix. A

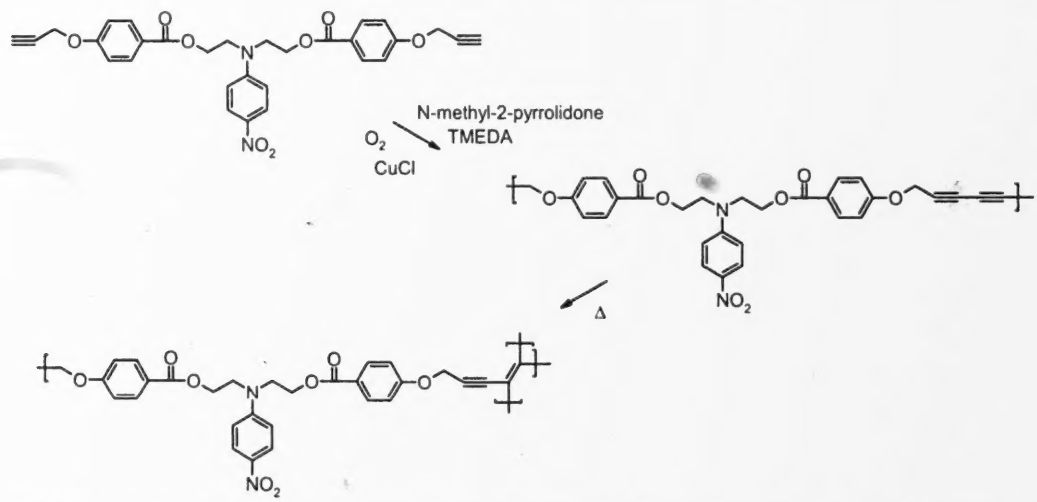

Figure 12. Oxidative coupling of terminal bis(acetylene)s yields thermally cross-linked poly(diacetylene)s [14]

structurally simple example was recently published[14] which generates a polymer containing diacetylene units via the oxidative coupling of terminal acetylenes (Figure 12). Cross-linking of the diacetylene groups was initiated thermally. In another variation on the polyurethane motif seen in previous sections, a 3-D network polymer incorporating the CLD-5 NLO chromophore (Figure 13) has been prepared via a multi-functional prepolymer.[15]

(c) Secondary Bonding Interactions

Instead of using covalent bonding to retain the desired orientation of the NLO chromophores, it is also possible to use secondary bonding interactions, such as hydrogen bonding, to serve the same purpose. The most common approach is a host-guest system in which the polymer acts as a host, and molecules of the NLO chromophore dopant are

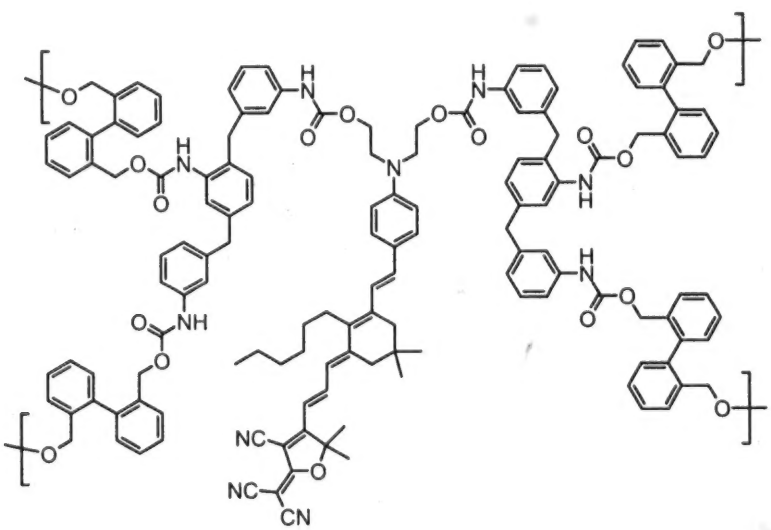

Figure 13. A 3D polyurethane network, resulting from reaction between a multifunctional prepolymer and an α,ω-diol chromophore [15]

guests. One example uses dipole-dipole interactions between a dicyanoethenyl-pyrazole derivative and a poly(ether ketone) host polymer (Figure 14).[16] In a more recent system, illustrated in Figure 15, a novel 2-dimensional NLO chromophore, based on

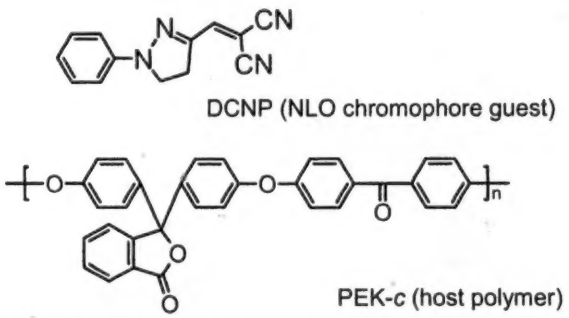

Figure 14. Dipole-dipole interactions between the host polymer and the chromophore dopant help stabilize the resulting material [16]

carbazole with nitro acceptors, is used as a dopant in a poly(ether imide) host.[17] In this system, a combination of both dipole-dipole interactions and a particularly large rotational cone volume for the chromophore contributed to a restriction of rotational freedom.

(d) Polymeric Chromophore

Another method used to fix chromophore orientation is to incorporate the chromophore into the polymer backbone, thus anchoring both ends of the dipolar structure at the same time. Two very different examples of this approach have recently been published. One uses a σ-π alternating polymer, poly(disilanylene-2,2′-bipyridine-5,5′-diyl), and its ruthenium(II) complex (Figure 16) to generate the NLO material.[18] In

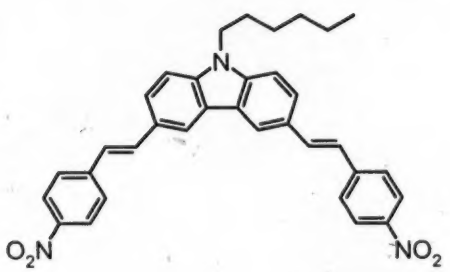

Cz_2PhNO_2 (2D NLO chromophore guest)

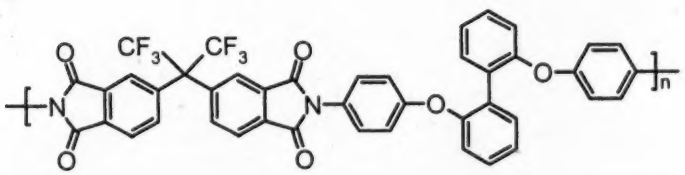

6FPEI (polymer host)

Figure 15. Another variation on the host-guest system, incorporating a novel 2D NLO chromophore [17]

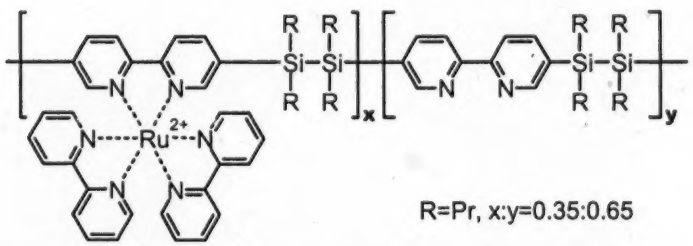

R=Pr, x:y=0.35:0.65

Figure 16. Complexation of Ru(II) with a poly(bipyridine) chain creates an NLO chromophore on a σ-π alternating polymer backbone [18]

this system, the ruthenium complex generates a charge, and the σ-π alternating polymer acts as both the charge transport channel and the second-order NLO chromophore. The second example consists of a "fully-functionalized polymer," in which the NLO chromophore is covalently bound to a photoconductive polymer that can undergo photo-induced orientation (Figure 17).[19]

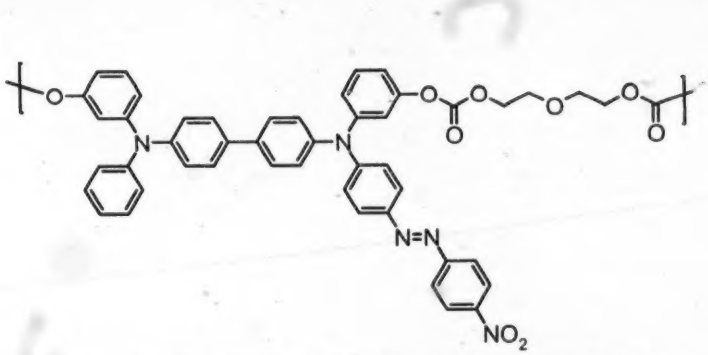

Figure 17. Azo coupling to a polymer with an aromatic system in the backbone provides another path to main-chain chromophore materials [19]

2. Non-Covalent Interactions

The precise definition of non-covalent interactions, establishing what is covalent and what is not, is a matter of significant debate in certain fields. For the purposes of this work, the definition shall encompass interactions among permanent dipoles within a molecular structure, such that all original bonding in the individual molecules is retained. More specifically, discussion will be restricted to a particular type of this sort of interaction, that of hydrogen bonding. Special attention will be paid to the cooperative effect of secondary interactions in molecules containing multiple adjacent hydrogen bonds, and the utility of this phenomenon in incorporating hydrogen bonding motifs into the design of an organic synthesis.

A. Hydrogen Bonding

Hydrogen bonds, commonly abbreviated H-bonds, connect atoms X and Y that have electronegativities larger than that of hydrogen, specifically C, N, O, F, P, S, Cl, Se, Br and I.[20] The XH group is typically referred to as the proton donor (D), whereas Y is

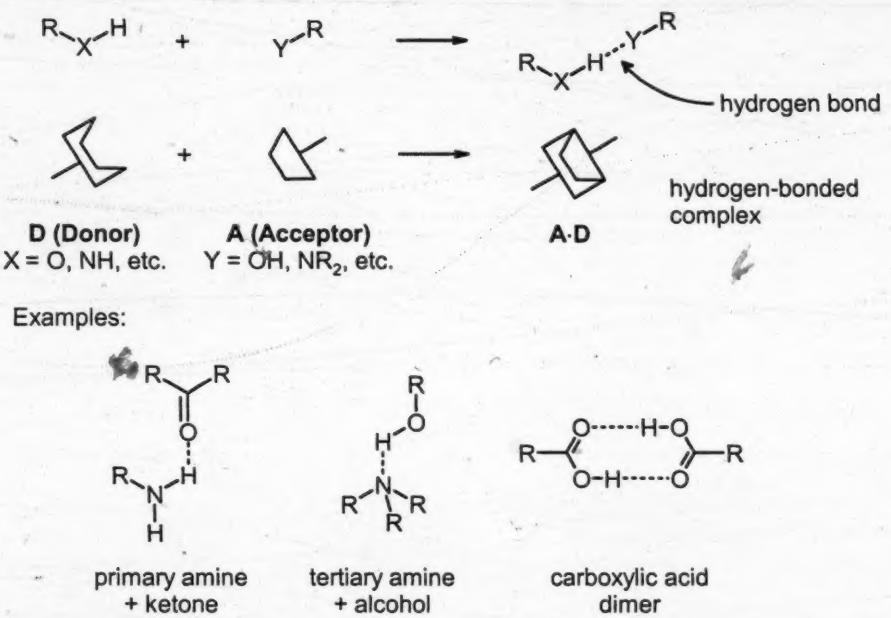

Figure 18. Interactions between proton donors (XH,D) and proton acceptors (Y,A) yield hydrogen bonds

called the proton acceptor (A). The strength of H-bonds increases with an increase in the dipole moment of the X-H bond and the electron lone pair on Y, so that the strongest H-bonds are formed between N, O, and F acting as X and Y.[20] Figure 18 illustrates this general interaction, and gives some simple examples involving common organic functional groups. C-H can also act as a weak donor, however, and the electrons of unsaturated double or triple bonds can act as weak acceptors, generating so-called "π" H-bonds.[21]

The typical energy of a H-bond in the gas phase is in the range of 2-20 kcal mol^{-1}, much weaker than covalent bonds, but much stronger than dipolar or London dispersion force energies (< 2 kcal mol^{-1}).[20] The electronic attraction is amplified in cases where

either the donor or acceptor is charged, and as a result, the H-bonds become much stronger (10-45 kcal mol^{-1}).[22]

Since H-bonds do not, for the most part, involve any physical transfer, but rather the close association of oppositely charged portions of dipolar species, they are dynamic and reversible in nature.[23] As a result, the strengths of H-bonds are generally expressed as thermodynamic stabilities or binding constants.[24] So, for the formation of a dimeric complex (A_2) from two monomer units A

$$2\,A \rightleftharpoons A_2$$

the binding constant or association constant, K_{ass}, may be expressed as:

$$K_{ass} = \frac{[A_2]}{[A]^2}$$

Due to the dynamic, reversible nature of H-bonds, their strengths are dependent on chemical environment, such as solvent and temperature.[23] They are usually strongest in apolar solvents without H-bonding properties, like alkanes, and are lower for solvents that can act as either a H-bond donor or acceptor themselves, due to competitive solvation of donor and acceptor sites by solvent molecules.[20]

B. Secondary Interactions and Schneider's Rule

In 1967, a study by Rich and co-workers, comparing the experimental binding data for triply H-bonded dimeric complexes in $CHCl_3$, found very different stabilities for the complexes, with values for binding constants ranging from ~10^2 to 10^4-10^5 M^{-1}.[25] Over 20 years later, Jorgensen and co-workers showed that these variations could be attributed largely to attractive and repulsive secondary interactions that result from the close proximity of the dipoles in the adjacent H-bonds.[26] Stabilization can result from

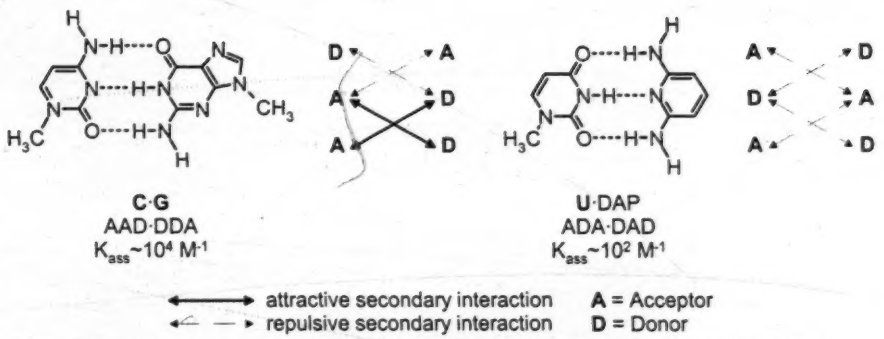

Figure 19. Attractive and repulsive secondary interactions account for the 10.7 kcal mol^{-1} difference in thermodynamic stability for the 1-methylcytosine·9-methylguanine (C·G) dimer and the 1-methyluracil·2,6-diaminopyridine (U·DAP) dimer [20]

electrostatic attraction between positively and negatively polarized atoms in adjacent H-bonds, while destabilization can similarly result from electrostatic repulsion between two positively or negatively polarized atoms (see Figure 19).[24] Simulations using Monte Carlo and molecular dynamics methods showed that the dimer formed by 1-methylcytosine and 9-methylguanine (C·G, an AAD·DDA array) is 10.7 kcal mol^{-1} lower in energy than the dimer of 1-methyluracil and 2,6-diaminopyridine (U·DAP, an ADA·DAD array). This result compares favorably with experimental binding data for the complexes.[27] As indicated, the C·G dimer involves two attractive and two repulsive secondary interactions, while the U·DAP dimer involves four repulsive secondary interactions. Extending this model, the highest association constant for a triply H-bonded complex is expected for an AAA·DDD array, in which all four secondary interactions are attractive. Experimental evidence of this was obtained by Murray and Zimmerman, one year later.[28] Further comparison of experimental binding data for 58 different synthetic H-bonded complexes led Sartorius and Schneider to develop an empirical rule that can be used to predict the binding strength of a given complex. Under this treatment, the free

energy of dimerization consists of only two increments: a contribution of 1.88 kcal mol^{-1} for each H-bond and ±0.7 kcal mol^{-1} for each attractive or repulsive secondary interaction.[29]

C. Hydrogen Bonding Complexes and Cooperativity

As individual entities, H-bonded dimers are fairly well-behaved and have relatively straightforward association characteristics. However, as multiple H-bonding motifs are covalently combined into larger arrays or multidentate modules, the phenomenon of cooperativity comes into play, in which the binding energy of the entire array is greater than the simple sum of the individual binding energies of the components. Put more simply, in an oligomeric system displaying positive cooperativity, $\Delta G_{n\text{-mer}} > n\Delta G_{\text{monomer}}$.[24] In combination with the previously mentioned secondary interactions, this can lead to a number of interesting motifs, broadly categorized here as those involving 1, 2, 3 and 4 H-bonds.

C.1 Complexes Involving 1 H-Bond

Generally speaking, assemblies based on a single H-bond have relatively low association constants. If necessary, however, the stability of such assemblies can be increased by connecting series of individual 1-H-bond motifs into multidentate modules, which can associate through the formation of multiple H-bonds.[30] This approach has led to the development of so-called "zipper complexes" (Figure 20). The system studied by Hunter and co-workers, $\mathbf{1}_2$, is held together by a combination of multiple H-bonding interactions between amide units and additional edge-to-face π-π interactions in the spacer unit.[31,32] The overall thermodynamic stability of the multidentate complexes increases exponentially with the number of connected binding sites, a clear

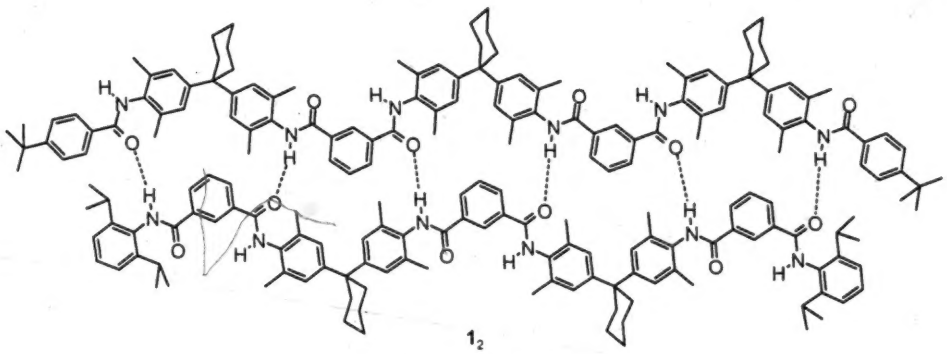

$\mathbf{1}_2$

$K_{ass} \sim 1.1 \times 10^3\ M^{-1}$

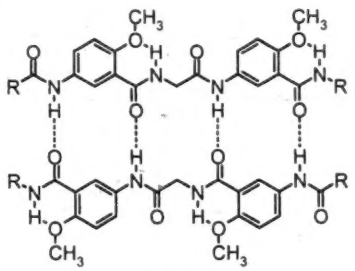

$\mathbf{2}_2$

$K_{ass} > 4.4 \times 10^4\ M^{-1}$

Figure 20. Multidentate zipper complexes reported by Hunter and co-workers ($\mathbf{1}_2$) and Gong and co-workers ($\mathbf{2}_2$) [31-34]

demonstration of positive cooperativity. A similar system prepared by Gong and co-workers describes the dimerization of self-complementary oligoamides synthesized from readily available starting materials, such as isophthalic acid and 1,3-phenylenediamine ($\mathbf{2}_2$, Figure 20).[33,34]

C.2 Complexes Involving 2 H-Bonds

Many commonly-encountered polar functionalities dimerize through the formation of two H-bonds, as in carboxylic acids, *cis*- and *trans*- amides, and several others.[24] Such dimers represent a motif that may be denoted AD·DA. In this motif, however, the presence of two repulsive secondary interactions limits the enthalpic gain such that it is usually insufficient to completely compensate for the entropic loss, and the complexes

are only stable at high concentrations (>10^{-2} M). The alternate motif, AA·DD, however, shows an increased stability, due to two attractive secondary interactions.[23] This can be further increased through the addition of secondary interactions, as, for example, in the DDD·AA complex shown in Figure 21, which contains a bifurcated (three-center) H-bond.[35] As with the 1-H-bond motifs, cooperativity can also occur here, as exemplified

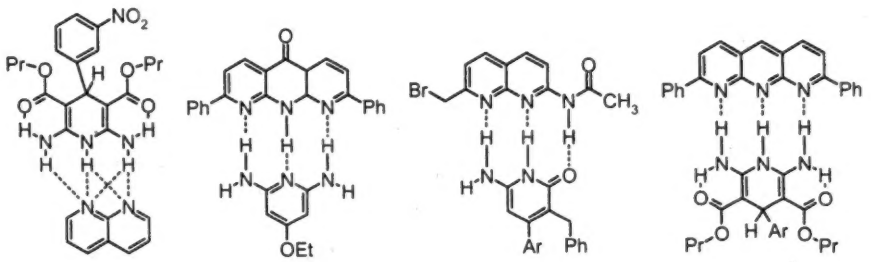

Figure 21. Examples of a DDD·AA dimer (**3**) stabilized by a bifurcated H-bond, and various 3-H-bonded dimers (**4**, **5** and **6**) with their corresponding stability constants [35]

by the 2-pyridone motif (**7** and **8**, Figure 22) developed by Wuest and co-workers, which can exhibit different association patterns with different orientations of the pyridone moiety.[36]

C.3 Complexes Involving 3 H-Bonds

As may be expected, complexes involving 3 H-bonds generally show much greater stability than 2-H-bond systems, with the third H-bond contributing favorably to the enthalpy of association. However, secondary interactions can counteract this stabilization to some extent, depending on the arrangement of donor and acceptor sites within the array. Studies by Zimmerman and co-workers of the differences in thermodynamic stability of dimeric complexes confirmed the expected result, that

is,increasing stabilities with increasing numbers of favorable secondary interactions. The values obtained were on the order of 10^2 M^{-1} for **4** (0 favorable secondary interactions),

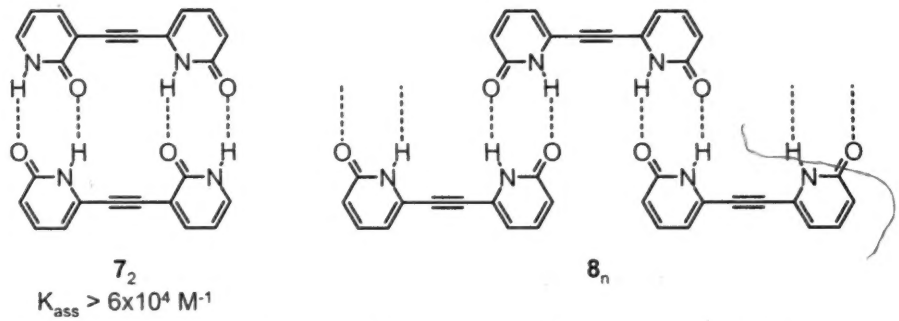

Figure 22. Self-assembly behavior of the self-complementary (C_{2v}) and non-self-complementary (C_s) dipyridone modules **7** and **8** [36]

10^3-10^4 M^{-1} for **5** (2 favorable interactions), and >10^5 M^{-1} for **6** (4 favorable interactions).[25,37] Some specific examples of these motifs are also shown in Figure 21.

C.4 Complexes Involving 4 H-Bonds

Once again, as expected, the addition of another H-bond confers increased stability to complexes containing 4 H-bonds. Unlike 3-H-bond motifs, however, these allow for self-complementarity, in some cases greatly simplifying their incorporation into an organic synthesis and providing attractive options for applications in polymeric materials and molecular capsules.[24] Meijer and co-workers were the first to describe a series of compounds that can dimerize through the formation of four H-bonds.[38,39] These 2-ureido-4(1*H*)-pyrimidone derivatives allow access to two different dimerization motifs, AADD·DDAA and ADAD·DADA, through tautomerism (Figure 23).

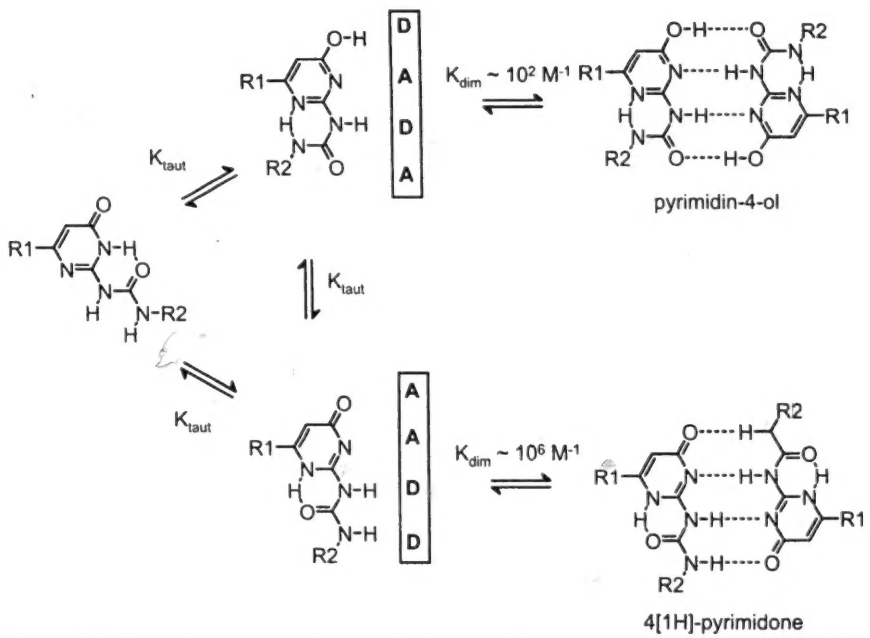

Figure 23. Equilibria between tautomeric forms and between monomer and dimer of 2-ureido-4(1*H*)-pyrimidone derivatives [39]

One interesting property of this system is that, although Schneider's rule predicts almost three orders of magnitude difference in dimerization constants between these motifs, the observed difference is only one order of magnitude, a discrepancy attributed to additional stabilization by an internal H-bond. Dimerization constants of structural analogues that are unable to form the internal H-bond are in much better agreement with Schneider's rule.[34]

D. Hydrogen Bonding in NLO Materials

A number of systems using the structural control of hydrogen bonding to elicit the useful bulk properties of NLO materials have been reported recently. Some of these use co-crystallization of two compounds with little or no bulk NLO properties to generate organic crystals with significantly increased NLO responses. Specific examples are

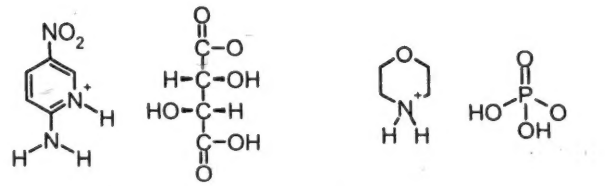

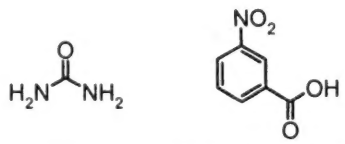

Figure 24. Co-crystallization of these pairs of compounds yields NLO materials with high mechanical and thermal stability [40a-c]

shown in Figure 24, and include ionic crystals, in both organic and organic-inorganic hybrid forms, and non-ionic binary organic complexes. All of these examples show significant mechanical and thermal stability of their NLO responses, an effect attributed to very close crystal packing due to strong hydrogen bonding.[40a-c]

Another approach using hydrogen bonding to enhance the stability of NLO materials incorporates siloxane linkages into urethane-urea copolymers.[41] Poled samples of these polymeric materials have orientational stabilities exceeding those of analogous polymers lacking the siloxane linkages, an effect ascribed to strong hydrogen bonding effects between X and Y. In addition, these linkages result in low optical loss materials, due to a decreased number density of C-H bonds in the polymer matrix.

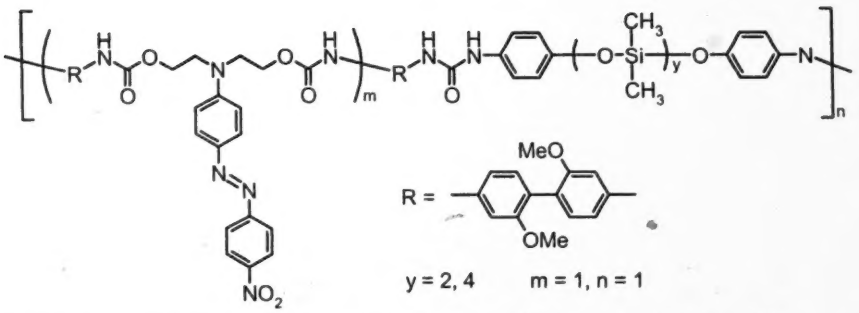

Figure 25. Strong hydrogen bonding between the urethane-urea carbonyls and the rigidity of the Si-O bonds are credited with the high thermal stability of these copolymers [41]

A fairly exotic system, developed as part of an investigation into the design of functional liquid crystalline materials, uses the self-assembly of gelling agents in liquid crystals via hydrogen bonding to generate anisotropic physical gels.[42] These gels have been found to possess electro-optical properties, dependent on the concentration of the gelling agent, as well as on various alignment forces generated by phase changes in the liquid crystal. An example of the type of heterogeneous structures that can be generated through these self-assembly processes is shown in Figure 26. An advantage to NLO materials generated in this manner is that the self-assembly processes are dynamic, and tend to re-establish the anisotropy of the materials. This is in contrast to poled polymeric materials, in which the tendency is for the NLO chromophores to lose their alignment over time.

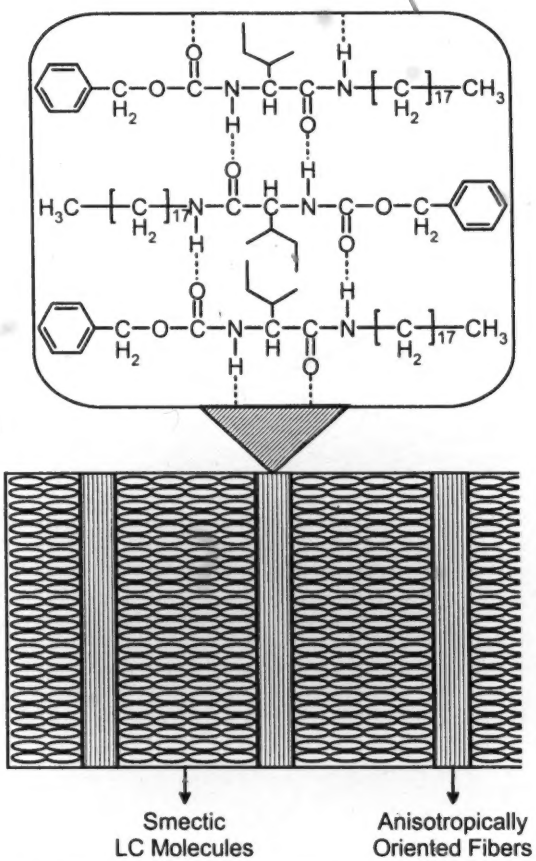

Figure 26. Schematic illustration of the anisotropic structure of the mixture of a smectic liquid crystal and the hydrogen-bonded complexes shown above [42]

3. Thesis Proposal

There exists significant technological potential for materials that show second order NLO responses *and* possess long-term stability.[1-5] Coupled with the relatively recent

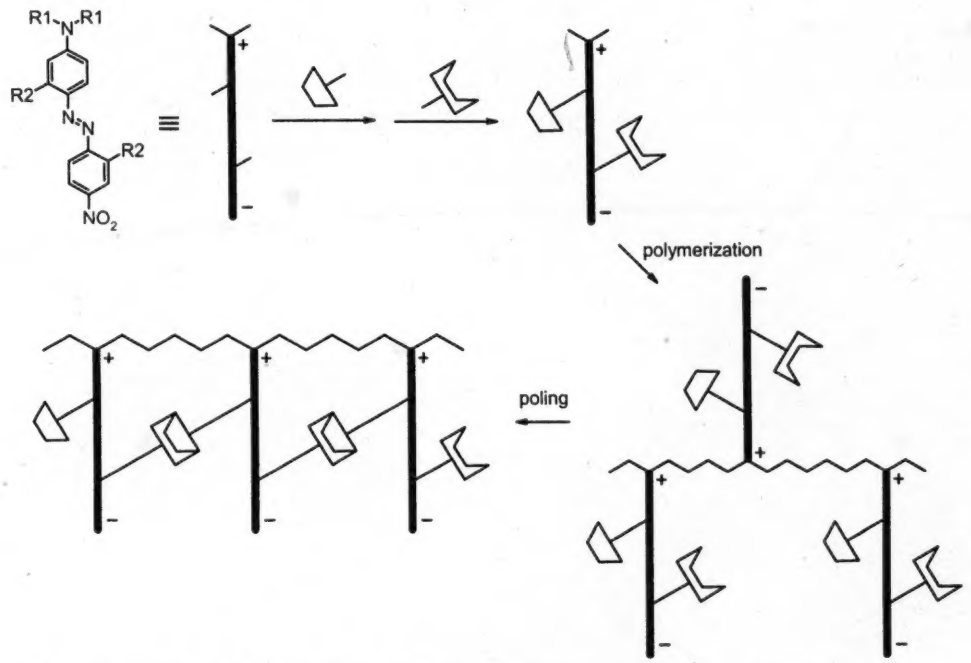

Figure 27. Schematic of primary research goal. Hydrogen-bonding interactions resist electrostatically-driven relaxation to a centrosymmetric arrangement

development of H-bonding complexes with very high association constants, this guided the major focus of the research presented in this thesis towards the integration of a known, reliable NLO chromophore and a strongly-associating H-bonding motif into a polymeric system. This goal is expressed schematically in Figure 27. Briefly, an appropriate polymer backbone carries pendant NLO chromophores, which are further functionalized with electronically separate H-bonding groups. When the polymer is poled, the dipolar chromophores will align with the poling field, bringing the H-bonding

moieties into close proximity. When the poling field is removed, the strong association between the H-bonding groups should stabilize the material against long-term degradation of its NLO response. The specific target **9** is illustrated in Figure 28, and incorporates the known 4-dialkylamino-4′-nitroazobenzene chromophore, two instances of the self-complementary ureidopyrimidone motif, attached to the chromophore with flexible ethylene spacers, and polymerization potential through appropriate functionality at the dialkylamino terminus. The azobenzene chromophore was chosen for its relative ease of synthesis, as well as for its known NLO behavior.[43] Ethylene spacers were

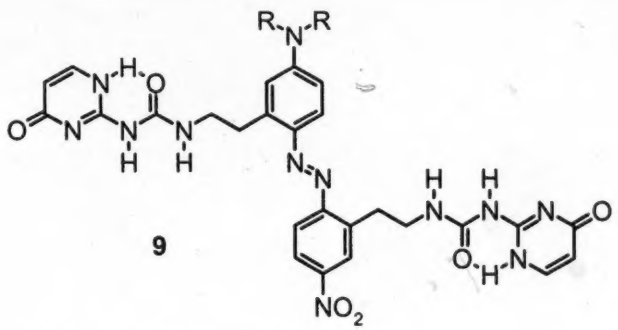

9

Figure 28. Specific synthetic target **9**

chosen to attach the ureidopyrimidone moieties based on preliminary molecular modeling studies, to provide sufficient flexibility to allow optimal association of the ureidopyrimidones, as well as to eliminate electronic contact with the chromophore. In order to maximize control over the extent of polymerization in the material, 4-pentenyl groups were chosen as the polymerization handles, to enable acyclic diene metathesis (ADMET) via Grubbs' ruthenium catalysts.

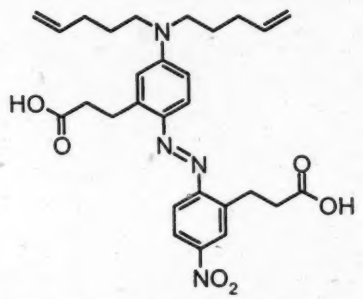

Figure 29. Key intermediate, used to optimize metathesis conditions and generate oligomeric material for NLO studies

In order to access the target material, a synthetic method was developed and used to generate a series of azobenzene chromophores. This led to the synthesis of the key intermediate shown in Figure 29, which was used to optimize conditions for metathesis polymerization. The oligomeric material thus generated was then cast into thin films, subjected to poling conditions, and its spectroscopic and optical properties characterized and compared to those of the parent monomer.

II. RESULTS AND DISCUSSION

1. Chromophore Synthesis

The synthesis of the azobenzene chromophores in this project was primarily a two-branched convergent synthesis. Retrosynthetically, it was based on an initial cleavage of the desired N=N double bond, easily the most chemically sensitive bond in the molecule, and thus a logical candidate for inclusion at the extreme late stages of the synthesis.

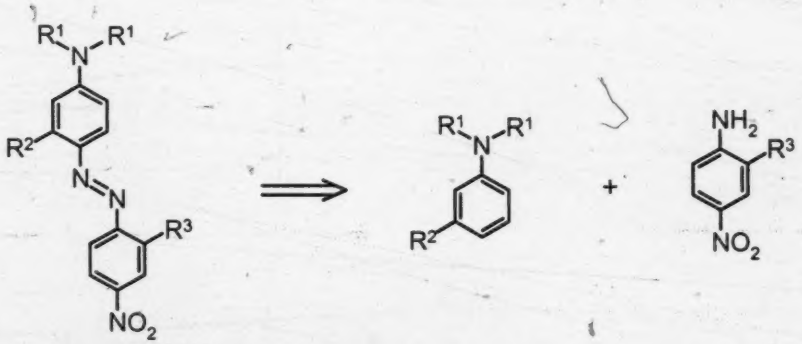

Scheme 1. Key synthons for the chromophore synthesis arise from disconnection of the N=N double bond

Disconnection at this bond yields the synthons shown in Scheme 1. The bulk of the design of the synthesis, then, was directed at generating these synthons with appropriate substitutents at the R^1, R^2 and R^3 positions. Having achieved this, the final azobenzene structure could be easily generated via well-documented azo coupling protocols.[44]

A. Nitro Terminus

The nitro terminus was completely conserved throughout the series of azobenzene chromophores that were generated. Early attempts to access the desired substitution pattern centered on 4-nitroaniline as a starting material, since it was thought that having

most of the needed functionality already in place would simplify the synthetic pathway. With this goal in mind, the route in Scheme 2 was attempted, in which 4-nitroaniline (**10**) was first converted to 3-chloropropionyl-(4-nitroanilide) (**11**) by reaction with 3-chloropropionyl chloride.[45] A Friedel-Crafts type alkylation was then attempted,[46] in

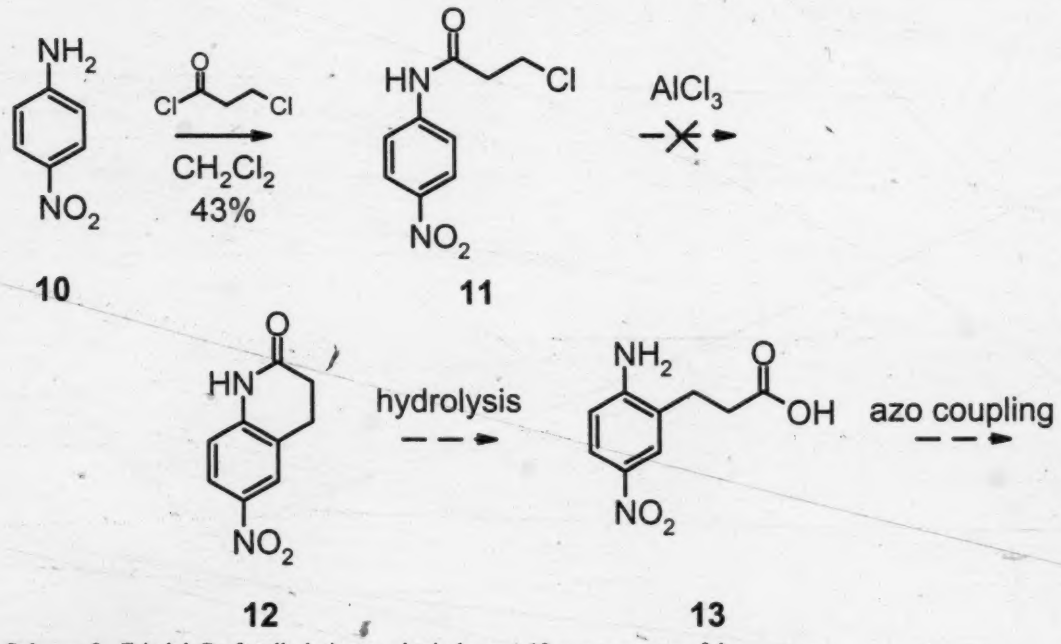

Scheme 2. Friedel-Crafts alkylation to obtain lactam **12** was unsuccessful

order to provide **12**, with the desired C-C bond at the C-2 position. Unfortunately, however, despite varying solvent, temperature, and co-catalysts, the desired alkylation was unsuccessful, and a new approach was developed (Scheme 3).

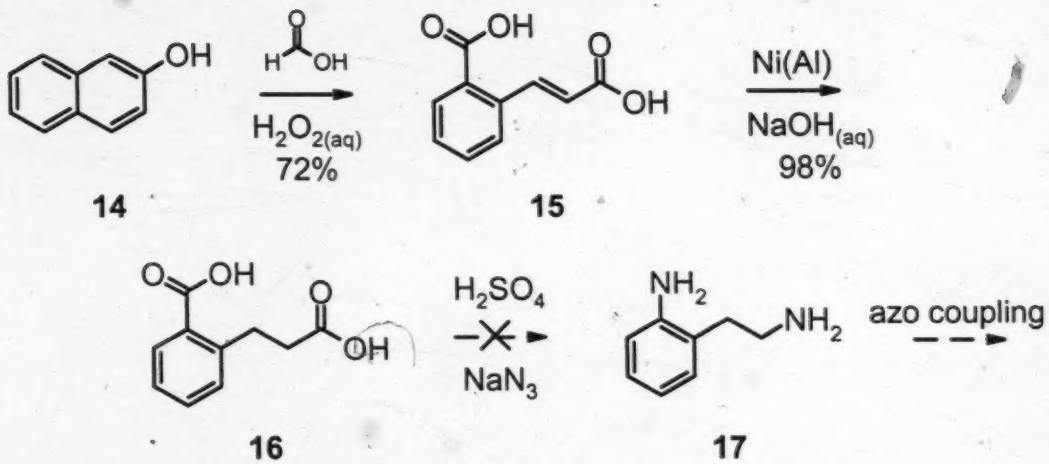

Scheme 3. The attempted double Curtius rearrangement/Schmidt reaction of **16** led to an anomalous product

Oxidation of 2-naphthol (**14**) in the presence of formic acid and aqueous hydrogen peroxide yielded 2-carboxy-*trans*-cinnamic acid (**15**).[47] Reduction of the double bond with Raney nickel gave 3-(2-carboxyphenyl)propionic acid (**16**),[48] from which it was hoped that the corresponding diamine **17** could be generated via a double Schmidt reaction/Curtius rearrangement.[49] The only product isolated from this reaction, however, did not show a sufficient number of amine hydrogens in the ^{1}H NMR spectrum. If the transformation had proceeded as planned, the resulting product should contain two aniline-type protons, and two primary alkyl amine protons. The ^{1}H NMR spectrum showed only a single proton not bonded to carbon. Furthermore, the chemical shift did not conform to either type of amine, but instead suggested an aromatic amide. It was thought that one of the acid groups had undergone the desired transformation to an amine much more quickly than the other, and that under the strongly acidic reaction conditions,

it had formed a lactam via reaction with the remaining acid group. This premise was confirmed by mass spectrometry and FTIR analysis, and the lactam was identified as 3,4-

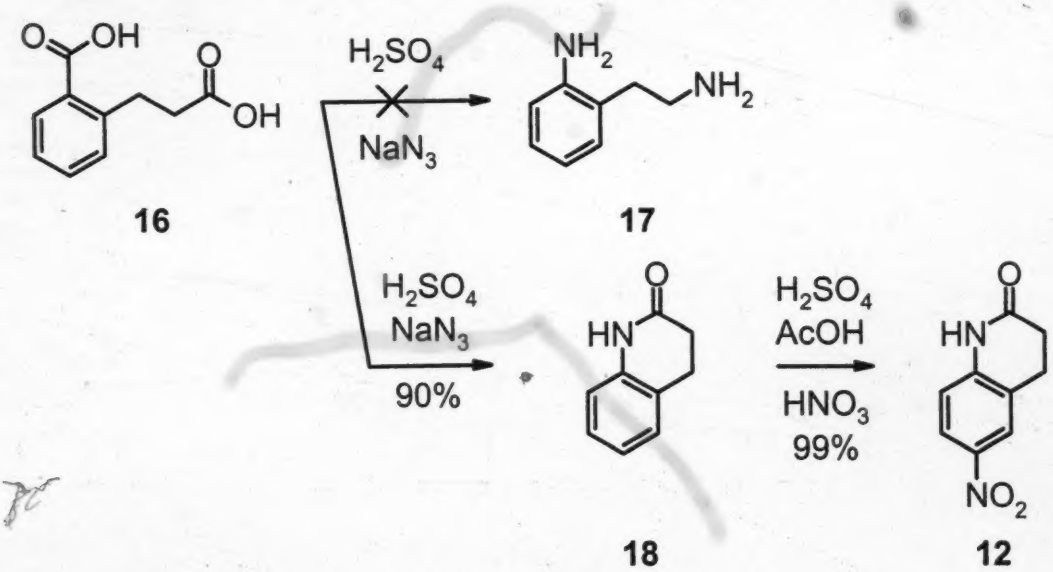

Scheme 4. Identification of the anomalous product resulted in a new route to lactam **12**

dihydro-2(1*H*)-quinolinone (**18**) (Scheme 4). This lactam was easily converted to 3,4-dihydro-6-nitro-2(1*H*)-quinolinone (**12**), the desired product in the earlier synthesis (Scheme 2), using standard nitration conditions.[50]

Resuming the earlier synthesis (Scheme 2) with the newly-acquired intermediate, reaction of **12** under basic hydrolysis conditions[51] afforded a highly-colored solid that was assumed to correspond to the sodium carboxylate salt of **13** (**Na-13**). Several attempts to isolate the free acid by careful neutralization yielded only starting material, presumably due to rapid re-cyclization of the amino acid. Mass spectrometry and ^{1}H NMR spectroscopic analysis in D_2O, however, indicated that the basic solution did, in fact, contain **Na-13**. It was believed that this compound would give satisfactory results in an azo coupling, so the solution was concentrated and dried under vacuum, and the

resulting solid carried on without further purification. All azo couplings carried out in this project used this carboxylate salt as the key precursor, under similar conditions.[40] A detailed description of the chromophores thus generated appears later in this chapter.

B. Amino Terminus

Given the simpler substitution pattern of the synthon for the amino terminus, it was anticipated that its synthesis would be relatively simple. The initial conception of this portion of the synthesis involved 3-bromoaniline (**19**) as a starting material (Scheme 5). 3-Bromoaniline was dimethylated in the presence of phosphorus pentoxide to yield *N,N*-dimethyl-3-bromoaniline (**20**).[52] Unfortunately, this product was almost completely

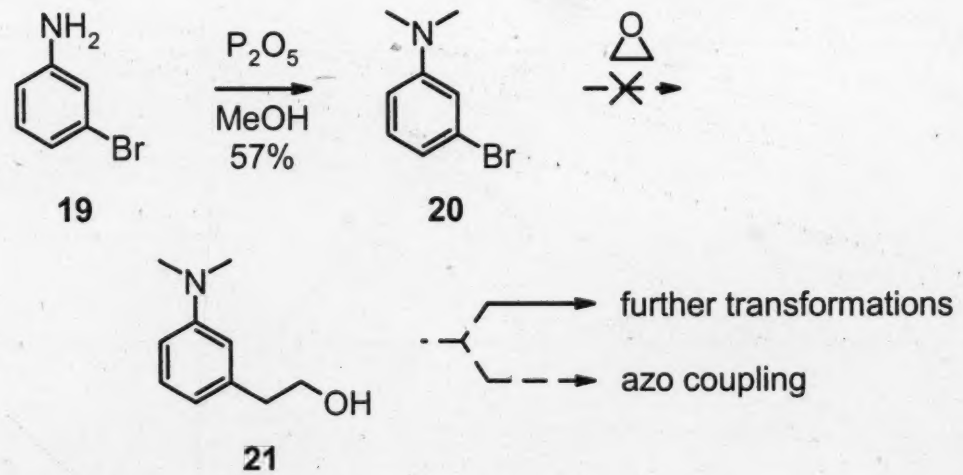

Scheme 5. Aryl bromide **20** proved unreactive to substitution

unreactive toward substitution at the C-3 position, so a revised synthesis was proposed (Scheme 6). 3-Toluidine (**22**) was dimethylated in trimethylphosphate at reflux to obtain *N,N*-dimethyl-3-toluidine (**23**).[53] Bromination at the benzylic position was then

attempted via photochemical methods,[54] but the reaction yielded a complex mixture of products that could not be resolved.

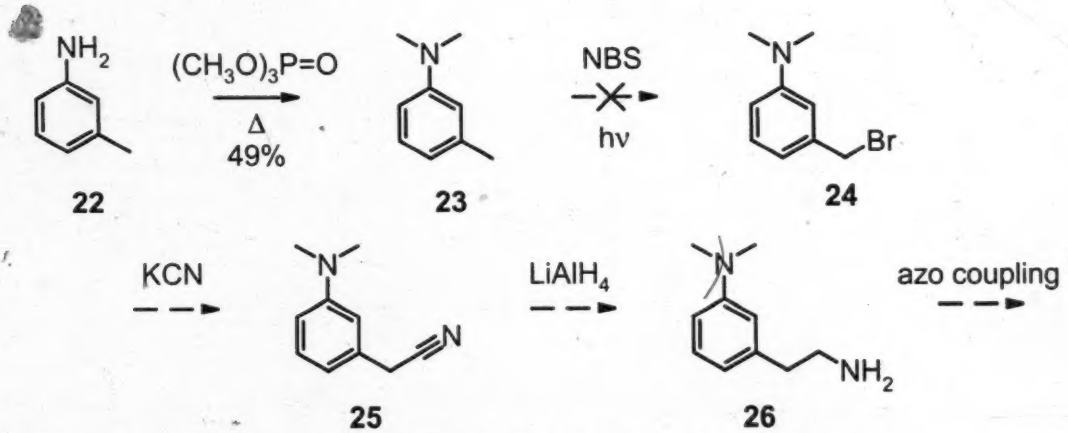

Scheme 6. Attempts at benzylic bromination of toluidine **23** did not yield useful products

B.1 Amine Series

It was thought at this point that the difficulties encountered thus far could have resulted from incompatibility between the aniline functionality and the various bromides. It had been hoped that the aniline nitrogen would be sufficiently non-nucleophilic to render this a moot point. Given the negative results described above, however, a new approach was proposed that ensured that the two functionalities had no opportunity to interact (Scheme 7). 3-Nitrotoluene (**27**) was brominated under photochemical conditions[51] to yield 3-nitrobenzyl bromide (**28**). Nucleophilic substitution using aqueous potassium cyanide afforded (3-nitrophenyl)acetonitrile (**29**),[55] which was reduced to (3-aminophenyl)-acetonitrile (**30**) via catalytic hydrogenation by palladium on

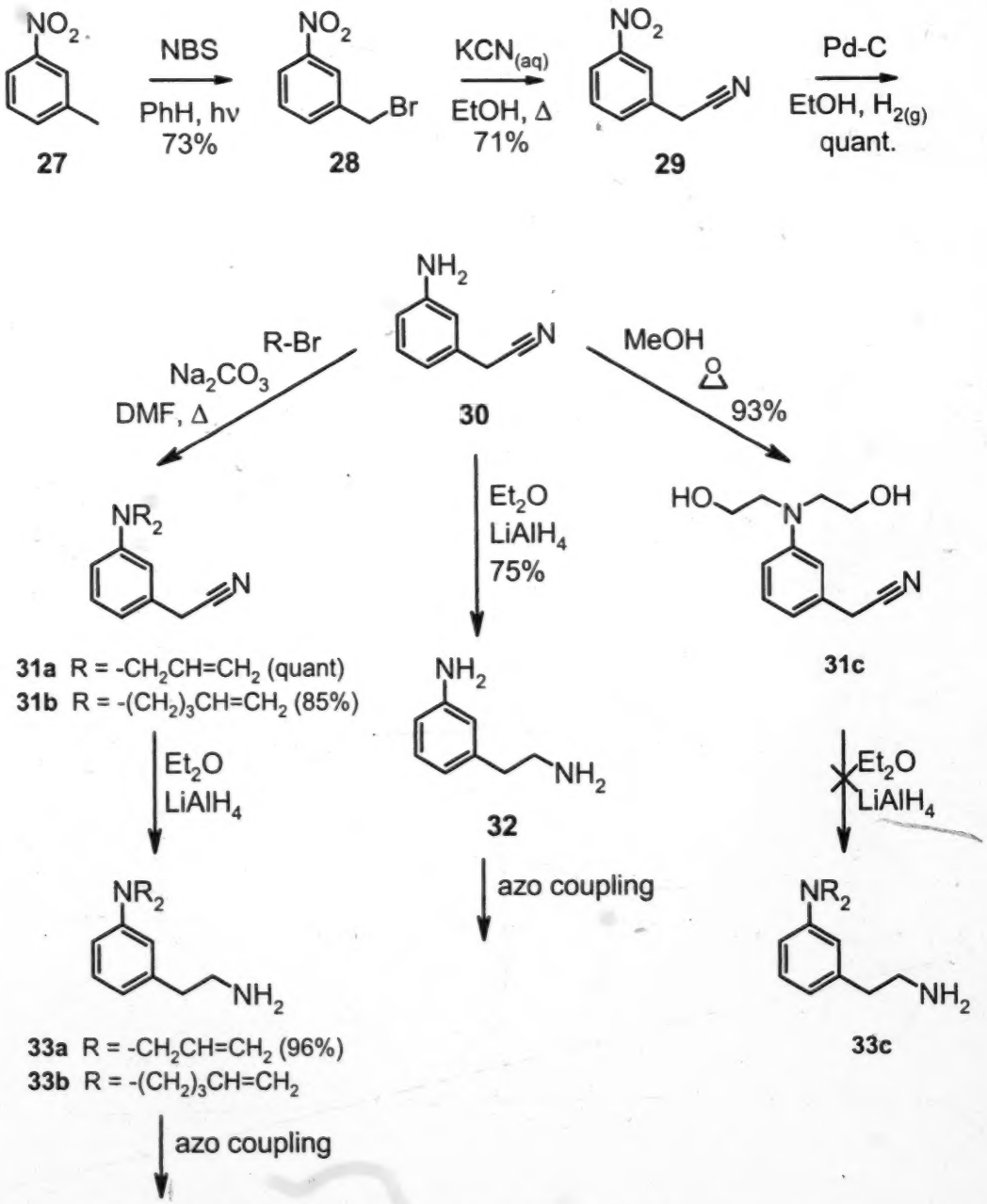

Scheme 7. Synthesis of the amine series for the amino terminus of the chromophore

carbon.[56] This compound was converted to the *N,N*-diallyl- and *N,N*-bis(4-pentenyl)aniline derivatives (**31a,b**) by reaction with two equivalents each of the

corresponding bromides,[57] and to the *N,N*-bis(2-hydroxyethyl)aniline derivative (**31c**) by reaction with an excess of ethylene oxide.[58] Also generated was *N,N*-diallyl-3-toluidine (**34**), as a test compound for the dialkylation reactions (Scheme 8). The alkylated derivative **31a** and the free aniline **30** were then reduced with lithium aluminum hydride[59] to yield the corresponding amines (**32**, **33a**). These amines were carried on to the azo coupling step. The reductions of **31b** and **31c** yielded complex mixtures of products, but the reaction conditions were not optimized, as the amine series was being replaced by the acid series described in the section below.

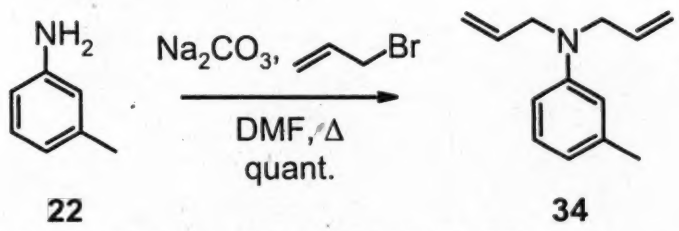

Scheme 8. Preparation of *N,N*-diallyl-3-toluidine (**34**)

B.2 Acid Series

Following the success of the amine series detailed above, it was recognized that the long-term goal of incorporating a ureidopyrimidone motif into the chromophore structure would be more easily realized if both functionalized alkyl chains contained the same functional group. Furthermore, an acid group would be more directly useful than a primary amine, due to the established method of generating the ureidopyrimidone moiety,[39] as well as the inherent restrictions imposed by the synthesis of the nitro terminus of the chromophore. As a result, the synthesis of a new series was pursued, based on the synthesis of the amine series, whereby the primary amine in the end products was replaced by a carboxylic acid (Scheme 9).

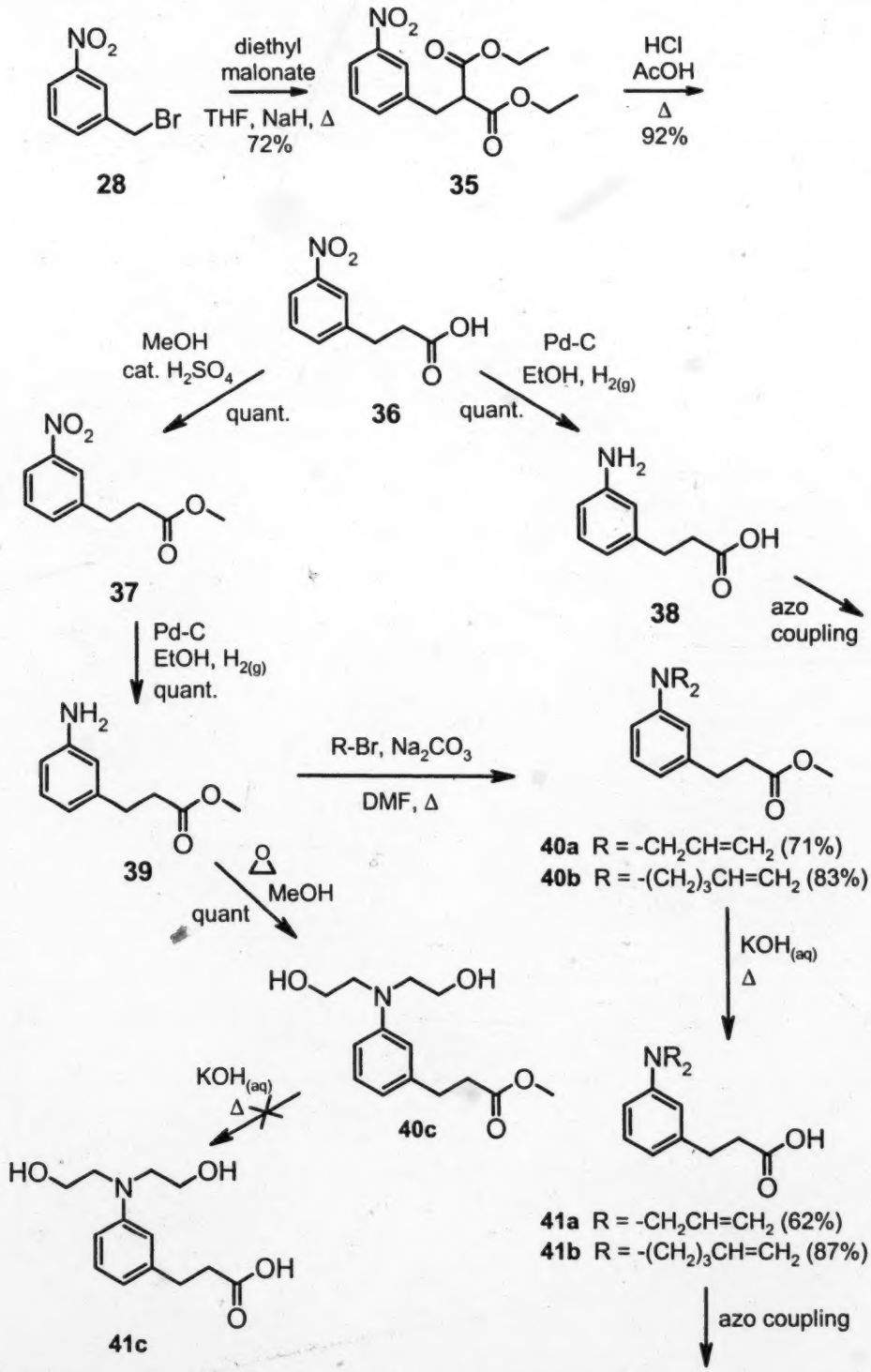

Scheme 9. Synthesis of the carboxylic acid series for the amino terminus of the chromophore

Starting from 3-nitrobenzyl bromide (**28**), reaction with diethyl malonate and sodium hydride afforded 2-(3-nitrobenzyl)malonic acid diethyl ester (**35**).[60] Acid hydrolysis and partial decarboxylation yielded 3-(3-nitrophenyl)propionic acid (**36**),[61] which was protected as the methyl ester to give methyl 3-(3-nitrophenyl)propionate (**37**).[62] The propionic acid derivative **36** and the methyl ester **35** could both be reduced by palladium on carbon to yield 3-(3-aminophenyl)-propionic acid (**38**) and methyl 3-(3-aminophenyl)propionate (**39**), respectively.[53] Compound **38** was carried on without further modification to an azo coupling reaction. Alkylation of **39** as in the amine series (see **31a-c**) yielded the *N,N*-diallyl-, *N,N*-bis(4-pentenyl)- and *N,N*-bis(2-hydroxyethyl)aniline derivatives **40a-c**. Finally, hydrolysis of the methyl esters **40a** and **40b** under basic conditions[48] yielded the free acids **41a** and **41b**, which were also subsequently used in azo coupling reactions, as was the ester **40c**. Hydrolysis of **40c** in an attempt to access the free acid resulted in a complex mixture of products, which could not be resolved easily.

C. Azo Coupling

All of the azobenzene chromophores in this project were generated using the same general reaction,[40] differing only in the work up procedure due to variations in solubility of the products. The results of these coupling reactions are summarized in Schemes 10 and 11. Generally, **Na-13** was diazotized using aqueous sulfuric acid and sodium nitrite in the presence of a trace of pyridine. The resulting diazonium salt solution was neutralized with urea and filtered. The appropriate aniline, dissolved in a minimal amount of pyridine, was then added to the filtrate. The reaction started immediately and visibly in all cases, with the mixture of the two yellow solutions instantly developing a

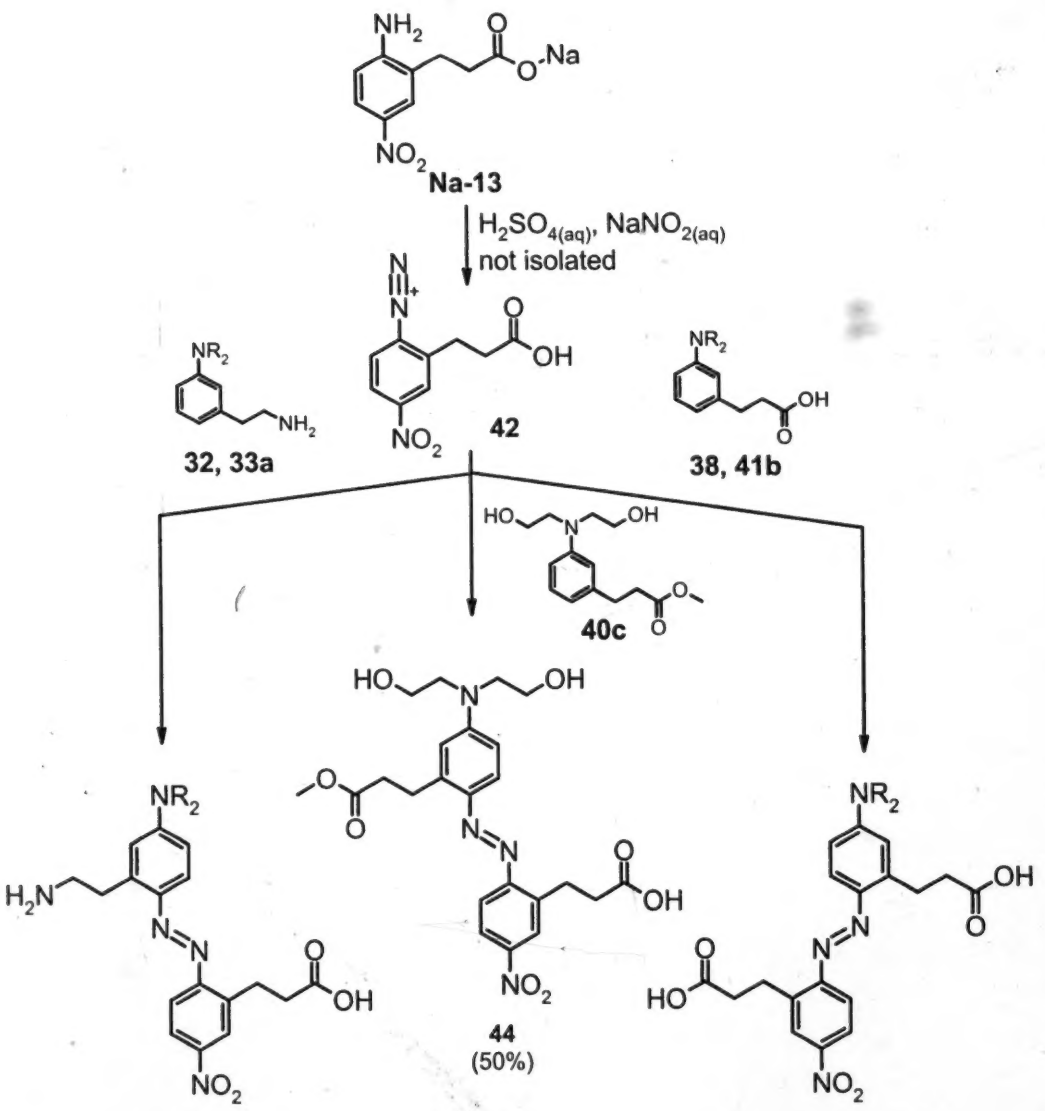

Scheme 10. Synthesis of the chromophores via azo coupling reactions

pink to deep red-purple color, which continued to develop over time. After allowing the mixture to sit for a time ranging from 10 minutes to 16 hours, a work up procedure appropriate to the solubility characteristics of the generated chromophore was applied.

The desired compounds (**43a,b**, **44**, **45a,b**, **46a,b**) were isolated via differential solubility, typically with a purity of >95% by ^{1}H NMR spectral analysis, in yields ranging from 25% to 75%.

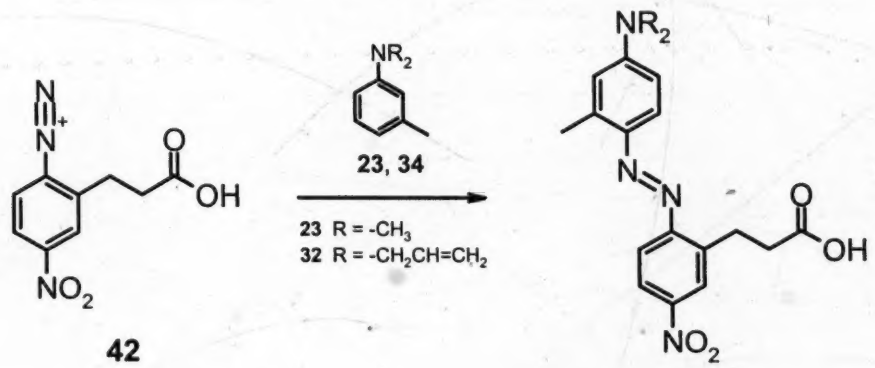

Scheme 11. Synthesis of related chromophores, lacking one functionalized alkyl chain

2. Metathesis Oligomerization

A variety of polymerization methods were considered for the incorporation of the azobenzene chromophores into a polymer matrix, but ultimately it was decided that acyclic diene metathesis (ADMET) polymerization via Grubbs-type catalysis offered the greatest potential for control over chain length, mildness of reaction conditions, and experimental simplicity.

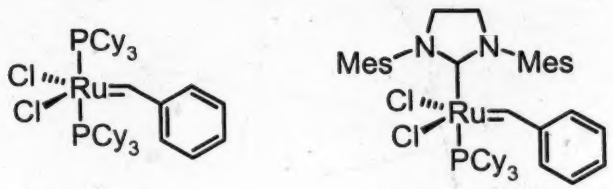

47 **48**

Cy = cyclohexyl
Mes = 2,4,6-trimethylphenyl

Scheme 12. Structures of the ruthenium catalysts used for ADMET oligomerization

A recent review[63] gives an excellent account of current trends in ruthenium metathesis catalysts, particularly those incorporating *N*-heterocyclic carbene ligands. Initial attempts involving the so-called first-generation Grubbs' catalyst, bis(tricyclohexylphosphine)benzylidene ruthenium(IV) dichloride (**47**, Scheme 12), were largely unsuccessful, since the monomer was only sparingly soluble in solvents such as dichloromethane, which are considered ideal for metathesis reactions involving dialkenylanilines.[64] Conversely, solvents in which the monomer was much more soluble, such as ethyl acetate or acetone, tended to deactivate the catalyst, presumably through coordination to ruthenium. A compromise was arrived at in the form of aromatic solvents, specifically benzene, in which the monomer was somewhat more soluble, and the catalyst was not adversely affected. However, even under these conditions, the chain lengths attained were not deemed useful, as the products consisted primarily of dimers and trimers.

Attention then shifted to the second-generation Grubbs' catalyst, tricyclohexylphosphine[1,3-bis(2,4,6-trimethylphenyl)-4,5-dihydroimidazol-2-

ylidene][benzylidene]ruthenium (IV) dichloride (**48**, Scheme 12), which is known to have higher activity, especially in combination with elevated temperatures.[65]

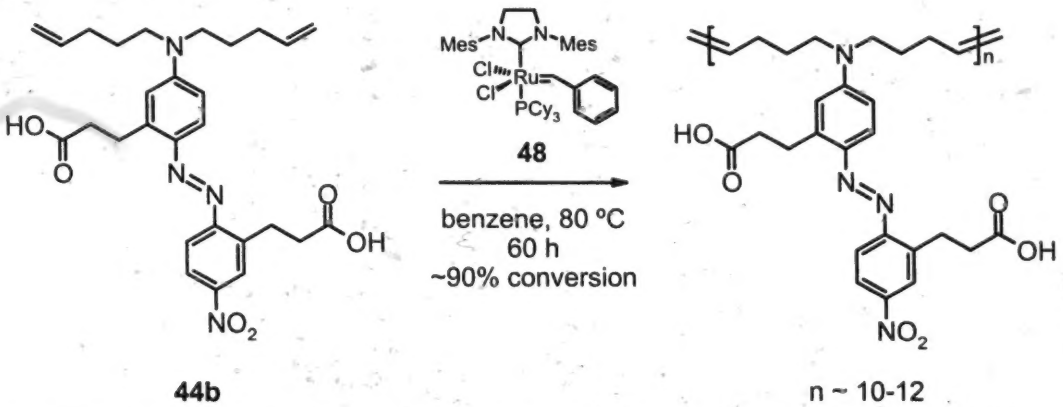

44b n ~ 10-12

Scheme 13. ADMET oligomerization yielded chain lengths of 10-12 repeat units, suitable for preparation of thin films

Application of catalyst **48** under similar conditions to the first-generation attempts yielded much more promising results, and further optimization led to the reliable generation of oligomers in the range of 10-12 repeat units (Scheme 13), as determined by ^{1}H NMR spectroscopy and MALDI MS. Isolation of the oligomeric materials consisted primarily of removing the reaction solvent (typically benzene) under high vacuum, dissolving the residue in freshly-distilled THF, and once more removing the solvent under high vacuum to obtain an easily-handled solid.

3. Properties of the Azobenzene Chromophore Series

A. UV-Vis Spectroscopy and pH

The electronic properties of the azobenzene chromophore series were probed via UV-Vis spectroscopy, and encompass a wide range of absorption characteristics. Table I shows a comparison of the chromophores in a common solvent. Methanol was chosen so as to allow a comparison of all of the chromophores at similar concentrations, while minimizing absorption bands from the solvent itself. The spectra were in all cases dominated by the π–π^* transition, found at or near 475 nm. The values obtained for λ_{max} show a variation of over 30 nm, based exclusively on structural variation. One of the most notable differences is that induced by the replacement of the free $-NH_2$ of the aniline with a dialkylated amine. Comparison of compounds **45a** and **45b** reveals a 14 nm bathochromic shift with the addition of alkyl groups, while a similar comparison between **43a** and **43b** reveals a bathochromic shift of 76 nm. A somewhat smaller influence was noted as a result of extending the alkyl chains on the amino terminus (**46a** to **46b**, 5 nm hypsochromic shift).

Table I - Absorption Characteristics of the Azobenzene Series in Methanol at r.t.

Compound	λ_{max} /nm	ε /L·mol^{-1}·cm^{-1}
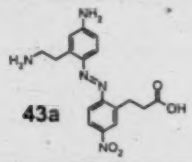 **43a**	392	21700
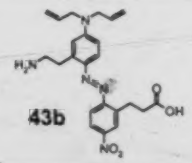 **43b**	468	21000
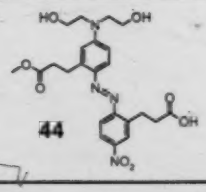 **44**	481	29600
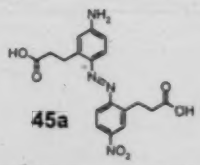 **45a**	485	28700
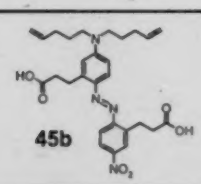 **45b**	499	34800
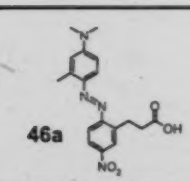 **46a**	479	27200
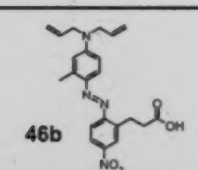 **46b**	474	34000

The rather substantial difference between the characteristic absorption of **43a** as opposed to the rest of the series is thought to be the result of a conformational change induced by intramolecular self-association of the amine and acid groups. This

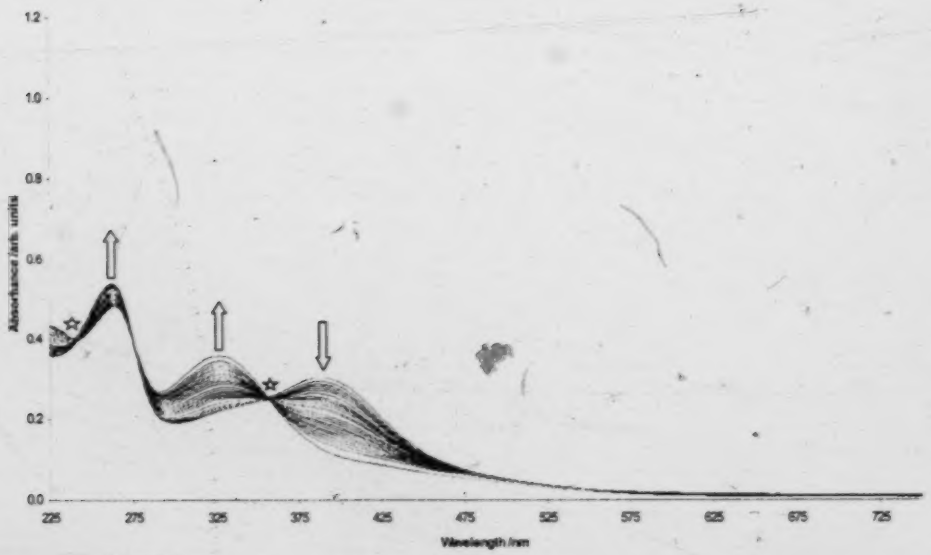

Figure 31. Titration of **43a** with ~ 5 M aqueous hydrochloric acid, pH 10–2. Isosbestic points indicated by (*)

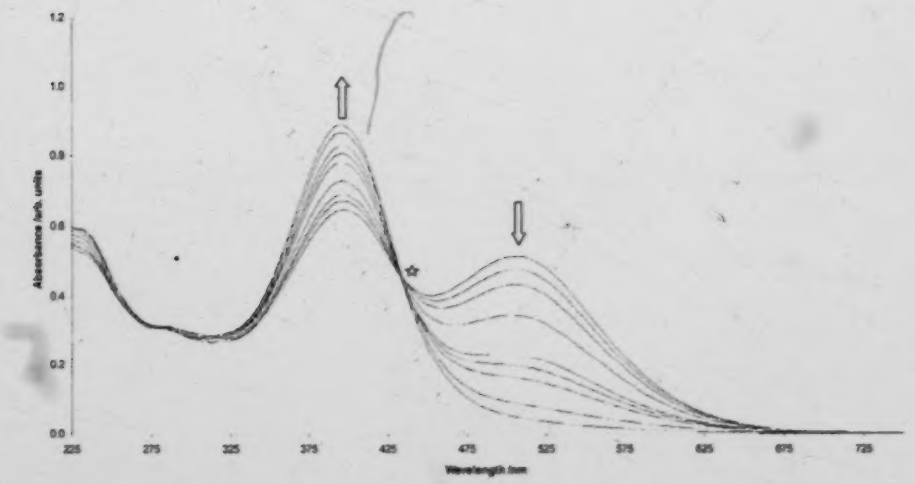

Figure 30. Titration of **43a** with ~ 5 M hydrochloric acid, pH 12-10. Isosbestic point indicated by (*)

association would force the central chromophore out of planarity, reducing the effective conjugation length, and thus shifting λ_{max} to much lower wavelengths. It was recognized that this process would be dynamic, and pH-dependent, and so studies were made of the effect of pH on the absorption characteristics of the chromophore. The results of this study are shown in Figures 30 and 31. The graphs are extracted from a single titration, beginning with a ~ 50 μM solution of **43a** in 12 M aqueous sodium hydroxide, followed by microliter-scale additions of ~ 5 M aqueous hydrochloric acid. The first graph (Figure 30) illustrates results over a pH range of 10 to 2, while the second (Figure 31)

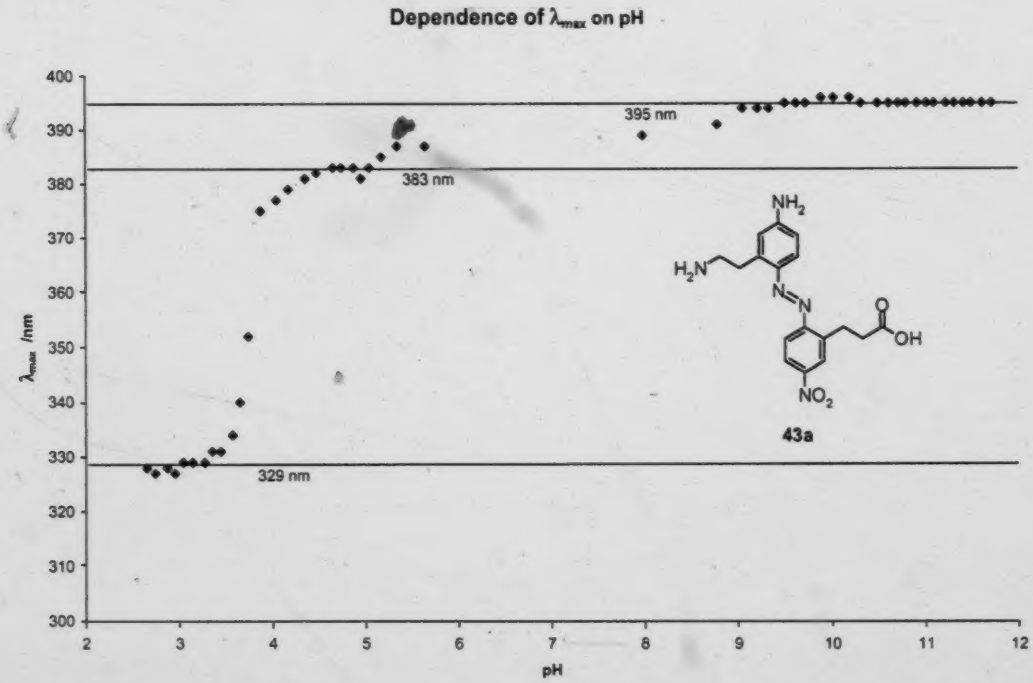

Figure 32. Three distinct absorption bands between 300 and 400 nm can be seen as a function of pH

covers a pH range of 12-10. In each case, there are clear isosbestic points, indicating that the observed change in absorption is due to a conversion between clearly-defined species in solution. Thus, over a pH range of 2–12, there exist at least four distinct protonation

states of the chromophore. However, it is possible that the state corresponding to intermediate pH values actually consists of an equilibrium between two states with very similar UV-Vis absorption characteristics. This is supported by a comparison of the wavelengths associated with the pH changes through this region, as illustrated in Figure 32. As a result, the overall picture of the protonation states involved across a pH range of 2–12 may be summarized as in Figure 33. At high pH, the chromophore exists as the primary amine at both the alkyl and aromatic positions, and as the carboxylate anion at the other alkyl side chain. In this state, there is minimal association between the amine and carboxylate, and the chromophore is free to adopt the preferred planar conformation, with λ_{max} of 505 nm.

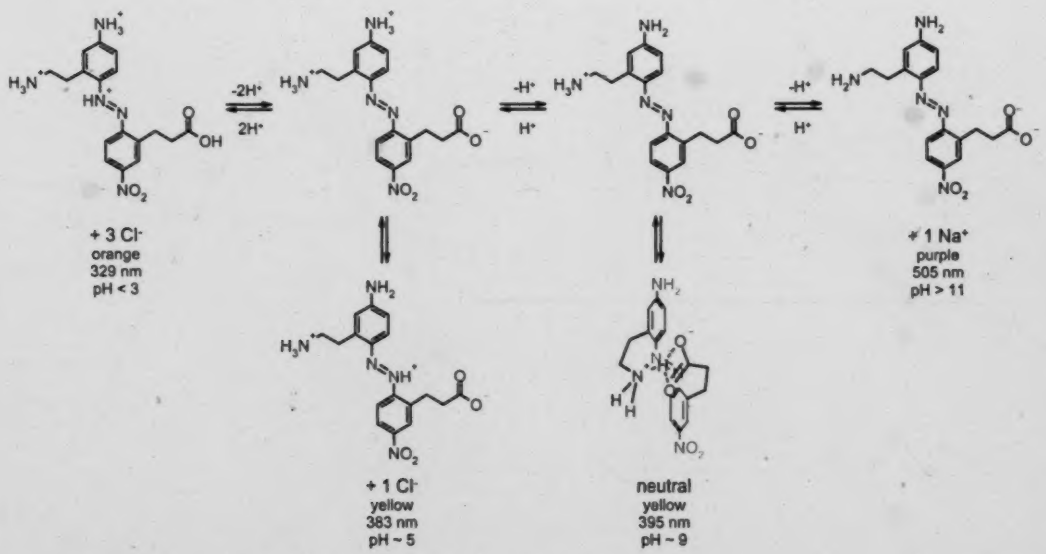

Figure 33. Proposed protonation states of **43a** from pH 2–12.

Upon moving to more moderate pH, around 9, the alkyl amine becomes protonated, generating a zwitterionic species that can form a strong intramolecular self-association complex. The formation of this complex requires a small conformational twist of the

chromophore, but one that is apparently sufficient to diminish conjugation between the two rings. As a result, λ_{max} shifts to 395 nm, consistent with a reduction in the effective conjugation length. A move to lower pH (~ 5) results in another protonation, this time of the chromophore itself, resulting in an equilibrium of the two net singly-charged tautomers shown.[66] Finally, moving to strongly acidic pH (< 3) results in another protonation of the chromophore, yielding the highly-charged species indicated, a still more shortened conjugation length, and a new absorption peak at 329 nm.

B. Nuclear Magnetic Resonance Spectroscopy

B.1 ^{13}C NMR Chemical Shifts

Further support for the proposed "twisted" conformation of **43a** at neutral pH is provided by its NMR spectroscopic data, obtained in CD_3OD. Relative to the other chromophores in the series, possessing similar substitution patterns on the azobenzene core, the chemical shifts in both the ^{13}C NMR spectra of **43a**, and to a lesser extent **45a**, show significant variations from the other members of the series. Table II contains the ^{13}C chemical shift data for the aromatic carbons of the chromophore series, numbered according to the scheme shown, with the notable variations shaded. Generally, the resonances of tertiary carbons are shifted upfield relative to those of the other chromophores, while the resonances of quaternary carbons are shifted downfield. Also, these resonance shifts significantly exceed the average variance among the other chromophores. These variations are consistent with a large change in the electron density on the aromatic rings, an effect to be expected with the modification of the "push-pull" system generated by electronic communication between the amino and nitro

termini. The effect can be seen much more clearly through a comparison among structurally similar azobenzene derivatives and monocyclic fragments, as summarized in

Table II - ^{13}C Chemical Shifts of the Chromophore Series As Measured at r.t.

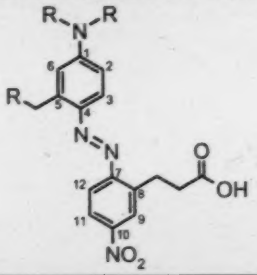

Solvent	CD_3OD	DMSO-d_6	acetone-d_6	DMSO-d_6	acetone-d_6	DMSO-d_6	acetone-d_6
Position	**43a**	**43b**	**44**	**45a**	**45b**	**46a**	**46b**
1	130.3	152.3	153.5	154.4	153.0	153.4	153.4
2	117.3	111.8	112.1	115.2	111.6	110.5	111.7
3	119.2	122.4	123.4	125.6	123.4	116.3	117.3
4	141.0	141.6	146.2	144.7	142.2	141.8	143.5_5
5	117.7	140.1	141.1	141.6	146.7	142.4	143.6_0
6	123.6	112.5	113.0	122.9	112.6	112.4	113.7
7	135.1	154.2	155.6	154.6	155.7	154.3	155.6
8	117.0	141.4	142.4	142.5	148.0	139.6	141.0
9	127.0	117.7	118.6	123.6	118.8	125.5	126.6
10	145.4	146.7	147.8	149.6	141.0	146.4	148.0
11	126.9	116.6	117.2	123.5	117.2	122.6	123.3
12	130.7	125.7	126.6	129.5	126.6	117.5	118.6

Table III. The azobenzene derivatives include 4-dimethylamino-4′-nitroazobenzene (DANAB), 4-amino-4′-nitroazobenzene (ANAB) and 4-aminoazobenzene (AAB). The monocyclic fragments include aniline (An), *p*-phenylenediamine (*p*PDA), nitrobenzene

(NB) and *p*-nitroaniline (*p*NA). Figure 34 illustrates each of these reference compounds. Structurally, compounds **43a** and **45a** most closely resemble ANAB, while **43b** and **45b**

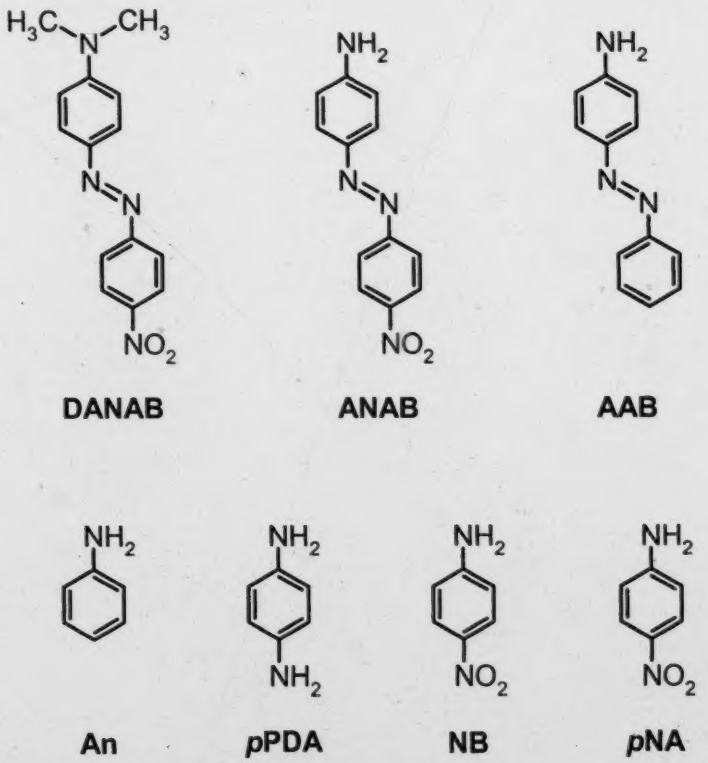

Figure 34. Structures of the azobenzene derivatives (top row) and monocyclic fragments (bottom row)

most closely resemble DANAB, neglecting the alkyl side chains attached to the ring. Thus, it could be anticipated that the chemical shift data for these closely related compounds should show some similarities as well. In the case of **43b**, **45b** and DANAB, this holds true, as there is no more than about 5 ppm variation in chemical shift for a given carbon atom in the three compounds. Similarly, if one compares **45a** and ANAB, a reasonable correlation is observed, with a net variation of no more than 5 ppm, and typically no more than 3 ppm, between comparable carbon atoms in the two compounds.

Comparison of **43a** with its structural analogue, ANAB, however, reveals a striking variance of over 20 ppm in two cases, suggesting a change in the character of the system. The nature of this change can be rationalized to some extent through comparison of the individual rings to corresponding monocyclic fragments. For example, the chemical

Table III - Comparison of ^{13}C Chemical Shifts of New Chromophores, Azobenzene Reference Compounds, and Key Structural Fragments

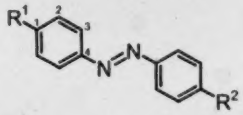

(a)

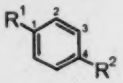

(b)

Index	R^1	R^2	$\delta(C_1)$	$\delta(C_2)$	$\delta(C_3)$	$\delta(C_4)$
43a	NH_2	NO_2	130.3	117.3	119.2	141.0
43b	NR_2	NO_2	152.3	111.8	122.4	141.6
45a	NH_2	NO_2	154.4	115.2	125.6	144.7
45b	NR_2	NO_2	153.0	111.6	123.4	142.2
DANAB	NMe_2	NO_2	153.3	111.4	124.6	143.7
ANAB	NH_2	NO_2	156.1	113.3	122.2	141.0
AAB	NH_2	H	149.7	114.5	125.1	145.4
An	NH_2	H	146.5	115.1	129.3	118.4
*p*PDA	NH_2	NH_2	138.6	116.7	116.7	138.6

shift data for the amino ring of **43a** compares excellently with that for *p*-phenylenediamine (*p*PDA), while the data for the nitro ring compares still more favorably with that for nitrobenzene (NB). Effectively, then, the electronic distribution in **43a** is more consistent with two electronically isolated ring systems, rather than with the linearly-conjugated "push-pull" system expected. These observations strongly

support the proposal that the rings have, in fact, been electronically separated via a loss of planarity in the chromophore, as suggested by the UV-Vis spectroscopic data presented earlier.

Table III (cont'd) - Comparison of ^{13}C Chemical Shifts of New Chromophores, Azobenzene Reference Compounds, and Key Structural Fragments

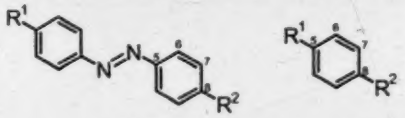

(a) (b)

Index	R^1	R^2	$\delta(C_5)$	$\delta(C_6)$	$\delta(C_7)$	$\delta(C_8)$
43a	NH_2	NO_2	135.1	130.7	126.9	145.4
43b	NR_2	NO_2	154.2	125.7	116.6	146.7
45a	NH_2	NO_2	154.6	129.5	123.5	149.6
45b	NR_2	NO_2	155.7	126.6	117.2	141.0
DANAB	NMe_2	NO_2	156.8	122.6	126.0	147.4
ANAB	NH_2	NO_2	154.4	126.1	124.7	146.7
AAB	NH_2	H	153.0	122.3	129.0	129.8
NB	H	NO_2	134.7	129.4	123.5	148.3
*p*NA	NH_2	NO_2	155.6	112.4	126.3	135.8

B.2 ^1H NMR Chemical Shifts

The effects in the ^{13}C NMR spectra described above are reflected to a lesser extent in the ^1H NMR spectra for the same compounds. Table IV contains the ^1H chemical shift data for the aromatic protons indicated, as well as for the methylene protons common to all the compounds in the series. Again, notable variations are shaded gray.

It can be seen from these data that the aromatic protons are most strongly affected by the change in the electronic communication within the molecule, as might be expected.

Table IV - ^{1}H Chemical Shifts of the Chromophore Series As Measured at r.t.

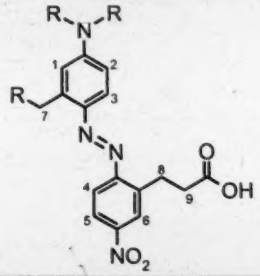

Solvent	CD_3OD	CD_3OD	acetone-d_6	DMSO-d_6	acetone-d_6	acetone-d_6	acetone-d_6
Position	**43a**	**43b**	**44**	**45a**	**45b**	**46a**	**46b**
1	7.09	6.71	6.84	7.05	6.82	6.71_8	6.73
2	7.35	6.75	6.79	7.30	6.74	6.71_7	6.69
3	7.36	7.81	7.80	7.36	7.84	7.82	7.77
4	7.69	7.70	7.78	7.77	7.81	7.80	7.77
5	8.05	8.08	8.14	8.10	8.15	8.16	8.14
6	8.16	8.26	8.30	8.16	8.32	8.32	8.30
7	3.13	3.23	3.42	2.85	3.44	2.72	2.68
8	2.96	3.42	3.48	3.12	3.50	3.50	3.48
9	2.52	2.62	2.77	2.59	2.80	2.79	2.78

Of these, the protons attached to the amino terminus are the most notably affected, with shifts of at least 0.25 and 0.56 ppm downfield for the *ortho* protons at C_1 and C_2, respectively, and 0.47 ppm upfield for the *meta* proton at C_3. The corresponding resonances on the nitro terminus show much less significant changes, specifically 0.10, 0.03 and 0.08 ppm upfield for the protons at C_4, C_5 and C_6, respectively. These

observations are consistent with the proposed twisted conformation, as such a twist would cause an alteration in the effective substitution pattern of each of the azobenzene rings. Neglecting the alkyl side chain, the ring at the amino terminus represents a "push-pull" system if there are no disruptions of planarity, consisting of an amine electron-donating group *para* to a *p*-nitrophenylazene electron-withdrawing group. The resulting chemical shifts resemble those found in nitrobenzene, as seen in the "normal" elements of the series. After the proposed conformational change, the two rings are no longer in electronic contact, and the chemical shifts on the amine ring return to values more characteristic of an isolated aniline moiety. This effect is particularly noticeable in the chemical shift of the proton on C_3, which changes from ~ 7.80 ppm in the "normal" chromophores (compared to 8.19 for nitrobenzene) to 7.36 ppm in **43a** (compared to ~ 7.1 ppm in aniline derivatives). By contrast, the nitro terminus experiences almost no such change, reflected in the small associated changes in chemical shifts for the corresponding aromatic protons. This is consistent with the apparent nature of the nitro ring in **43a**, as suggested by the ^{13}C NMR chemical shift data, which indicate a nitrobenzene-like moiety. For example, the loss of planarity in the chromophore would be anticipated to yield a change at C_4 from ~ 7.9 ppm to ~ 7.5 ppm, based on chemical shifts of the structural analogues, ANAB and NB. The actual change, based on a comparison of **43a** and **45a**, is from 7.77 to 7.69.

The methylene protons at C_7, C_8 and C_9 also show significant changes in chemical shift across the series. For protons at C_7, such alterations are virtually indistinguishable from the changes expected from variation of the functional groups attached to the alkyl chain, and thus are not particularly diagnostic. Protons at C_8 and C_9, however, both

experience upfield shifts of 0.46 and 0.10 ppm, respectively, consistent with an alteration in either the ring anisotropy of the nitro terminus, or a change in position of these protons relative to the completely planar system. Since the aromatic protons of the nitro terminus are relatively less affected, it seems likely that most of this effect on the methylene protons is due to a restriction of free rotation via the proposed intramolecular self-association. Further evidence of this can be seen in a comparison of the splitting patterns for these protons between, for example, **43a** and compounds with no capacity for this intramolecular interaction, such as **46a** and **46b**. In the spectra for the latter two compounds, the methylene triplets are very sharp and clearly defined, with not even a suggestion of further splitting. Compound **43a**, however, shows significant peak broadening of these triplets, in some cases resolving into fine splitting, consistent with a differentiation of the individual protons via the proposed restriction of free rotation.

C. Infrared Spectroscopy

The solid state infrared spectrum for **43a** shows strong, broad absorptions extending from above 3000 cm^{-1} to about 2000 cm^{-1}, indicating the presence of the salt of a primary amine ($-NH_3^+$). Also, the carbonyl absorption appears at 1588 cm^{-1}, consistent with a carboxylate anion. This suggests that the native protonation state of **43a** corresponds to that associated with the 395 nm UV-Vis absorption, shown in Figure 33. Further evidence for this may be found in the UV-Vis spectroscopic analysis. In methanol, which would most readily dissolve this neutral state of the chromophore, the observed λ_{max} is 392 nm.

4. Properties of the Metathesis Monomer (**45b**)

The chromophore carried into metathesis polymerization reactions, **45b**, was studied in some detail with respect to its electronic properties. A strong solvatochromic effect was noted and was studied in a series of nine solvents spanning a large range of polarity and hydrogen-bonding ability. The results of this study are summarized in Table V.

Table V - Solvatochromism of Compound 45b at r.t.

Solvent	λ_{max} /nm	ε /L·mol^{-1}·cm^{-1}
Carbon Tetrachloride	453 / 470 *sh*	39500
Toluene	460 *sh* / 487	32900
Benzene	465 *sh* / 490	26600
Ethyl Acetate	494	42600
Methanol	499	34800
Tetrahydrofuran	502	47100
Acetone	505	33600
N,N-Dimethylformamide	513	27800
Dimethyl Sulfoxide	525	33400

Values for λ_{max} refer to the peak wavelength for the strongest absorption band, while the associated values for ε refer to the molar absorptivity at λ_{max}, in L·mol^{-1}·cm^{-1}. These were calculated from data fit to a Beer's Law curve across a concentration range of approximately 1 to 20 μM, with an R^2 value exceeding 0.9980 in all cases but one (CCl_4, 0.9946, due to poor solubility).

A notable feature of these UV-Vis spectra is the presence of an additional absorption band in certain solvents, such as carbon tetrachloride or toluene, perhaps due to a dynamic equilibrium between two states of the chromophore. This is attributed to

incomplete intramolecular self-association of the carboxylic acid dimer, even in mostly nonpolar solvents, as this would result in an equilibrium involving the twisted and planar conformations of the chromophore. Alternately, there could be several degrees of twist possible, depending on the strength of association in a given solvent, and the additional peak could then correspond to another twisted state. In either case, the adherence of these compounds to Beer's Law (as, for example, in Figure 35) strongly supports an intramolecular association rather than intermolecular, since intermolecular association would be expected to yield a strong concentration dependence of the absorption wavelength, which is not seen. In more polar solvents, the twisted state is suppressed.

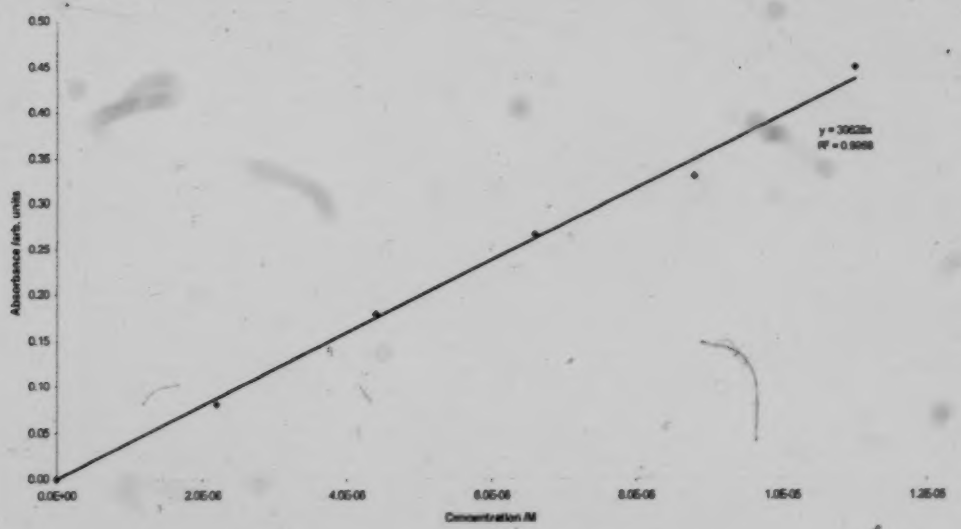

Figure 35. Representative Beer's Law curve for **45b** in carbon tetrachloride

The low energy values of λ_{max} vary by almost 55 nm across the range of solvents, a range approaching that observed in the pH studies of **43a**. This range, and particularly the values defining its extremes, suggest a correlation between solvent polarity and the conformation of the chromophore. More specifically, the value of λ_{max} in carbon

tetrachloride approaches that observed for the "twisted" conformation of the chromophore proposed previously, found in slightly acidic aqueous solution. Conversely, the λ_{max} value observed in dimethyl sulfoxide more closely matches the value observed for the completely planar chromophore seen in strongly basic aqueous solution. The observed UV-Vis spectra in carbon tetrachloride, dimethyl sulfoxide, and a number of solvents of intermediate polarity are shown in Figure 36.

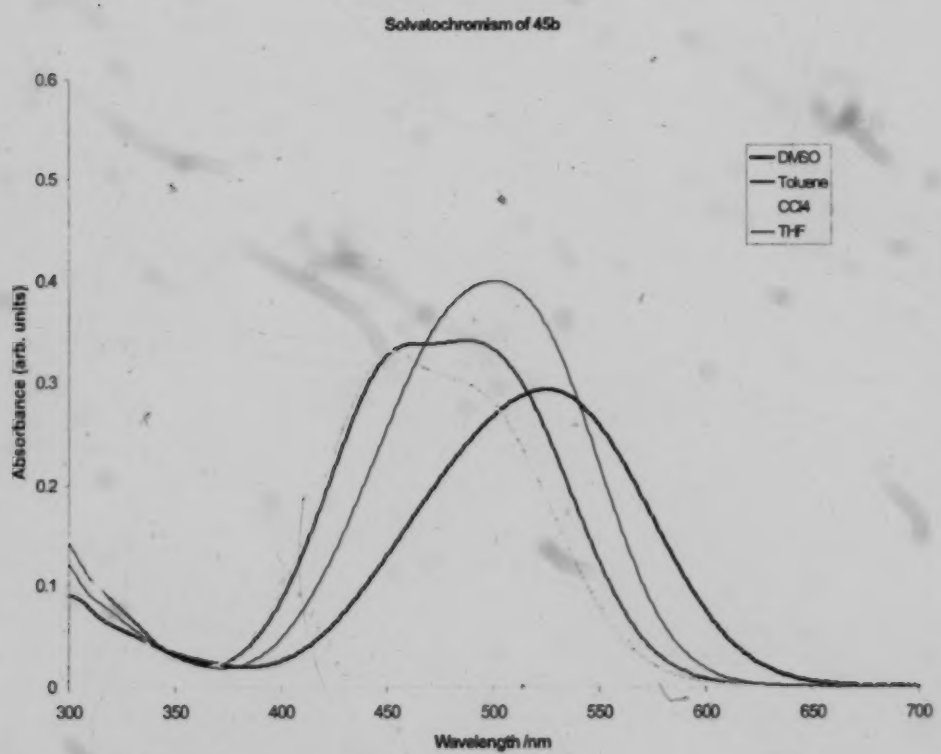

Figure 36. Solvatochromism of **45b** in selected solvents, at r.t.

These observations can be partially explained on the basis of the ability of a given solvent to solvate strongly a polar functional group. In nonpolar solvents, such as carbon tetrachloride, the carboxylic acid groups cannot be efficiently solvated, and tend to

intramolecularly self-associate, forming an internal dimer. This results in a conformational effect similar to that proposed for **43a**, in which a twist is induced in the normally planar chromophore. The break of planarity reduces the effective conjugation length of the chromophore, and shifts the characteristic absorption band to shorter wavelengths. In polar solvents, such as dimethyl sulfoxide, the carboxylic acid groups are efficiently solvated through the formation of multiple intermolecular hydrogen bonds, effectively eliminating the twisted conformation and favoring instead the completely planar chromophore. This results in a larger effective conjugation length, and shifts the characteristic absorption band to longer wavelengths. Of course, a simple solvatochromic effect would also contribute to the observed shifts, as the increased dielectric constant of the more polar solvents lowers the energy of the π–π^* transition. However, these effects are typically limited in the extent of the shift that they generate, and are likely insufficient to completely rationalize the observed shifts.

5. Properties of the Metathesis Oligomers

A. Nuclear Magnetic Resonance Spectroscopy

The progress of the metathesis reactions used to generate oligomeric materials was monitored via nuclear magnetic resonance spectroscopy (NMR). In the δ 6–5 region of the ^{1}H NMR spectrum, the integral ratios develop over time in a manner consistent with the degree of polymerization of the oligomers being generated. In this region, the monomer shows three resonances: One (δ 5.90, ddt) corresponds to the =C**H**– proton of the terminal alkene, while the other two (δ 5.10, 2 × dd) correspond to the =C**H**$_2$ protons (Figure 37). As the polymerization reaction proceeds, a fourth resonance (δ 5.55) appears and grows larger. The degree of polymerization (DP) of the isolated

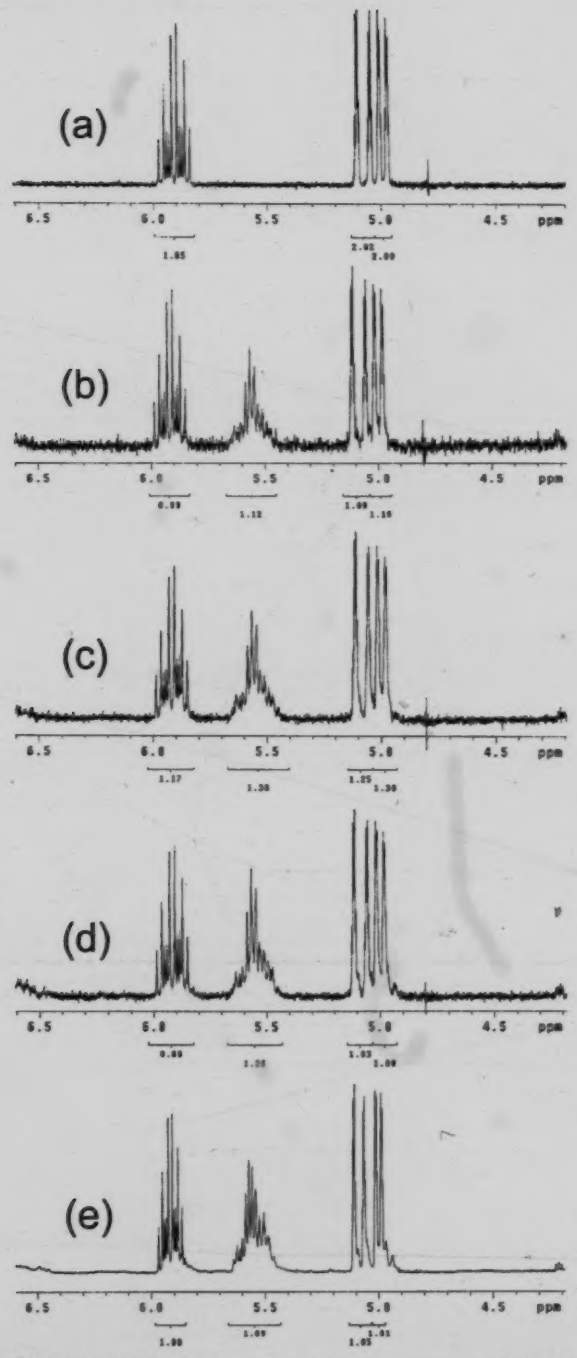

Figure 37. The ^{1}H NMR integral ratios of the alkene resonances of **45b** develop over time, as shown at (a) 0h00, (b) 3h00, (c) 5h20, (d) 22h30 and (e) 56h00, as measured in $(CD_3)_2CO$, at r.t.

material can thus be approximated by a calculation based on the integral of the new resonance (N_{int}) and the sum of the integrals of the original three resonances (N_{end}), as follows:

$$DP = 3 \times \left(\frac{N_{int}}{N_{end}} \right) + 1 \quad (13)$$

On this basis, the degree of polymerization of the oligomeric materials used to prepare thin films for NLO studies was calculated as 10–12, depending on the specific sample.

B. Mass Spectrometry

Analysis of the oligomers by mass spectrometry proved challenging, due to their polycarboxylate nature. Ionization by electron impact (EIMS) proved ineffective, as anticipated due to similar results from the monomer. Negative mode electrospray ionization (ESIMS) allowed the resolution of a number of short chain oligomers (DP = 3–5) (Figure 38). In the mass spectra, the repeat unit was considered to be approximately *m/z* 495, although peaks for each consecutive unit appeared as clusters of peaks differing by *m/z* 14 each, the origin of which is currently unclear. Thus, the spectrum shown in Figure 38 clearly suggests the presence of up to five repeat units (DP = 5, *m/z* 2475). Analysis of the same sample by ^{1}H NMR spectroscopy, as described in the previous section, suggested a DP of about 12. This disparity led to speculation that ESIMS was not revealing the true extent of polymerization and that other analytical methods would be required. The use of matrix-assisted laser desorption ionization, with time-of-flight detection (MALDI-TOF) was then explored. After some experimentation with various matrix compounds, retinoic acid yielded results much more satisfactory than those obtained via ESIMS (Figure 39). These results indicated the presence of oligomers

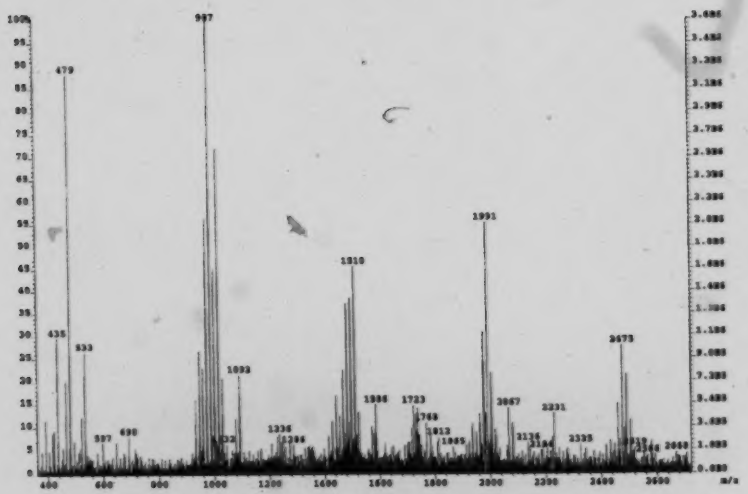

Figure 38. Negative mode ESIMS of an oligomer sample, indicating about 5 repeat units

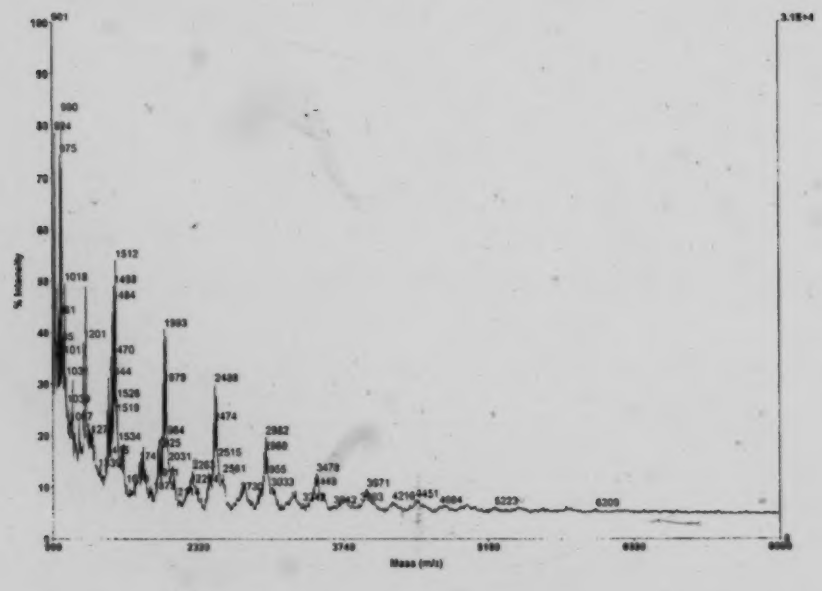

Figure 39. MALDI-TOF of the oligomer sample, indicating up to 11 repeat units

containing up to 11 repeat units (DP = 11, *m/z* 5445), an acceptable correlation with the NMR results from the same samples.

B.1 Cooperativity Effects and MS Analysis

Qualitatively, although the MALDI MS analyses discussed above provide evidence for the existence of oligomeric chain lengths up to 11 repeat units, they are not entirely satisfactory as mass spectra of a polymerization product. For such a product, it could be anticipated that the general shape of the spectrum would appear as a pseudo-Gaussian curve, with its peak at the average molecular weight (M_w) of the polymer sample, as shown in Figure 40. This shape stems from the fact that a polymerization reaction will

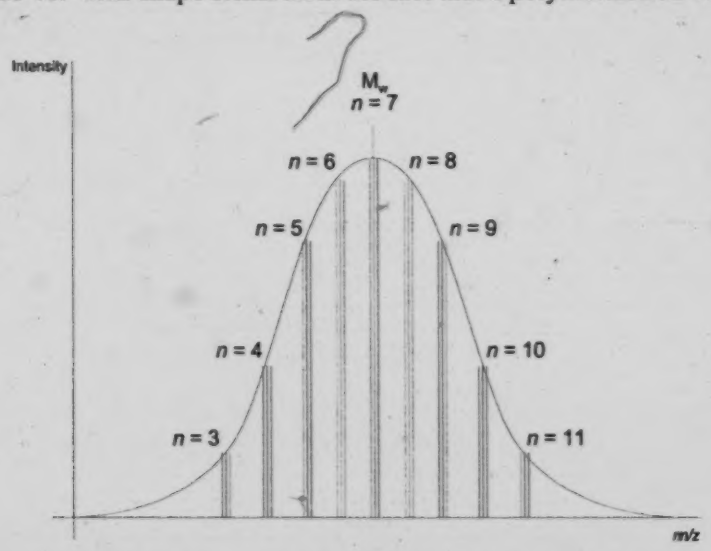

Figure 40. Schematic representation of the expected shape of the mass spectrum of a polymer sample, where *n* is the degree of polymerization of the specific oligomer, and M_w is the average molecular weight of the sample

tend to yield an average chain length with $m/z = M_w$, and relatively much smaller amounts of both slightly larger and slightly smaller chains, assuming that all of these chain lengths are detectable. The shape actually seen in every sample of these oligomers is pseudo-exponential, as illustrated in Figure 41. A possible interpretation of the

schematic spectrum shown is that the polymerization reaction yielded primarily dimers, with lesser

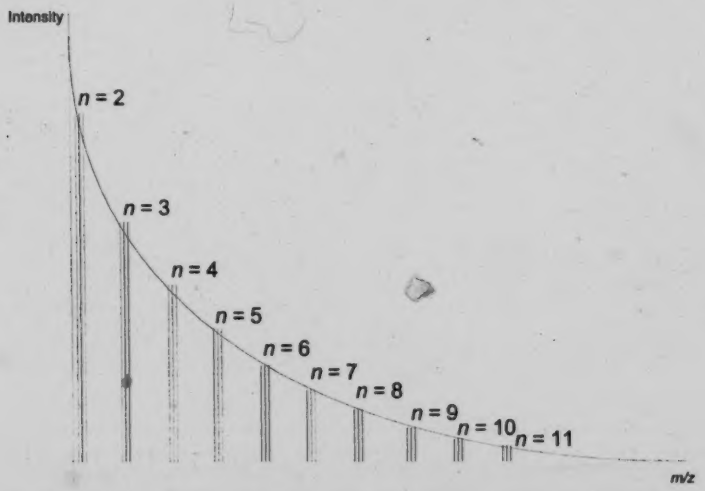

Figure 41. Schematic representation of the observed shape of the mass spectra obtained, where *n* is again the degree of polymerization of the specific oligomer

amounts of the higher oligomers. However, metathesis reactions, such as the one used to generate the oligomeric samples, tend to yield very well-defined molecular weight distributions, and it is unlikely, though not impossible, that a spread this wide would be seen with such short oligomers. There is definite evidence for the existence of oligomers containing up to 11 repeat units, obtained from multiple experiments, different catalyst batches, different monomer batches, and so on. This estimate is supported as well by ^{1}H NMR spectroscopic analysis. Thus, it appears that, while longer oligomers are present, they are not as easily ionized or vaporized as the shorter oligomers, leading to the atypical weight distribution observed in the mass spectra of the oligomeric samples. This is consistent with the polycarboxylate nature of the oligomers, since a strong intermolecular association would be expected and would increase substantially with

increased chain length. The increase could in fact be almost exponential in nature, due to a cooperativity effect similar to those seen in the zipper complexes described by Hunter and coworkers and Gong and coworkers.[28-31] Future attempts to generate longer oligomers and true polymers could be hampered by this effect, and it seems likely that further development or significant modification of the mass spectroscopic techniques used here will be necessary in order to adequately characterize such samples.

C. Solvatochromism

As with the monomer (**45b**), the oligomeric materials prepared via metathesis reactions also showed a strong solvatochromic effect. This was studied in a series of six solvents, selected from the original nine solvents on the basis of solubility. The results of the study are summarized in Table VI. Values of λ_{max} in this case vary by almost 30 nm,

Table VI - Solvatochromism of 45b and Its Oligomers

Solvent	Monomer (**45b**) λ_{max} /nm	Oligomers λ_{max} /nm
Methanol	499	491
Ethyl Acetate	494	495
Tetrahydrofuran	502	501
Toluene	487	503
Acetone	505	504
Dimethyl Sulfoxide	525	522

a range similar to that seen for the monomer in the same solvents. However, there are some differences in the specifics of these data. Perhaps one of the most significant is the lack of shoulder peaks in any of the solvents, including toluene. The spectrum of **45b** in toluene had yielded a double peak, attributed to a conformational variation stemming

from intramolecular self-association, and resulting in a change in conjugation length. However, in the oligomeric material, this shoulder is no longer present, suggesting that perhaps the intramolecular association has given way either to intermolecular association, or to intrachain association within the individual oligomer molecules. Neither of these modes of association would require any conformational shift within the chromophore core, and thus would not be expected to yield the same shoulder peaks. Another notable difference can be found in the values obtained for toluene. A comparison of the other five solvents reveals an average hypsochromic shift of about 2 nm from the monomer to the oligomer. In toluene, however, a bathochromic shift of 16 nm is seen. A possible explanation of this observation may arise from the aromatic nature of toluene, as this allows a mode of solvation largely unavailable to the other five solvents, namely π–π interactions, or "π-stacking." This mode of solvation could favor the planar form of the chromophore, since this would provide a larger π-system with which the solvent molecules could interact. In this case, the absorption band would tend towards longer wavelengths, for reasons elaborated in the earlier discussion of the solvatochromism of **45b**.

D. Thermal Analysis

D.1 Differential Scanning Calorimetry

Initial DSC analysis of the monomer (**45b**) indicated a melting point of 157 °C, and two exothermic transitions, one at 200 °C and the other at 260 °C. Analysis of the oligomeric material under identical conditions indicated no clear melting point, although to visual inspection, an apparent glass transition temperature (T_g) occurred around

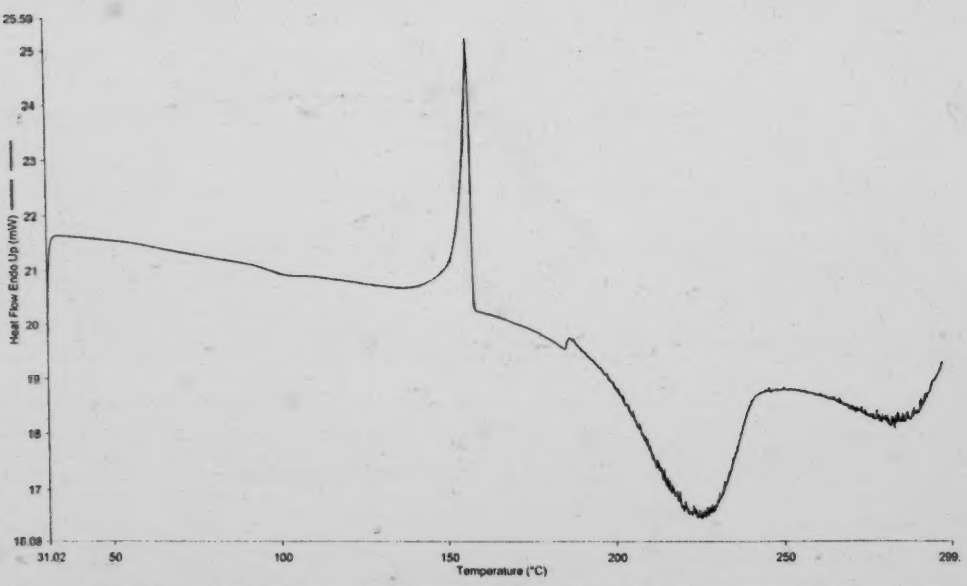

Figure 42. Differential scanning calorimetry (DSC) analysis of **45b**, showing a melting point at 157 °C and two exotherms, at 200 °C and 260 °C

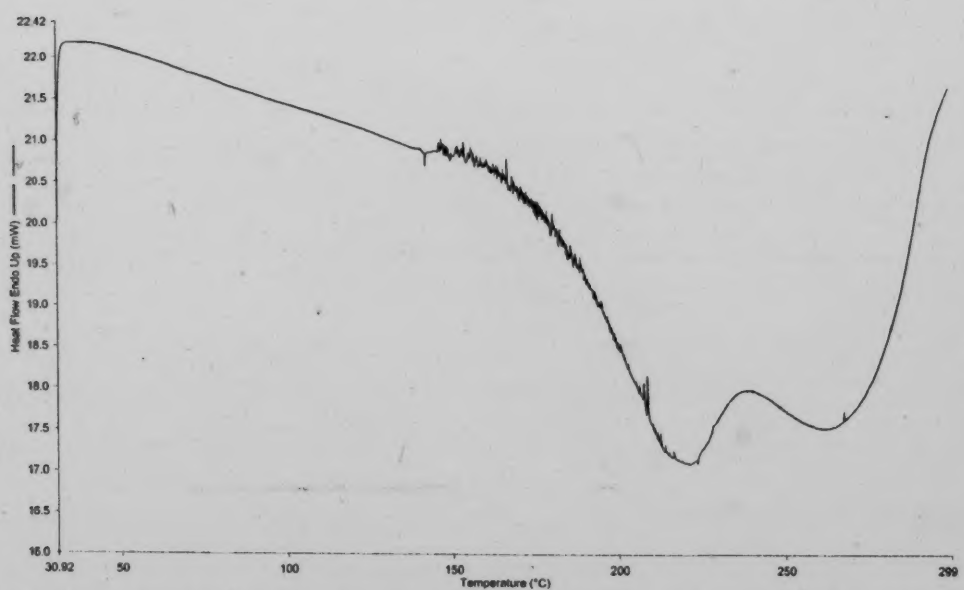

Figure 43. DSC analysis of the oligomeric material, showing two exotherms, at 200 °C and 250 °C

100 °C. However, there still existed two exothermic transitions, this time at 200 °C and 250 °C. The relevant curves are shown in Figures 42 and 43.

D.2 Thermal Gravimetric Analysis

TGA of **45b** under the same heating conditions as used in the DSC results discussed above showed a 5% mass loss at 200 °C, and substantial loss above 220 °C. In

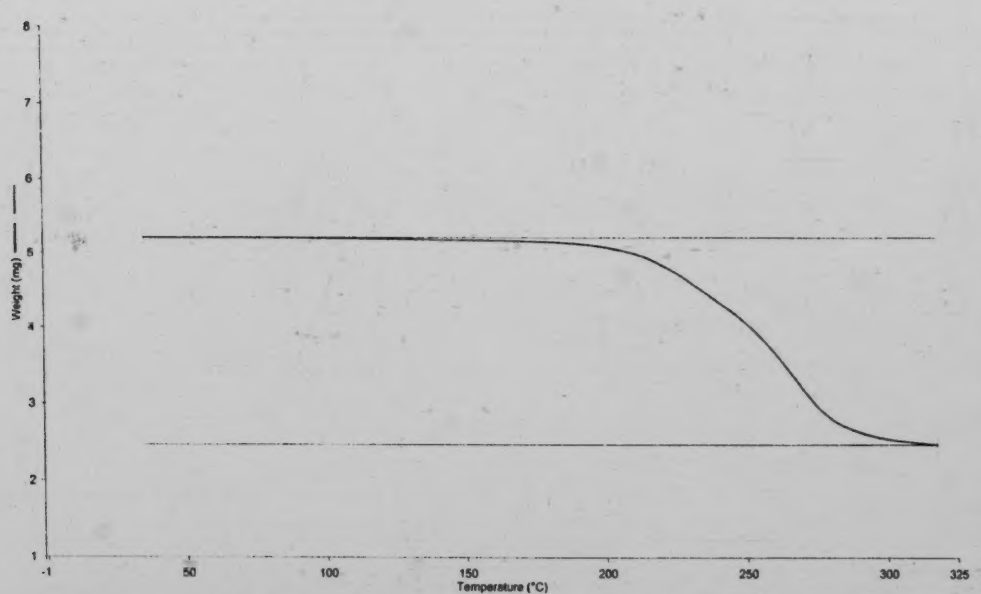

Figure 44. Thermal gravimetric analysis (TGA) of **45b**, showing 5% mass loss at 200 °C and substantial mass loss above 220 °C

combination with the two exotherms seen in the DSC analysis, this is consistent with a two-stage decomposition of the chromophore, one stage involving the reactive azo group, the other involving decarboxylation at one or both carboxylic acid sites. Analysis of the oligomeric material showed 5% mass loss at 160 °C, and substantial loss above 220 °C. The lower temperature of the 5% mass loss is likely due to elimination of residual benzene, the solvent from the metathesis reaction, as it is forced out of the polymer

matrix. The remaining substantial loss is consistent with a two-stage decomposition, virtually identical to that proposed for the monomer. The relevant curves are shown in Figures 44 and 45.

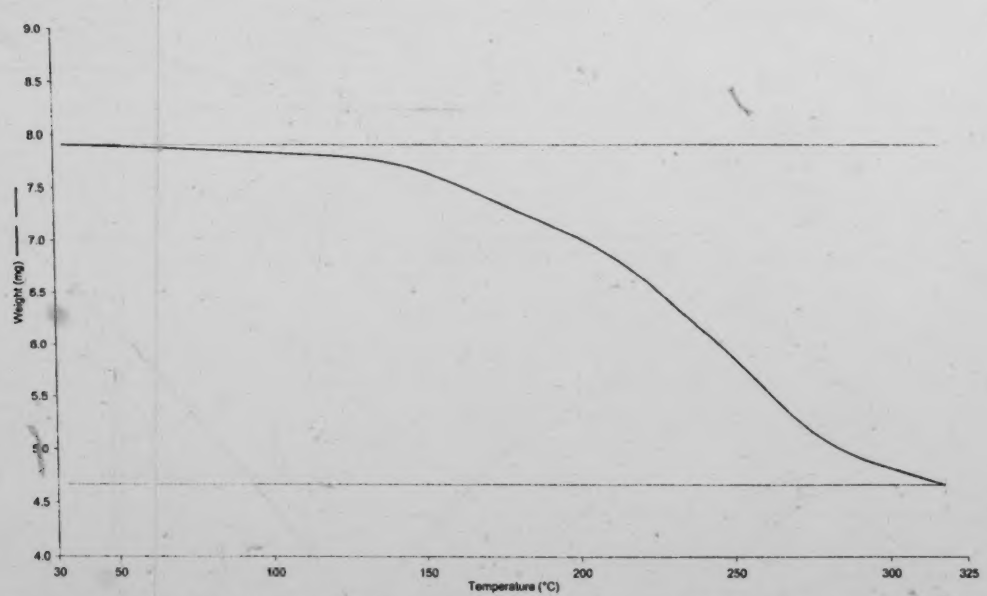

Figure 45. TGA of oligomeric material, showing 5% mass loss at 160 °C, and substantial mass loss above 220 °C

E. Thin Films

E.1 Electronic Properties

In addition to solution state, the electronic properties of the oligomers were also studied in the solid state, in the form of casts on quartz cuvette walls. Overall, a strong correlation was observed among these results, shown in Table VII, in that in the absence of solvent, the absorption characteristics of the film were fairly consistent. Two anomalous results were noted in films cast from methanol and acetone, yielding absorption wavelengths significantly higher and lower than the average, respectively. The origin of these anomalies is unclear, and does not seem convincingly to correlate to

any obvious property of the casting solvents, such as polarity or hydrogen-bonding ability, or even boiling point or vapor pressure of the solvents. It would seem apparent that more detailed studies are needed to elucidate the cause of this peculiar effect.

Table VII - Solvatochromism of Oligomers in Solution and Thin Film Casts

Solvent	Solution λ_{max} /nm	Thin Film† λ_{max} /nm
Methanol	491	507‡
Ethyl Acetate	495	525
Tetrahydrofuran	501	522
Toluene	503	527
Acetone	504	549‡
Dimethyl Sulfoxide	522	520

† Thin films were cast from the solvent indicated
‡ Anomalous values

E.2 Nonlinear Optical Effects - The Electro-Optic Effect

Spin-casting of thin films, vapor deposition of the gold electrode, and poling experiments were conducted in collaboration with Hue Nguyen of TR Labs.

In order to begin to study the nonlinear optical properties of the oligomers, it was necessary to generate uniform thin films on an appropriate surface. The preferred surface for studying these properties is a glass substrate coated with indium tin oxide (ITO), a transparent electrode material. Thus, attempts at generating these films were carried out directly on 0.7" × 0.7" ITO-coated plates. Initial spot tests on unmodified glass surfaces seemed to suggest that THF would serve as a casting solvent. Casts from a THF solution onto the ITO plates yielded very rough films, however, apparently due to the rapid

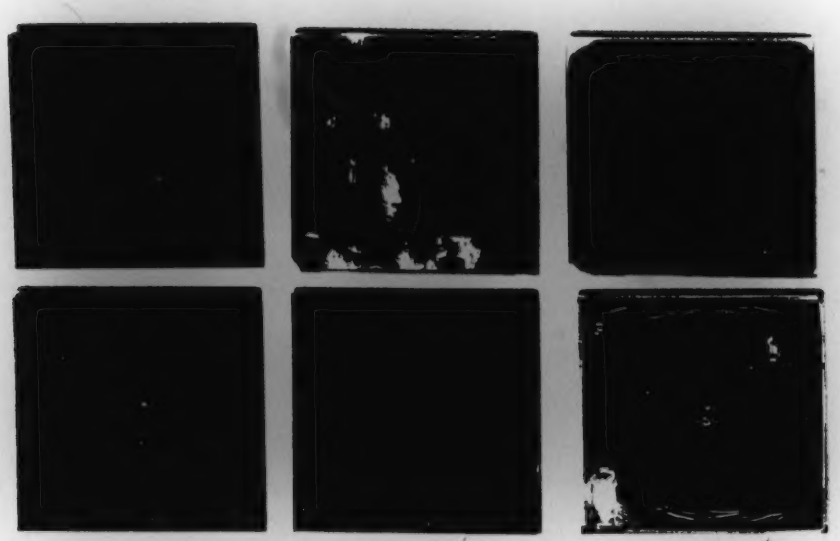

Figure 46. 0.49 in^2 ITO plates coated with polymer films cast from tetrahydrofuran (THF, top left), *N,N*-dimethylformamide (DMF, top center), *N,N*-dimethylacetamide (DMAc, top and bottom right), pyridine (bottom left) and 2,6-lutidine (bottom center). A gold electrode has been deposited on the bottom right film, cast from DMAc, visible as a pale circular area

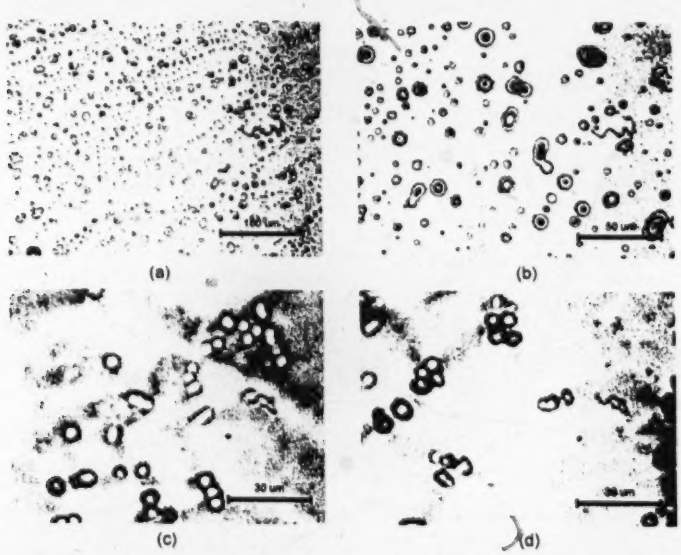

Figure 47. Micrographs of the films cast from *N,N*-dimethylacetamide, at low magnification (a), medium magnification (b), and high magnification (c) and (d). The average diameter of the surface defects is approximately 15 μm, and the average depth is approximately 0.4 μm, as measured by profilometry studies

evaporation rate of the solvent (Figure 45, top left). Attention was then focused on solvent with higher boiling points and, thus, lower evaporation rates. *N,N*-dimethylformamide (DMF) evaporated much more slowly, but failed to completely coat the ITO surface, instead forming very rough streaks across the plate (Figure 45, top center).

N,N-dimethylacetamide (DMAc), finally, yielded films that appeared very uniform to visible inspection (Figure 45, top right). These films were used in an attempt to acquire preliminary NLO data: First, a gold electrode was sputtered onto the film (Figure 45, bottom right), and then an attempt was made to pole the film, by heating to near its apparent glass transition temperature (T_g ~ 110 °C) and applying an electric field. The poling attempt was unsuccessful, however, and closer inspection of the DMAc films revealed μm-scale defects, or pinholes, throughout the films. It was thought that these defects were interfering with the poling process (Figure 46). Recent attempts to generate more uniform films using solvent such as pyridine and 2,6-lutidine (Figure 45, bottom left and center) have been similarly unsuccessful. The resulting lack of high-quality films has made studies of the NLO properties of these oligomers impossible to date, but efforts are ongoing to improve the film quality.

III. CONCLUSIONS

In the preceding chapters, efforts to generate NLO materials with high temporal stability resulting from intramolecular hydrogen bonding were detailed. A synthetic pathway was developed, leading to the synthesis of a series of azobenzene-based chromophores. The synthesis is flexible, allowing a variety of substitution patterns to be generated on the amino terminus of the chromophores. Solubility of the members of the series was highly variable, ranging from those soluble in aqueous solutions, whether acidic, basic or neutral, to those soluble in relatively nonpolar solvents, such as chloroform or toluene. One chromophore in particular (**43a**) exhibited evidence for a pH-induced conformational control over the azobenzene core, induced by intramolecular self-association of side chain functional groups. Some chromophores (**45a** and **45b**) are key precursors for the preparation of a self-complementary quadruple hydrogen bond motif, and one of these (**45b**) was designed to allow polymerization via acyclic diene metathesis (ADMET) protocols.

Compound **45b** was carried on into attempts at metathesis polymerization, and after a certain amount of optimization, oligomeric materials were obtained, possessing chain lengths of ~ 10–12 repeat units. Simultaneously, mass spectrometric methods to estimate chain length were developed to overcome the inherent difficulties of analyzing polycarboxylate chains via mass spectrometry. Strong solvatochromism of the oligomeric material was noted in solution, reflecting that of the corresponding monomer, and this effect translated, somewhat unexpectedly, to a strong dependence of the absorption characteristics of thin film casts on the solvent from which the films had been cast. This was tentatively attributed to an extension of the conformational control noted

in the monomeric compounds, this time induced by solvation efficiency, rather than protonation states. Preparation of high-quality thin films for NLO measurements was attempted, but remains a challenge, presumably due to insufficient chain lengths of the oligomeric material. Casts from *N,N*-dimethylacetamide and 2,6-lutidine yielded high-quality films to visual inspection, but possessed large numbers of microscale defects (~ 15 μm). Attempts to pole these films were made anyway, but were unsuccessful, due to short-circuiting between the ITO and gold electrodes. This effect was attributed to the noted microscale defects, many of which completely penetrated the films, although it is possible that trace amounts of ruthenium from the metathesis catalyst could be contributing as well.

Future developments of this work may follow a variety of pathways. A number of the chromophores generated could be incorporated into other types of polymeric materials, such as polyurethanes, polycarbonates, and others. These could allow improvements in temporal stability of the NLO response via a high-T_g polymer matrix, as previously reported, or through hydrogen bonding between pendant chromophores and the polymer backbone. Some of these compounds also have potential utility as aqueous sensors for free boronic acids, via reaction with the diethanolaniline moiety. More generally, the strong sensitivity of the chromophore to its immediate environment, combined with appropriate functionality on the alkyl side chains and the ability to be polymerized, could lead to a class of tunable solid state sensor materials. Also, the addition of known "molecular switch" components, such as dithienylethene derivatives, could allow bulk properties, such as NLO response, or the sensor activity mentioned above, to be toggled between two or more states by external stimuli.

Other developments are possible regarding the preparation of thin films of the oligomeric materials. Further experimentation with casting solvents (such as, e.g., *N*-methylpyrrolidinone) could yield higher quality films than those generated to date. Annealing of the existing films could help as well, although early attempts with films cast from THF were not encouraging, since the oligomers begin to decompose at > 150 °C. The potential interference from traces of ruthenium could be minimized by washing the oligomers in DMSO or in the presence of triphenylphosphine.[67] The most probable cause of the poor film quality is the relatively short chain lengths of the oligomeric material, and even if high-quality films are possible from the shorter chains, extended chain lengths should improve the processability of the material. This extension could be accessed via protection of the carboxylic acid groups as esters, which should increase the solubility of both the monomer and the forming polymer chain, a factor suspected in the limited chain lengths obtained thus far. Also, carrying out the metathesis reaction prior to the azo coupling step could help, both for solubility reasons and by reducing the size of the monomer unit. However, this method would likely result in a significant decrease in the number density of the chromophores in the resulting material, and may adversely affect the desired intramolecular hydrogen bonding interactions by placing "adjacent" units too far away from each other.

IV. EXPERIMENTAL

General. Reagents were purchased reagent grade from commercial suppliers and used without further purification. Solvent removal was done at water-aspirator pressure on a rotary evaporator, followed by final evaporation *in vacuo* on a mechanical vacuum pump. Column chromatography: Silica gel 60 (230-400 mesh) from Silicycle. Thin Layer Chromatography (TLC): Plastic sheets coated with silica gel 60 treated with the fluorescent indicator UV_{254} from Macherey-Nagel; visualization by UV light at 254 nm. Mp: *Fisher-Johns Melting Point Apparatus*, uncorrected. DSC: *Pyris 1 Differential Scanning Calorimeter*. TGA: *Pyris 1 Thermal Gravimetric Analyzer*. UV-Vis Spectra: *Varian Cary 400* at room temperature; λ_{max} in nm (ε in L mol^{-1} cm^{-1}). IR Spectra: *Nicolet Magna-IR 750* (casts and neat films) with *Nic-Plan IR Microscope* (solids), bands in cm^{-1}. ^1H and ^{13}C NMR spectra: *Bruker AM-300, Varian Inova 300, 400, 500* or *600*, or *Varian Unity 500*, at room temperature in $(CD_3)_2CO$ (acetone-d_6, solvent peaks: 2.05 ppm for ^1H and 206.3 ppm and 29.8 ppm for ^{13}C), $CDCl_3$ (solvent peaks: 7.24 ppm for ^1H and 77.0 ppm for ^{13}C), $(CD_3)_2SO$ (DMSO-d_6, solvent peaks: 2.49 ppm for ^1H and 39.5 ppm for ^{13}C) or CD_3OD (solvent peaks: 3.30 ppm for ^1H and 49.0 ppm for ^{13}C). EIMS: *Kratos MS-50*, peaks as *m/z*. ESIMS: *Micromass ZabSpec Hybrid Sector-TOF*, in either positive or negative ion mode, peaks as *m/z*. MALDI: *Applied Biosystems Voyager Elite*, with delayed extraction and reflectron (ion mirror), peaks as *m/z*. Elemental analyses: *Carlo Erba 1108 Elemental Analyzer*. Compounds whose spectral data are not listed were identified via comparison with literature values, typically ^1H NMR spectral data and mass spectral data, in the references indicated.

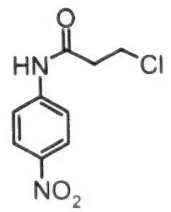

11

3-Chloropropionyl-(4-nitroanilide) (11).[45] 4-Nitroaniline (10.02 g, 72.57 mmol) was suspended in CH_2Cl_2 (125 mL) and cooled to –2 °C in a salted ice-water bath. 3-chloropropionyl chloride (3.5 mL, 37 mmol) was dissolved in CH_2Cl_2 (25 mL) and added over 2 h, dropwise, with vigorous stirring. The reaction mixture was filtered to remove unreacted starting materials, and the filtrate was concentrated under vacuum. The resulting residue was washed with water, dissolved in 1:1 CH_2Cl_2/acetone (~ 100 mL), dried over $MgSO_4$ and concentrated under vacuum to give **11** (3.637 g, 43%) as a crystalline yellow solid.

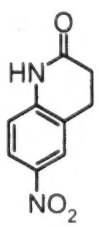

12

3,4-Dihydro-6-nitro-2(1*H*)-quinolinone (12).[46] 3,4-Dihydro-2(1H)-quinolinone (**18**, 3.236 g, 21.99 mmol) was dissolved in concentrated sulfuric acid (40 mL), glacial acetic acid (30 mL) was added while cooling in an ice-water bath to maintain temperature below 40 °C, and the resulting solution was cooled to 10 °C. Cooling was continued as concentrated nitric acid (13 mL) was added, dropwise, so as to maintain the temperature

between 10 °C and 15 °C. The solution was allowed to warm to room temperature, poured over crushed ice, filtered, and dried under vacuum to yield **12** (4.199 g, 99%) as a pale yellow powder.

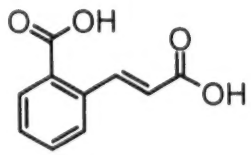

15

2-Carboxy-*trans*-cinnamic acid (15).[47] 2-Naphthol (20.04 g, 0.1390 mol) was added to a solution of 90% w/v formic acid (110 mL), and stirred for 10 min. 30% w/v $H_2O_{2(aq)}$ (125 mL) was added, and stirring was continued while the solution temperature was monitored. When the temperature reached 35 °C, a lightly-iced water bath was applied so as to maintain the temperature between 33 °C and 37 °C. Once the visible reaction (i.e., foaming) had slowed, 30% w/v $H_2O_{2(aq)}$ (100 mL) was added, and stirring and temperature control were continued until foaming stopped, and temperature stopped rising. The reaction mixture was filtered, washed with cold water, then benzene, and air-dried to give **15** (19.28 g, 72%) as a beige powder.

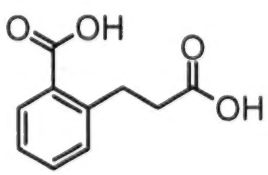

16

3-(2-Carboxyphenyl)propionic acid (16).[48] 2-Carboxy-*trans*-cinnamic acid (**15**, 10.00 g, 52.06 mmol) was dissolved in 10% w/v $NaOH_{(aq)}$ (390 mL) and heated to 100 °C while stirring vigorously. The heat source was removed, and Ni(Al) alloy powder (31.60 g,

0.3688 mol) was added in small portions, pausing after each addition to allow foaming to subside. The mixture was heated to 100 °C and maintained at this temperature for 70 min, during which evaporated water was replenished as needed to maintain a constant volume. The hot reaction mixture was filtered, and the metallic residue was washed with hot 10% $NaOH_{(aq)}$ (50 mL) and hot water (2 × 50 mL) before dissolving the metal residue in dilute aqueous hydrochloric acid for disposal. The filtrate was cooled to room temperature and dropped over 2 h into concentrated hydrochloric acid (200 mL) while stirring vigorously and cooling in an ice-water bath to maintain a temperature of less than 36 °C. The resulting mixture was cooled to 10 °C, filtered and air-dried to give **16** (9.952 g, 98%) as a pale yellow powder.

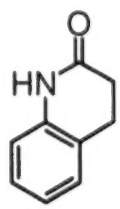

18

3,4-Dihydro-2(1*H*)-quinolinone (18).[46] 2-(2-Carboxyphenyl)propionic acid (**16**, 6.254 g, 32.21 mmol) was added to concentrated sulfuric acid (100 mL) and stirred for 15 min to ensure complete dissolution. Sodium azide (2.312 g, 35.57 mmol) was added in very small portions over 20 min, pausing after each addition to allow foaming to subside. The solution was stirred at room temperature for 24 h, poured over crushed ice, neutralized to pH ~ 6 with 20% w/v $NaOH_{(aq)}$, filtered, and air-dried to give **18** (4.251 g, 90%) as a beige powder.

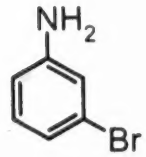

19

3-Bromoaniline (19).[68] Calcium chloride (0.169 g, 1.52 mmol) was dissolved in water (5 mL) and combined with 3-bromonitrobenzene (2 g, 10 mmol) in ethanol (10 mL). The mixture was heated to boiling, iron powder (2 g, 36 mmol) was added in one portion, and the resulting mixture was heated at reflux for 30 min. The reaction mixture was cooled to room temperature and filtered, and the ethanol was distilled off of the filtrate. The resulting solution was acidified with concentrated HCl (10 mL) and washed with ether, basified with 40% w/v $NaOH_{(aq)}$ and extracted with ether. The extracts were concentrated under vacuum to yield **19** (0.661 g, 39%) as a brown-orange oil.

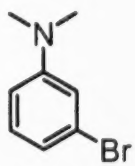

20

***N,N*-Dimethyl-3-bromoaniline (20).**[52] Phosphorus pentoxide (10.24 g, 72.17 mmol) and methanol (8 mL, 0.2 mol) were combined and heated until the mixture became fluid (~ 120 °C). 3-bromoaniline (**19**, 0.959 g, 5.57 mmol) was added, and the mixture was heated to 150 °C overnight, and cooled to room temperature. Excess phosphoric acid glass was dissolved with 10% w/v $NaHCO_{3(aq)}$. The resulting solution was extracted with

ether, and the extracts were dried over $MgSO_4$ and concentrated under vacuum to afford **20** (0.635 g, 57%) as a brown oil.

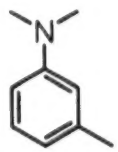

23

***N,N*-Dimethyl-3-toluidine (23).**[69] 3-Toluidine (11 mL, 0.10 mol) and trimethyl phosphate (13 mL, 0.11 mol) were combined in a large flask and heated at reflux for 2 h. The mixture was cooled to ~ 50 °C, and aqueous NaOH (14 g in 100 mL) was added, and the solution was heated to reflux for an additional 2 h. The reaction mixture was cooled to room temperature, and water (150 mL) was added to dissolve the phosphate salts. The resulting mixture was extracted with diethyl ether (3 × 150 mL), and the extracts were dried over $MgSO_4$ and concentrated to yield **23** (6.675 g, 49%) as a medium brown viscous oil.

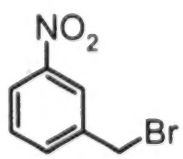

28

3-Nitrobenzyl bromide (28).[70] 3-Nitrotoluene (9.908 g, 72.25 mmol) was dissolved in benzene (250 mL) and bubbled with argon for 30 min while stirring vigorously. *N*-bromosuccinimide (13.05 g, 73.31 mmol) was added and argon bubbling was continued for an additional 5 min. The reaction flask was fitted with a reflux condenser, irradiated with a 140 W Hanovia quartz ultraviolet lamp for 2 h, and cooled to room temperature.

The solution was washed with water (4 × 250 mL), dried over $MgSO_4$, and concentrated under vacuum to give a yellow-orange oil, which was purified by flash chromatography (SiO_2, hexanes/diethyl ether 9:1) to give **28** (11.40 g) as a pale yellow lachrymatory powder comprised of a mixture of mono- and dibrominated products, which was carried on to the next step(s) without separation. Content of monobrominated product was estimated by ^1H NMR via comparison of integral ratios of the benzylic protons, and varied from 65–85% wt. $R_f = 0.1$ (SiO_2, hexanes/diethyl ether 9:1).

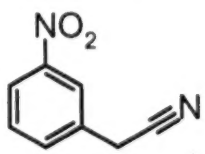

29

(3-Nitrophenyl)acetonitrile (29).[55] Potassium cyanide (1.370 g, 21.04 mmol) was dissolved in water (30 mL), the solution was heated to 90 °C, and 3-nitrobenzylbromide (**28**, 5.965 g, 19.05 mmol of monobrominated product) dissolved in absolute ethanol (110 mL) was dropped into the hot solution over 1h40. The resulting solution was heated to reflux for 20 h, cooled to room temperature and filtered, and the solvent was removed from the filtrate. The residue was diluted with water and extracted with $CHCl_3$ (3 × 150 mL), and the combined extracts were dried over $MgSO_4$, and concentrated to give a dark brown liquid. Purification by flash chromatography (SiO_2, hexanes/diethyl ether 1:1) yielded **29** (2.190 g, 71%) as a yellow waxy powder. $R_f = 0.2$ (SiO_2, hexanes/diethyl ether 1:1).

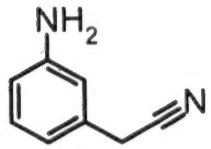

30

(3-Aminophenyl)acetonitrile (30).[71] (3-Nitrophenyl)acetonitrile (**29**, 2.190 g, 13.50 mmol) and 10% palladium on carbon (0.367 g, 345 μmol) were combined dry, and absolute ethanol (140 mL) was added. The mixture was stirred until the starting material had completely dissolved, and was shaken under 50 psi $H_{2(g)}$ for 30 min. The reaction mixture was filtered, the solid mass washed with diethyl ether, and the combined filtrate and washings were concentrated to give **30** (1.785 g, quantitative) as an orange oil.

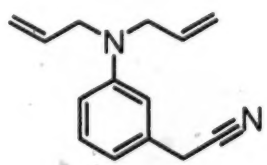

31a

3-(*N,N*-Diallylamino)phenylacetonitrile (31a). (3-Aminophenyl)acetonitrile (**30**, 0.673 g, 5.09 mmol) and allyl bromide (3.75 mL, 45.1 mmol) were dissolved in *N,N*-dimethylformamide (10 mL), and Na_2CO_3 (2.566 g, 24.21 mmol) was added. The resulting mixture was heated to reflux for 1 h, and cooled to room temperature and filtered, and the solid mass was washed with diethyl ether (100 mL). The combined filtrate and washings were poured into water (120 mL), the layers were separated, and the aqueous portion was extracted with diethyl ether (3 × 150 mL). All organic portions were combined, washed with water, dried over Na_2SO_4, and concentrated to yield **31a**

(1.081 g, quantitative) as a clear orange oil. R_f = 0.5 (SiO_2, hexane/acetone 3:1). IR (neat film) 3081, 3008, 2980, 2912, 2250 (C≡N), 1604, 1499, 1244, 989, 922, 770, 692 cm^{-1}; ^1H NMR (300 MHz, $CDCl_3$) δ 7.16 (t, J = 8.1 Hz, 1H); 6.7–6.5 (m, 3H), 5.84 (ddt, J_1 = 18 Hz, J_2 = 10 Hz, J_3 = 4.8 Hz, 2H), 5.17 (dd, J_1 = 18 Hz, J_2 = 1.7 Hz, 2H), 5.17 (dd, J_1 = 10 Hz, J_2 = 1.7 Hz, 2H), 3.92 (dt, J_1 = 4.8 Hz, J_2 = 1.7 Hz, 4H), 3.65 (s, 2H); ^{13}C NMR (75.5 MHz, $CDCl_3$, APT) δ 149.2, 133.4, 130.8, 129.8, 118.1, 116.2, 115.6, 111.8, 111.4, 52.8, 23.9; EIMS *m/z* 212.1 (M^+, 100), 185.1 (97), 143.1 (39), 116.1 (35), 89.0 (26); HRMS calcd for $C_{14}H_{16}N_2$ (M^+) 212.1314, found 212.1310.

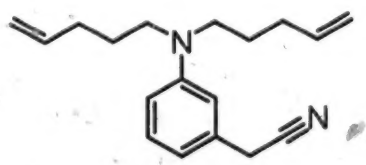

31b

3-[*N,N*-Bis(4-pentenyl)amino]phenylacetonitrile (31b). (3-Aminophenyl)acetonitrile (**30**, 1.120 g, 8.476 mmol) and 5-bromo-1-pentene (7.576 g, 50.84 mmol) were dissolved in *N,N*-dimethylformamide (10 mL), and Na_2CO_3 (4.363 g, 41.16 mmol) was added. The resulting mixture was heated to reflux for 1h30, cooled to room temperature and filtered, and the solid mass was washed with diethyl ether (200 mL). The combined filtrate and washings were poured into water (600 mL), the layers were separated, and the aqueous portion was extracted with diethyl ether (3 × 300 mL). All organic portions were combined, washed with water, dried over $MgSO_4$, and concentrated to yield **31b** (1.924 g, 85%) as an amber oil. IR (neat film) 3076, 2975, 2935, 2250 (C≡N), 1603, 1500, 1369, 1176, 993, 913, 766, 693 cm^{-1}; ^1H NMR (300 MHz, $CDCl_3$) δ 7.17 (t, J = 8.1 Hz, 1H), 6.7–6.5 (m, 3H), 5.84 (ddt, J_1 = 17 Hz, J_2 = 10 Hz, J_3 = 7.2 Hz, 2H), 5.06 (dd, J_1 = 17 Hz,

J_2 = 1.7 Hz, 2H), 5.01 (dd, J_1 = 10 Hz, J_2 = 1.7 Hz, 2H), 3.66 (s, 2H), 3.28 (dd, J_1 = 7.6 Hz, J_2 = 7.6 Hz, 4H), 2.10 (dt, J_1 = 7.6 Hz, J_2 = 7.2 Hz, 4H), 1.68 (p, J = 7.6 Hz, 4H); ^{13}C NMR (75.5 MHz, $CDCl_3$, APT) δ 148.5, 138.1, 130.9, 129.9, 118.2, 115.1, 114.7, 111.3, 110.9, 50.3, 31.1, 26.2, 23.9; EIMS *m/z* 268.2 (M^+, 19), 213.1 (68), 159.1 ([M – C_8H_{13}]$^+$, 100), 145.1 (41), 116.1 (11), 89.0 (9); HRMS calcd for $C_{18}H_{24}N_2$ (M^+) 268.1939, found 268.1937.

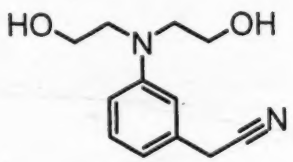

31c

3-[*N*,*N*-Bis(2-hydroxyethyl)amino]phenylacetonitrile (31c). (3-Aminophenyl)acetonitrile (**30**, 1.784 g, 13.50 mmol) was dissolved in methanol (25 mL) and cooled to –78 °C, and ethylene oxide (~ 13 mL) was added cold (–5 °C). The reaction vessel was sealed and allowed to warm to room temperature, and the mixture was stirred for 115 h. The reaction mixture was concentrated under vacuum to yield an orange oil, which was purified by flash chromatography (SiO_2, diethyl ether) to give **31c** (2.755 g, 93%) as a yellow oil. R_f = 0.1 (SiO_2, diethyl ether). IR (neat film) 3357, 2933, 2881, 2251 (C≡N), 1604, 1580, 1500, 1357, 1413, 1012, 770, 693 cm^{-1}; ^{1}H NMR (300 MHz, $CDCl_3$) δ 7.15 (t, J = 7.8 Hz, 1H), 6.6–6.5 (m, 3H), 4.27 (s br, 2H), 3.75 (t, J = 4.9 Hz, 4H), 3.61 (s, 2H), 3.49 (t, J = 4.9 Hz, 4H); ^{13}C NMR (75.5 MHz, $CDCl_3$, APT) δ 148.4, 130.9, 129.9, 118.3, 116.0, 111.9, 111.5, 60.3, 54.9, 23.8; EIMS *m/z* 220.1 (M^+, 24), 189.1 ([M – CH_2OH]$^+$, 100), 145.1 (62), 116.0 (15), 91.1 (9), 77.0 (5); HRMS calcd for $C_{12}H_{16}N_2O_2$ (M^+) 220.1212, found 220.1212.

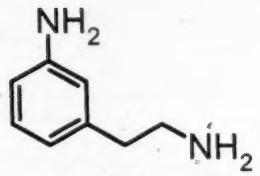

32

2-(3-Aminophenyl)ethylamine (32).[72] (3-Aminophenyl)acetonitrile (**30**, 0.827 g, 6.26 mmol) was dissolved in dry diethyl ether (50 mL) and added dropwise over 1.5 h into a slurry of lithium aluminum hydride (95%, 1.195 g, 29.92 mmol) and dry diethyl ether (50 mL), while cooling throughout addition in a cold water bath. An excess of $Na_2SO_4 \cdot 10H_2O$ was added portionwise, with continued cooling, until no further visible reaction occurred. The resulting mixture was filtered, and the solid mass was washed with diethyl ether, and the combined filtrate and washings were concentrated to give **32** (0.639 g, 75%) as a dark orange-brown oil.

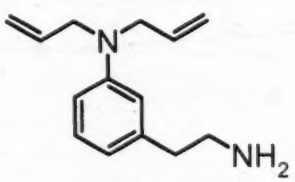

33a

2-(*N*,*N*-Diallyl-3-aminophenyl)ethylamine (33a). 3-(*N*,*N*-Diallylamino)phenylacetonitrile (**31a**, 1.107 g, 5.214 mmol) was dissolved in dry diethyl ether (80 mL), and added over 1.5 h, dropwise, into a slurry of lithium aluminum hydride (1.113 g, 29.33 mmol) in dry diethyl ether (80 mL). The mixture was stirred 5 min, and $Na_2SO_4 \cdot 10H_2O$ was added in excess, portionwise and while cooling in a water bath, until visible reactions had stopped. This mixture was filtered and concentrated to yield **33a** (1.082 g, 96%) as an orange oil. IR (CH_2Cl_2, cast) 3364, 3275, 3079, 2978, 2926, 2857,

1601, 1579, 1498, 1245, 1178, 990, 918, 772, 697 cm^{-1}; ^1H NMR (300 MHz, $CDCl_3$) δ 7.11 (t, J = 8.0 Hz, 1H), 6.6–6.4 (m, 3H), 5.84 (ddt, J_1 = 17 Hz, J_2 = 10 Hz, J_3 = 4.8 Hz, 2H), 5.16 (dd, J_1 = 17 Hz, J_2 = 1.5 Hz, 2H), 5.14 (dd, J_1 = 10 Hz, J_2 = 1.5 Hz, 2H), 3.90 (d, J = 4.8 Hz, 4H), 2.93 (t, J = 6.9 Hz, 2H), 2.66 (t, J = 6.9 Hz, 2H), 1.29 (s br, 2H); ^{13}C NMR (100.5 MHz, $CDCl_3$, APT) δ 148.7, 140.5, 133.9, 129.0, 116.8, 115.9, 112.8, 110.2, 52.8, 43.6, 40.6; EIMS *m/z* 216.6 (M^+, 92), 187.1 (86), 146.1 ([M – CH_2NH – C_3H_5]$^+$, 100), 118.1 (43), 91.1 (45), 77.0 (21); HRMS calcd for $C_{14}H_{20}N_2$ (M^+) 216.1626, found 216.1628.

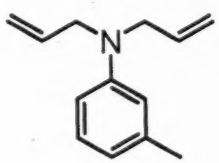

34

***N,N*-Diallyl-3-toluidine (34).**[57] 3-Toluidine (0.55 mL, 5.1 mmol) and allyl bromide (3.75 mL, 43.3 mmol) were dissolved in *N,N*-dimethylformamide (10 mL), and Na_2CO_3 (2.560 g, 24.16 mmol) was added. The resulting mixture was heated to reflux for 30 min, cooled to room temperature and filtered, and the solid mass was washed with diethyl ether (100 mL). The combined filtrate and washings were poured into water (80 mL), the layers were separated, and the aqueous portion was extracted with diethyl ether (3 × 100 mL). All organic portions were combined, washed with water, dried over Na_2SO_4, and concentrated to yield **34** (0.957 g, quantitative) as an orange oil.

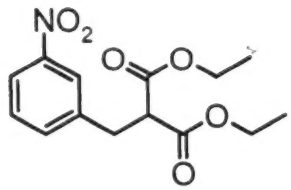

35

2-(3-Nitrobenzyl)malonic acid diethyl ester (35).[60] Diethyl malonate (9.623 g, 60.08 mmol) was dissolved in dry THF (100 mL) and the solution flushed with Ar, and sodium hydride (95%, 1.836 g, 72.70 mmol) was added portionwise to yield a clear solution after bubbling stopped. 3-nitrobenzylbromide (**28**, 5.612 g, 20.00 mmol of monobrominated product) was dissolved in dry THF (100 mL), and added over 2 h to the sodium malonate solution, over 1h30. The mixture was heated to reflux for 17 h, cooled to room temperature and filtered, and the solvent was removed from the filtrate. The residue was suspended in diethyl ether (250 mL) and washed with water (3 × 200 mL), the washings were back-extracted with diethyl ether (3 × 200 mL), and all organic portions were combined, dried over $MgSO_4$, and concentrated to yield 8.822 g of a yellow oil. Purification by flash chromatography (SiO_2, hexanes/diethyl ether 2:1) yielded **35** (4.298 g, 72%) as a pale yellow oil. $R_f = 0.5$ (SiO_2, hexanes/diethyl ether 2:1).

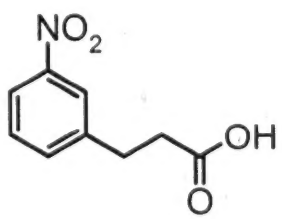

36

3-(3-Nitrophenyl)propionic acid (36).[61] 2-(3-Nitrobenzyl)malonic acid diethyl ester (**35**, 8.697 g, 29.45 mmol) was combined with concentrated hydrochloric acid (30 mL) and glacial acetic acid (2.6 mL), and the mixture was heated to reflux for 26 h. The reaction mixture was cooled to room temperature, filtered, and the solid mass was washed with water and air-dried to yield **36** (5.281 g, 92%) as a pale yellow powder.

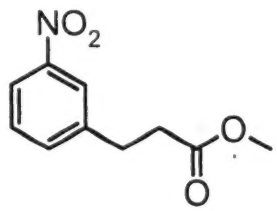

37

Methyl 3-(3-nitrophenyl)propionate (37).[73] 3-(3-Nitrophenyl)propionic acid (**36**, 2.229 g, 11.42 mmol) was dissolved in methanol (30 mL), and concentrated sulfuric acid (3 drops) were added. The solution was heated at reflux for 2h30, cooled to room temperature and poured into water (300 mL). The resulting mixture was extracted with diethyl ether (2 × 200 mL), and the extracts were dried over $MgSO_4$ and concentrated to afford **37** (2.394 g, quantitative) as a pale yellow oil.

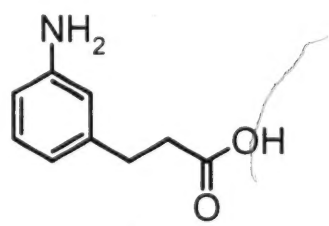

38

3-(3-Aminophenyl)propionic acid (38).[74] 3-(3-Nitrophenyl)propionic acid (**36**, 0.623 g, 3.19 mmol) was combined dry with Pd-C (73 mg, 69 μmol Pd), absolute ethanol (65 mL)

was added, and the mixture was stirred until the starting material had completely dissolved. The resulting suspension was shaken under 50 psi $H_{2(g)}$ for 30 min and filtered, and the filtrate was concentrated to yield **38** (0.526 g, quantitative) as a clear brown oil.

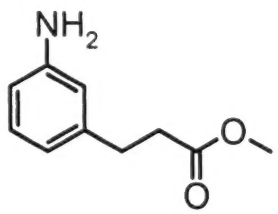

39

Methyl 3-(3-aminophenyl)propionate (39).[75] Methyl 3-(3-nitrophenyl)propionate (**37**, 2.389 g, 11.42 mmol) was combined with Pd-C (0.307 g, 289 μmol Pd), absolute ethanol (125 mL) was added, and the mixture was stirred until the starting material had completely dissolved. The resulting suspension was shaken under 50 psi $H_{2(g)}$ for 15 min and filtered, and the filtrate was concentrated to yield **39** (2.033 g, 99%) as an orange-brown oil.

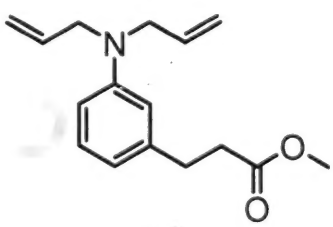

40a

Methyl 3-(*N*,*N*-diallyl-3-aminophenyl)propionate (40a). Methyl 3-(3-aminophenyl)propionate (**39**, 0.904 g, 5.05 mmol) and allyl bromide (3.75 mL, 43.3 mmol) were dissolved in *N*,*N*-dimethylformamide (10 mL), and Na_2CO_3 (2.554 g, 24.10

mmol) was added. The reaction mixture was heated at reflux for 30 min, cooled to room temperature and filtered, and the solid mass was washed with diethyl ether. Water (200 mL) was added to the combined filtrate and washings, and the aqueous solution was extracted with diethyl ether (3 × 250 mL). The combined organic portions were washed with water (3 × 300 mL), dried over $MgSO_4$, and concentrated to yield **40a** (0.927 g, 71%) as a yellow oil. R_f = 0.5 (SiO_2, hexane/acetone 3:1). IR (CH_2Cl_2, cast) 3080, 3005, 2979, 2950, 2861, 1739 (C=O), 1602, 1580, 1498, 1245, 1176, 990, 919, 773, 697 cm^{-1}; ^1H NMR (300 MHz, $CDCl_3$) δ 7.10 (t, J = 8.1 Hz, 1H), 6.6–6.4 (m, 3H), 5.85 (ddt, J_1 = 17 Hz, J_2 = 10 Hz, J_3 = 4.9 Hz, 2H), 5.16 (dd, J_1 = 17 Hz, J_2 = 1.8 Hz, 2H), 5.15 (dd, J_1 = 10 Hz, J_2 = 1.8 Hz, 2H), 3.90 (d, J = 4.9 Hz, 4H), 3.69 (s, 3H), 2.88 (t, J = 7.8 Hz, 2H), 2.61 (t, J = 7.8 Hz, 2H); ^{13}C NMR (150.9 MHz, $CDCl_3$, APT) δ 173.6, 148.9, 141.4, 134.0, 129.2, 116.2, 116.0, 112.2, 110.3, 52.7, 51.6, 35.8, 31.4; EIMS *m/z* 259.2 (M^+, 100), 232.1 (47), 172.1 (29), 158.1 (36), 91.1 (14), 77.0 (11); HRMS calcd for $C_{16}H_{21}NO_2$ (M^+) 259.1572, found 259.1572.

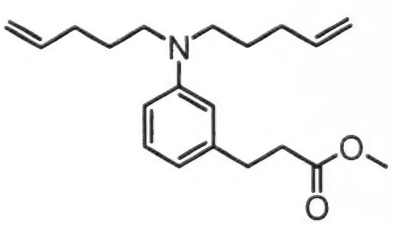

40b

Methyl 3-[*N,N*-bis(4-pentenyl)-3-aminophenyl]propionate (40b). Methyl 3-(3-aminophenyl)propionate (**39**, 2.358 g, 13.16 mmol) and 5-bromo-1-pentene (4.919 g, 33.00 mmol) were dissolved in *N,N*-dimethylformamide (15 mL), and Na_2CO_3 (6.716 g, 63.36 mmol) was added. The mixture was heated at reflux for 2 h, then more 5-bromo-1-

pentene (0.987 g, 6.62 mmol) was added and the mixture was heated at reflux for an additional 1 h. The reaction mixture was cooled to room temperature and filtered, and the solid mass washed with diethyl ether. Water (500 mL) was added to the combined filtrate and washings, and the aqueous solution was extracted with diethyl ether (3 × 200 mL). The combined organic portions were washed with water (3 × 250 mL), dried over $MgSO_4$, and concentrated to yield **40b** (3.437 g, 83%) as a yellow oil. R_f = 0.6 (SiO_2, hexane/acetone 3:1). IR (CH_2Cl_2, cast) 3076, 2947, 1739 (C=O), 1602, 1366, 1175, 992, 912, 771 cm^{-1}; ^1H NMR (300 MHz, $CDCl_3$) δ 7.09 (t, J = 8.0 Hz, 1H), 6.5–6.4 (m, 3H), 5.82 (ddt, J_1 = 17 Hz, J_2 = 10 Hz, J_3 = 6.6 Hz, 2H), 5.02 (dd, J_1 = 19 Hz, J_2 = 1.5 Hz, 2H), 4.98 (dd, J_1 = 10 Hz, J_2 = 1.8 Hz, 2H), 3.66 (s, 3H), 3.24 (t, J = 7.5 Hz, 4H), 2.87 (t, J = 8.0 Hz, 2H), 2.60 (t, J = 8.0 Hz, 2H), 2.07 (dt, J_1= 7.2 Hz, J_2 = 7.1 Hz, 4H), 1.65 (p, J = 7.5 Hz, 4H); ^{13}C NMR (75.5 MHz, $CDCl_3$, APT) δ 173.7, 148.3, 141.6, 138.2, 129.4, 115.4, 115.0, 111.8, 110.0, 51.6, 50.5, 35.9, 31.6, 31.3, 26.4; EIMS *m/z* 315.2 (M^+, 47), 260.2 (81), 206.1 ([M – CH_2=CHCH=CH_2 – CH_2=CHCHCH_3]$^+$, 100), 192.1 (28); HRMS calcd for $C_{20}H_{29}NO_2$ (M^+) 315.2198, found 315.2191.

40c

Methyl 3-[*N*,*N*-bis(2-hydroxyethyl)-3-aminophenyl]propionate (40c).[74] Methyl 3-(3-aminophenyl)propionate (**39**, 0.718 g, 4.00 mmol) was dissolved in methanol (15 mL) and cooled to –78 °C in a dry ice-acetone bath, and ethylene oxide (~ 4 mL) was added

cold (–5 °C). The reaction vessel was sealed and allowed to warm to room temperature, and the mixture was stirred for 120 h. The reaction mixture was concentrated under vacuum to yield **40c** (1.071 g, quantitative) as an amber oil.

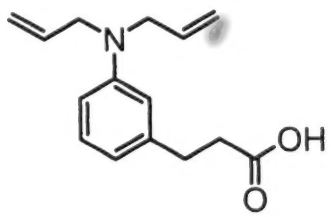

41a

3-(*N,N*-Diallyl-3-aminophenyl)propionic acid (41a). 3-(3-Aminophenyl)propionic acid (**38**, 0.444 g, 2.69 mmol) and allyl bromide (2.1 mL, 24 mmol) were dissolved in *N,N*-dimethylformamide (5.5 mL), and Na_2CO_3 (1.365 g, 63.36 mmol) was added. The mixture was heated at reflux for 40 min, cooled to room temperature and filtered, and the solid mass washed with diethyl ether. Water (80 mL) was added to the combined filtrate and washings, and the aqueous solution was extracted with diethyl ether (3 × 100 mL). The combined organic portions were washed with water, dried over $MgSO_4$, and concentrated to yield **41a** (0.410 g, 62%) as a pale yellow oil. IR (CH_2Cl_2, cast) 3080, 2979, 2916, 1709 (C=O), 1602, 1580, 1498, 1245, 1180, 990, 919, 772, 697 cm^{-1}; ^1H NMR (300 MHz, $CDCl_3$) δ 10.6 (s br, 1H), 7.12 (t, J = 7.8 Hz, 1H), 6.7–6.5 (m, 3H), 5.85 (ddt, J_1 = 17 Hz, J_2 = 10 Hz, J_3 = 4.9 Hz, 2H), 5.17 (dd, J_1 = 17 Hz, J_2 = 1.5 Hz, 2H), 5.16 (dd, J_1 = 10 Hz, J_2 = 1.5 Hz, 2H), 3.90 (d, J = 4.9 Hz, 4H), 2.89 (t, J = 7.8 Hz, 2H), 2.66 (t, J = 7.8 Hz, 2H); ^{13}C NMR (75.5 MHz, $CDCl_3$, APT) δ 179.2, 148.9, 141.1, 133.9, 129.3, 116.5, 116.3, 112.6, 110.8, 52.9, 35.7, 31.1; EIMS *m/z* 245.1 (M^+, 100), 218.1

(67), 172.1 (18), 158.1 (46), 91.1 (39), 77.0 (51); HRMS calcd for $C_{15}H_{19}NO_2$ (M^+) 245.1416, found 245.1414.

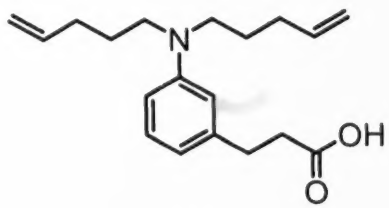

41b

3-[*N,N*-Bis(4-pentenyl)-3-aminophenyl]propionic acid (41b). Methyl 3-[*N,N*-bis(4-pentenyl)-3-aminophenyl]propionate (**40b**, 3.152 g, 9.991 mmol) and aqueous potassium hydroxide (5.661 g in 20 mL water) were combined and heated to reflux for 1h30. The mixture was cooled to room temperature, diluted with water (30 mL), acidified to pH ~ 2 with concentrated HCl and extracted with diethyl ether (4 × 250 mL). The extracts were dried over $MgSO_4$ and concentrated to afford **41b** (2.630 g, 87%) as a dark orange oil. IR (CH_2Cl_2, cast) 3076, 2934, 1709 (C=O), 1601, 1368, 1179, 992, 912, 770 cm^{-1}; ^1H NMR (300 MHz, $CDCl_3$) δ 7.11 (t, J = 7.8 Hz, 1H), 6.6–6.4 (m, 3H), 5.82 (ddt, J_1 = 17 Hz, J_2 = 10 Hz, J_3 = 7.0 Hz, 2H), 5.03 (dd, J_1 = 18 Hz, J_2 = 1.7 Hz, 2H), 4.98 (dd, J_1 = 10 Hz, J_2 = 1.7 Hz, 2H), 3.25 (t, J = 7.6 Hz, 4H), 2.89 (t, J = 7.9 Hz, 2H), 2.66 (t, J = 7.9 Hz, 2H), 2.08 (dt, J_1 = 7.0 Hz, J_2 = 7.0 Hz, 4H), 1.66 (p, J = 7.0 Hz, 4H); ^{13}C NMR (75.5 MHz, $CDCl_3$, APT) δ 179.1, 148.3, 141.3, 138.1, 129.4, 115.4, 115.1, 111.9, 110.2, 50.5, 35.7, 31.2; 26.3 (one coincident signal not observed); EIMS *m/z* 301.2 (M^+, 35), 246.1 ([M – CH_2=CHCHCH$_3$]$^+$, 100), 192.1 (96), 178.1 (28); HRMS calcd for $C_{19}H_{27}NO_2$ (M^+) 301.2042, found 301.2039.

General Procedure for Azo Coupling Reactions (43a,b, 44, 45a,b, 46a,b). 3,4-Dihydro-6-nitro-2(1*H*)-quinolinone (**12**, ~ 7 mmol) was suspended in aqueous base (~ 35 mmol NaOH in 10 mL water) and dioxane (15 mL) was added. The mixture was heated to reflux for 30 min, and concentrated under high vacuum. The resulting residue was dissolved in water (25 mL), and added dropwise, over 45 min, to a precooled (0 °C) solution of concentrated sulfuric acid (10 mL), water (5 mL), pyridine (0.5 mL) and $NaNO_2$ (1.4 g), while cooling during addition to maintain a temperature between 0 °C and 6 °C. This solution was stirred at 0 °C for 20 min, following which urea (5 g) was added, and the mixture stirred until foaming stopped (~ 30 min). The solution was filtered, and the filtrate cooled to 0 °C, and the desired aniline (~ 7 mmol) dissolved in pyridine (5 mL) was added over 20 min, dropwise, so as to maintain a temperature between 0 °C and 5 °C. A work up procedure appropriate to the solubility of the specific product was applied, as indicated below, along with specific reagent quantities.

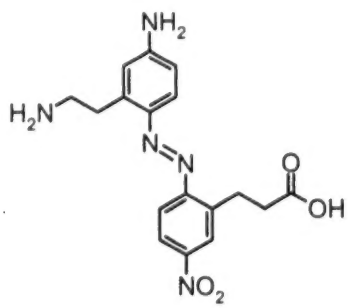

43a

4-Amino-2-(2-aminoethyl)-2′-(2-carboxyethyl)-4′-nitroazobenzene (43a). Compound **12** (1.353 g, 7.04 mmol) was dissolved in a mixture of dioxane (38 mL), NaOH (1.204 g, 30.10 mmol), and water (20 mL). The isolated residue was dissolved in water (24 mL) and added to a solution of conc H_2SO_4 (10.5 mL), water (5.1 mL), and $NaNO_2$ (1.003 g,

14.54 mmol), and the resulting diazonium salt was added to **32** (0.909 g, 6.67 mmol) in pyridine (30 mL). The reaction mixture was filtered, and the solid mass washed with a small amount of water and air-dried to yield a rusty red powder. This powder was stirred in 10% v/v aqueous ethanol (100 mL) for 30 min, filtered, washed with more water, then $CHCl_3$, and air-dried to afford **43a** (1.003 g, 42%) as an orange red powder. Mp >147 °C (dec). UV-Vis (MeOH) λ_{max} (ε) 392 (21700) nm; IR (uScope) 2925, 1588 (C=O), 1503, 1398, 1332, 1260, 1152 cm^{-1}; ^1H NMR (300 MHz, CD_3OD) δ 8.16 (d, J = 2.7 Hz, 1H), 8.05 (dd, J_1 = 9.0 Hz, J_2 = 2.7 Hz, 1H), 7.69 (d, J = 9.0 Hz, 1H), 7.35 (m, 2H), 7.09 (m, 1H), 3.16 (t, J = 7.4 Hz, 2H), 3.13 (t, J = 7.4 Hz, 2H), 2.96 (t, J = 7.6 Hz, 2H), 2.52 (t, J = 7.6 Hz, 2H); ^{13}C NMR (75.5 MHz, CD_3OD) δ 181.3, 145.4, 141.0, 135.1, 130.7, 130.3, 127.0, 126.9, 123.6, 119.2, 117.7, 117.3, 117.0, 43.1, 39.9, 37.5, 29.6; ESIMS *m/z* 358.2 ($[M+H]^+$, 100); EIMS *m/z* 329.1 ($[M–N_2]^+$, 1), 192.1 ($[M - C_8H_{11}N_3O]^+$, 100), 107.1 (35), 77.0 (20); HRMS calcd for $C_{17}H_{20}N_5O_4$ ($[M+H]^+$) 358.1515, found 358.1511.

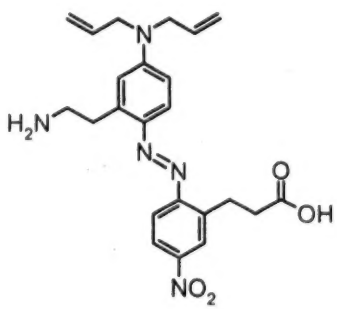

43b

4-Diallylamino-2-(2-aminoethyl)-2′-(2-carboxyethyl)-4′-nitroazobenzene (43b). Compound **12** (0.401 g, 2.09 mmol) was dissolved in a mixture of dioxane (12 mL), NaOH (0.405 g, 10.1 mmol) and water (6 mL). The isolated residue was dissolved in water (15 mL) and added to a solution of conc H_2SO_4 (3.0 mL), water (1.5 mL), $NaNO_2$

(0.310 g, 4.49 mmol), and pyridine (0.5 mL), and the resulting diazonium salt was added to **33a** (0.457 g, 2.11 mmol) in pyridine (10 mL). The reaction mixture was filtered, the solid mass washed with acetone, and air-dried to give **43b** (0.466 g) as a rust-red powder. The filtrate was concentrated under vacuum, washed with hexanes, dissolved in a minimum amount of acetone, diluted with water (2.5 equivalent volumes), filtered, and air-dried to give an additional 0.180 g of **43b** as a rust-red powder (net yield 0.646 g, 71%). Mp >155 °C (dec). UV-Vis (MeOH) λ_{max} (ε) 467 (21000) nm; IR (uScope) 3079, 2922, 1599 (C=O), 1513, 1382, 1336, 1233, 1080 cm^{-1}; ^1H NMR (300 MHz, CD_3OD) δ 8.26 (d, J = 2.1 Hz, 1H), 8.08 (dd, J_1 = 8.8 Hz, J_2 = 2.6 Hz, 1H), 7.81 (d, J = 9.3 Hz, 1H), 7.70 (d, J = 9.0 Hz, 1H), 6.75 (dd, J_1 = 9.2 Hz, 1H), 6.71 (d, J = 3.0 Hz, 1H), 5.92 (ddt, J_1 = 17 Hz, J_2 = 11 Hz, J_3 = 4.8 Hz, 2H), 5.21 (dd, J_1 = 9.3 Hz, J_2 = 1.5 Hz, 2H), 5.19 (dd, J_1 = 18 Hz, J_2 = 1.5 Hz, 2H), 4.10 (d, J = 4.8 Hz, 4H), 3.42 (t, J = 7.6 Hz, 4H), 3.23 (t, J = 7.8 Hz, 2H), 2.62 (t, J = 7.8 Hz, 2H); ^{13}C NMR (125 MHz, $(CD_3)_2SO$, APT) δ 173.6, 154.2, 152.3, 146.7, 141.6, 141.4, 140.1, 133.2, 125.7, 122.4, 117.7, 116.6, 116.5, 112.5, 111.8, 52.4, 40.7, 35.2, 30.0, 26.6; ESIMS *m/z* 438.2 ($[M+H]^+$, 100), 421.2 (12); HRMS calcd for $C_{23}H_{28}N_5O_4$ ($[M+H]^+$) 438.2141, found 438.2148.

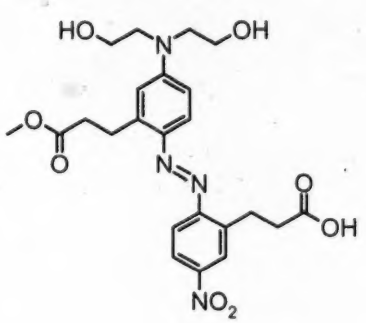

44

4-Bis(2-hydroxyethyl)amino-2-(methyl-2-carboxyethyl)-2′-(2-carboxyethyl)-4′-nitroazobenzene (44). Compound **12** (0.384 g, 2.00 mmol) was dissolved in a mixture of dioxane (10 mL), NaOH (0.381 g, 9.53 mmol) and water (6 mL). The isolated residue was dissolved in water (12 mL) and added to a solution of conc H_2SO_4 (2.9 mL), water (1.4 mL), $NaNO_2$ (0.394 g, 5.71 mmol) and pyridine (0.5 mL), and the resulting diazonium salt was added to **40c** (0.535 g, 2.00 mmol) in pyridine (2.5 mL). The reaction mixture was allowed to warm to room temperature, filtered and air-dried. The residue was dissolved in acetone and diluted with water, the acetone was removed, and the aqueous solution extracted with $CHCl_3$, dried over Na_2SO_4, and concentrated to yield **44** (0.489 g, 50%) as a dark purple-black powder. Mp 132–133 °C. UV-Vis (MeOH) λ_{max} (ε) 481 (29600) nm; IR (acetone, cast) 3290 (br, O–H), 2930, 1730 (C=O), 1598, 1515, 1336, 1198, 1153, 1078 cm^{-1}; ^1H NMR (400 MHz, $(CD_3)_2CO$) δ 8.31(d, J = 2.4 Hz, 1H), 8.15 (dd, J_1 = 8.8 Hz, J_2 = 2.8 Hz, 1H), 7.81(d, J = 9.2 Hz, 1H), 7.79 (d, J = 8.8 Hz, 1H), 6.84 (d, J = 2.8 Hz, 1H), 6.80 (dd, J_1 = 9.6 Hz, J_2 = 3.0 Hz, 1H), 4.17 (s br, 2H), 3.84 (t, J = 5.6 Hz, 4H), 3.74 (t, J = 5.8 Hz, 4H), 3.61(s, 3H), 3.49 (t, J = 7.6 Hz, 2H), 3.42 (t, J = 7.8 Hz, 2H), 2.78 (t, J = 7.8 Hz, 2H), 2.72 (t, J = 7.8 Hz, 2H); ^{13}C NMR (75.5 MHz, $(CD_3)_2CO$, APT) δ 173.9, 173.4, 155.6, 153.5, 147.8, 146.2, 142.4, 141.1, 126.6, 123.4, 118.6, 117.2, 113.0, 112.1, 60.1, 55.0, 51.6, 36.9, 35.6, 28.3, 27.8; EIMS *m/z* 488.2 (M^+, 6), 457.2 (24), 250.1 (24), 219.1 ($[M - C_{11}H_{13}N_2O_2]^+$, 100), 192.1 (68); HRMS calcd for $C_{23}H_{28}N_4O_8$ (M^+) 488.1907, found 488.1903. Anal. Calcd for $C_{23}H_{28}N_4O_8$: C, 56.55; H, 5.78; N, 11.47. Found: C, 56.39; H, 5.80; N, 10.96.

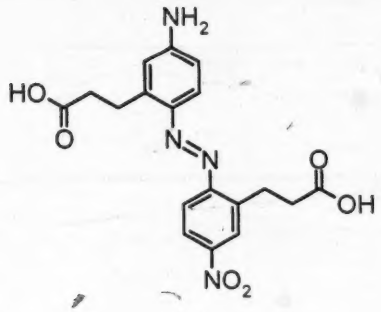

45a

4-Amino-2,2′-bis(2-carboxyethyl)-4′-nitroazobenzene (45a). Compound **12** (0.318 g, 1.66 mmol) was dissolved in a mixture of dioxane (9.5 mL), NaOH (0.333 g, 8.33 mmol) and water (4.8 mL). The isolated residue was dissolved in water (12 mL) and added to a solution of conc H_2SO_4 (2.4 mL), water (1.2 mL) and $NaNO_2$ (0.258 g, 3.74 mmol), and the resulting diazonium salt was added to **38** (0.277 g, 1.68 mmol) in pyridine (8 mL). The reaction mixture was allowed to warm to ~ 15 °C, filtered, and the solid mass washed with a small amount of water, then $CHCl_3$, and air-dried to give **45a** (0.421 g, 66%) as an orange-red powder. Mp >139 °C (dec). UV-Vis (MeOH) λ_{max} (ε) 497 (28700) nm; IR (uScope) 3195, 3037, 2964, 1703 (C=O), 1593, 1514, 1341, 1205, 1160, 746 cm^{-1}; ^1H NMR (300 MHz, $(CD_3)_2SO$) δ 12.2 (s br, 2H), 8.16 (d, J = 2.4 Hz, 1H), 8.10 (dd, J_1 = 9.0 Hz, J_2 = 2.4 Hz, 1H), 7.77 (d, J = 9.0 Hz, 1H), 7.36 (m, 1H), 7.30 (m, 1H), 7.05 (bs, 1H), 3.12 (t, J = 7.6 Hz, 2H), 2.85 (t, J = 7.6 Hz, 2H), 2.59 (t, J = 7.6 Hz, 2H), 2.56 (t, J = 7.6 Hz, 2H); ^{13}C NMR (125.7 MHz, $(CD_3)_2SO$, BB) δ 173.8, 173.7, 154.6, 154.5, 149.6, 144.7, 142.5, 141.6, 129.5, 125.6, 123.6, 123.5, 122.9, 115.2, 35.1, 34.2, 30.4, 29.6; ESIMS(–) *m/z* 385.1 ($[M–H]^-$, 100); EIMS *m/z* 192.1 ($[M - C_{11}H_9N_2O_2]^+$,

100), 164.1 (49), 91.1 (37), 77.0 (24); HRMS calcd for $C_{18}H_{17}N_4O_6$ ([M–H]$^-$): 385.1143, found 385.1144.

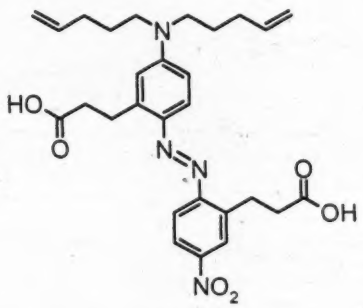

45b

4-Bis(4-pentenyl)amino-2,2′-bis(2-carboxyethyl)-4′-nitroazobenzene (45b). Compound **12** (1.364 g, 7.10 mmol) was dissolved in a mixture of dioxane (15 mL), NaOH (1.412 g, 35.30 mmol) and water (10 mL). The isolated residue was dissolved in water (25 mL) and added to a solution of conc H_2SO_4 (10 mL), water (5.2 mL), $NaNO_2$ (1.410 g, 20.44 mmol) and pyridine (0.5 mL), and the resulting diazonium salt was added to **41b** (2.138 g, 7.09 mmol) in pyridine (5 mL). The reaction mixture was stirred 10 min at 0 °C, allowed to warm to room temperature, and diluted with acetone (400 mL) and water (150 mL). The acetone was removed under aspirator vacuum, and the resulting aqueous suspension was filtered, washed with water, and air-dried to give **45b** (2.792 g, 75%) as a dark purple-black powder. Mp 157 °C. R_f = 0.3 (SiO_2, hexane/acetone/acetic acid 15:5:1). UV-Vis (MeOH) λ_{max} (ε) 499 (34800) nm; IR ($CHCl_3$, cast) 2927, 1708 (C=O), 1599, 1575, 1335, 1256, 912, 837 cm^{-1}; ^{1}H NMR (400 MHz, $(CD_3)_2CO$)) δ 8.32 (d, J = 2.7 Hz, 1H), 8.15 (dd, J_1 = 8.9 Hz, J_2 = 2.7 Hz, 1H), 7.84 (d, J = 9.6 Hz, 1H), 7.81(d, J = 8.9 Hz, 1H), 6.82 (d, J = 2.8 Hz, 1H), 6.74 (dd, J_1 = 9.6 Hz, J_2 = 2.8 Hz, 1H), 5.92 (ddt, J_1 = 17 Hz, J_2 = 10 Hz, J_3 = 7.0 Hz, 2H), 5.09 (dd, J_1 = 17 Hz, J_2 = 2.1 Hz, 2H),

5.00 (dd, J_1 = 10 Hz, J_2 = 2.1 Hz, 2H), 3.54 (t, J = 7.7 Hz, 4H), 3.50 (t, J = 7.7 Hz, 2H), 3.44 (t, J = 7.7 Hz, 2H), 2.80 (t, J = 7.7 Hz, 2H), 2.74 (t, J = 7.7 Hz, 2H), 2.18 (dt, J_1 = 7.4 Hz, J_2 = 7.0 Hz, 4H), 1.80 (p, J = 7.7 Hz, 4H); ^{13}C NMR (75.5 MHz, $(CD_3)_2CO$, APT) δ 174.0, 173.7, 155.7, 153.0, 148.0, 146.7, 142.2, 141.0, 138.9, 126.6, 123.4, 118.8, 117.2, 115.5, 112.7, 111.6, 51.1, 36.6, 35.6, 31.7, 28.2, 27.8, 27.3; EIMS *m/z* 522.2 (M^+, 3), 192.1 (47), 189.1 ([M – $C_{17}H_{21}N_2O_5$]$^+$, 100); HRMS calcd for $C_{28}H_{34}N_4O_6$ (M^+) 522.2479, found 522.2477. Anal. Calcd for $C_{28}H_{34}N_4O_6$: C, 64.35; H, 6.56; N, 10.72. Found: C, 64.22; H, 6.52; N, 10.46.

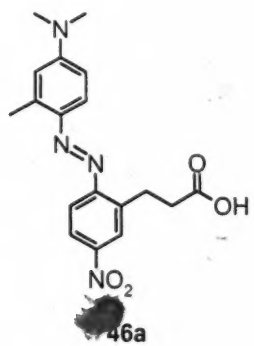

46a

4-Dimethylamino-2-methyl-2′-(2-carboxyethyl)-4′-nitroazobenzene (46a). Compound **12** (0.397 g, 2.06 mmol) was dissolved in a mixture of dioxane (12 mL), NaOH (0.386 g, 5.59 mmol) and water (6 mL). The isolated residue was dissolved in water (10 mL) and added to a solution of conc H_2SO_4 (3.0 mL), water (1.5 mL), $NaNO_2$ (0.307 g, 4.45 mmol) and pyridine (0.5 mL), and the resulting diazonium salt was added to **23** (0.274 g, 2.02 mmol) in pyridine (10 mL). The reaction mixture was filtered and the solid mass washed with water and air-dried to give **46a** (0.471 g, 65%) as a purple-black powder. Mp 204–206 °C. UV-Vis (MeOH) λ_{max} (ε) 479 (27200) nm; IR (uScope) 2911, 2667, 1702 (C=O), 1600, 1516, 1441, 1428, 1274, 1197, 1081, 893, 825 cm^{-1}; ^{1}H

NMR (300 MHz, $(CD_3)_2CO$)) δ 8.32 (d, J = 2.5 Hz, 1H), 8.16 (dd, J_1 = 8.9 Hz, J_2 = 2.5 Hz, 1H), 7.82 (d, J = 10 Hz, 1H), 7.80 (d, J = 8.9 Hz, 1H), 6.71_8 (d, J = 2.8 Hz, 1H), 6.71_7 (dd, J_1 = 10 Hz, J_2 = 2.8 Hz, 1H), 3.50 (t, J = 7.6 Hz, 2H), 3.15 (s, 6H), 2.79 (t, J = 7.6 Hz, 2H), 2.72 (s, 3H); ^{13}C NMR (75.5 MHz, $(CD_3)_2SO$, APT) δ 173.5, 154.3, 153.4, 146.4, 142.4, 141.8, 139.6, 125.5, 122.6, 117.5, 116.3, 112.4, 110.5, 34.9, 26.5, 17.9 (signal for $-N(\mathbf{C}H_3)_2$ not observed); EIMS *m/z* 356.1 (M^+, 43), 297.1 (12), 192.1 (10), 149.1 (53), 134.1 ([M – N_2 – $C_6H_4(CH_2CH_2COOH)NO_2]^+$, 100), 91.1 (20), 77.0 (10); HRMS calcd for $C_{18}H_{20}N_4O_4$ (M^+) 356.1485, found 356.1483.

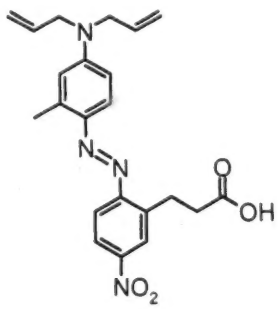

46b

4-Diallylamino-2-methyl-2′-(2-carboxyethyl)-4′-nitroazobenzene (46b). Compound **12** (0.399 g, 2.08 mmol) was dissolved in a mixture of dioxane (12 mL), NaOH (0.392 g, 9.80 mmol) and water (6 mL). The isolated residue was dissolved in water (15 mL) and added to a solution of conc H_2SO_4 (3.0 mL), water (1.5 mL), $NaNO_2$ (0.308 g, 4.46 mmol) and pyridine (0.5 mL), and the resulting diazonium salt was added to **34** (0.400 g, 2.14 mmol) in pyridine (10 mL). The reaction mixture was stirred 5 min, filtered, air-dried, and washed with a small amount of hexane. The residue was dissolved in the minimum amount of acetone, and water (2 equivalent volumes) were added. The acetone was evaporated from the solution, and the resulting suspension was filtered and air-dried

to give **46b** (0.451 g, 53%) as a dark purple-red microcrystalline solid. Mp 147–148 °C. UV-Vis (MeOH) λ_{max} (ε) 474 (34100) nm; IR (uScope) 3017, 2920, 1707 (C=O), 1597, 1510, 1377, 1332, 1235, 1198, 1079, 918, 837 cm^{-1}; ^1H NMR (300 MHz, $(CD_3)_2CO$)) δ 8.30 (d, J = 2.6 Hz, 1H), 8.14 (dd, J_1 = 8.9 Hz, J_2 = 2.6 Hz, 1H), 7.77 (d, J = 8.9 Hz, 2H), 6.73 (d, J = 3.0 Hz, 1H), 6.69 (dd, J_1 = 8.9 Hz, J_2 = 3.0 Hz, 1H), 5.94 (ddt, J_1 = 18 Hz, J_2 = 10 Hz, J_3 = 5.0 Hz, 2H), 5.23 (dd, J_1 = 9.5 Hz, J_2 = 1.6 Hz, 2H), 5.22 (dd, J_1 = 18 Hz, J_2 = 1.6 Hz, 2H), 4.12 (d, J = 4.8 Hz, 4H), 3.48 (t, J = 7.6 Hz, 2H), 2.78 (t, J = 7.6 Hz, 2H), 2.68 (s, 3H); ^{13}C NMR (125.3 MHz, $(CD_3)_2CO$, APT) δ 173.7, 155.6, 153.4, 148.0, 143.6_0, 143.5_5, 141.0, 134.1, 126.6, 123.3, 118.6, 117.3, 116.7, 113.7, 111.7, 53.4, 35.6, 27.8, 18.4; EIMS *m/z* 408.2 (M^+, 52), 349.2 (12), 201.1 (41), 192.1 ($[M - C_{13}H_{16}N_2O]^+$, 100), 186.1 (28), 91.1 (31), 77.0 (23); HRMS calcd for $C_{22}H_{24}N_4O_4$ (M^+) 408.1798, found 408.1786.

Metathesis Polymerization of 4-bis(4-pentenyl)amino-2,2′-bis(2-carboxyethyl)-4′-nitroazobenzene (44c). 4-bis(4-pentenyl)amino-2,2′-bis(2-carboxyethyl)-4′-nitroazobenzene (**45b**, 0.501 g, 959 μmol) and tricyclohexylphosphine[1,3-bis(2,4,6-trimethylphenyl)-4,5-dihydroimidazol-2-ylidene][benzylidene]ruthenium (IV) dichloride (**48**, 31 mg, 37 μmol) were combined dry, and the containing flask was cycled from high vacuum to an Ar atmosphere five times before adding dry benzene (5 mL). The mixture was kept at a temperature just under reflux for 115 h, and the solvent was removed under high vacuum. The residue was dissolved in freshly-distilled THF and concentrated under vacuum to give 0.480 g (90%) of oligomeric material as a dark purple-black powder with a yellow-green reflective tinge. UV-Vis (MeOH) λ_{max} 491 nm; IR (CH_2Cl_2) 3646, 2959, 2927, 1705 (C=O), 1597, 1518, 1383, 1336, 1260, 1197, 1080, 1025, 804 cm^{-1}; ^1H NMR

(400 MHz, $(CD_3)_2CO$)) δ 10.7 (s br, 4H), 8.31 (d, J = 2.8 Hz, 2H), 8.15 (dd, J_1 = 8.6 Hz, J_2 = 2.2 Hz, 2H), 8.10 (m, 1H), 7.83 (m, 4H), 7.24 (m, 3H), 7.15 (m, 5H), 6.83 (m, 2H), 6.73 (m, 2H), 5.92 (ddt, J_1 = 16 Hz, J_2 = 10 Hz, J_3 = 6.8 Hz, 2H), 5.53 (m, 3H), 5.09 (dd, J_1 = 16 Hz, J_2 = 2.0 Hz, 2H), 5.00 (dd, J_1 = 10 Hz, J_2 = 2.0 Hz, 2H), 3.6-0.8 (m, ~70H); ^{13}C NMR (75.5 MHz, $(CD_3)_2SO$, BB) δ 188.1, 187.8, 168.6, 165.9, 160.6, 159.7, 155.1, 153.9, 144.3, 173.8, 139.8, 139.2, 137.8_5, 137.8_0, 137.0, 136.9, 132.0, 130.3, 129.5, 125.6, 124.9, 81.3, 64.1, 50.2, 49.2, 48.7, 44.7, 43.9, 43.5, 41.2, 41.0, 40.8, 40.5, 40.1, 39.4, 38.5, 31.5; MALDI-TOF (retinoic acid/THF) *m/z* 5470 (2), 4970 (3), 4450 (4), 3970 (5), 3480 (7), 2980 (10), 2490 (22), 1990 (34), 1510 (50), 1020 (50).

Preparation of Thin Films for NLO Studies. Samples of the polymer (~ 100 mg) were dissolved in the desired solvent (1 mL), filtered through a 0.22 μm Teflon filter, and cast onto a stationary glass plate, pre-coated with a layer of indium tin oxide (ITO). In the case of THF as a solvent, the casts were allowed to evaporate at room temperature; the other casts were dried in a closed chamber in the presence of concentrated sulfuric acid to accelerate evaporation of the basic solvents. In preparation for poling, a gold electrode was sputtered onto the film surface, and standard photolithography processes were used to generate a waveguide on the ITO plate. Poling was attempted at the apparent glass transition temperature of the oligomeric material, ~ 100 °C, under standard conditions.

Bibliography

1. Stucky, G.D.; Marder, S.R.; Sohn, J.E. In *Materials for Nonlinear Optics: Chemical Perspectives*; Marder, S.R., Sohn, J.E., Stucky, G.D., Eds.; ACS Symposium Series 455; American Chemical Society: Washington, DC, 1991; pp 2-30.
2. (a) Zernike, F., Midwinter, J.E.; *Applied Nonlinear Optics*; John Wiley & Sons: New York, NY, 1973. (b) Kaminow, I.P. In *An Introduction to Electrooptic Devices*; Kaminow, I.P., Ed.; Academic Press: New York, NY, 1974; pp 1-70. (c) Prasad, P.N., Williams, D.J.; *Introduction to Nonlinear Optical Effects in Molecules & Polymers*; John Wiley & Sons: New York, NY, 1991.
3. Williams, D.J. *Angew. Chem. Int. Ed. Engl.* **1984**, *23*, 690-703.
4. Williams, D.J. In *Nonlinear Optical Properties of Organic and Polymeric Materials*; Williams, D.J., Ed.; ACS Symposium Series 233; American Chemical Society: Washington, DC, 1983; pp ix-xi.
5. *Organic Nonlinear Optical Materials*; Bosshard, Ch., Sutter, K., Prêtre, Ph., Hulliger, J., Flörsheimer, M., Kaatz, P., Günter, P.; Gordon and Breach Publishers: Switzerland, 1995.
6. Meredith, G.R.; Vandusen, J.G.; Williams, D.J. In *Nonlinear Optical Properties of Organic and Polymeric Materials*; Williams, D.J., Ed.; ACS Symposium Series 233; American Chemical Society: Washington, DC, 1983; pp 109-133.
7. Marder, S.R.; Perry, J.W. *Science* **1994**, *263*, 1706-1707.
8. Davey, M.H.; Lee, V.Y.; Wu, L.-M.; Moylan, C.R.; Volksen, W.; Knoesen, A.; Miller, R.D.; Marks, T.J. *Chem. Mater.* **2000**, *12*, 1679-1693.

9. Sui, Y.; Lu, J.-X.; Yin, J.; Wang, D.; Zhu, Z.-K.; Wang, Z.-G. *J. Appl. Polym. Sci.* **2002**, *85*, 944-949.

10. Artal, C.; Ros, M.B.; Serrano, J.L.; Pereda, N.; Etxebarria, J.; Folcia, C.L.; Ortega, J. *Macromolecules* **2001**, *34*, 4244-4255.

11. Zhang, C.; Wang, C.; Dalton, L.R.; Zhang, H.; Steier, W.H. *Macromolecules* **2001**, *34*, 253-261.

12. Takase, H.; Natansohn, A.; Rochon, P. *J. Polym. Sci. B: Polym. Phys.* **2001**, *39*, 1686-1696.

13. Serhatli, İ.E.; Yagci, Y.; Hattemer, E.; Zentel, R.; Schmälzlin, E.; Hohenadl, S.; Bräuchle, C.; Meerholz, K. *J. Polym. Sci. A: Polym. Chem.* **2001**, *39*, 1589-1595.

14. Hernández, S.; Ogawa, T. *Polym. Bull.* **2001**, *47*, 127-134.

15. Zhang, C.; Wang, C.; Yang, J.; Dalton, L.R.; Sun, G.; Zhang, H.; Steier, W.H. *Macromolecules* **2001**, *34*, 235-243.

16. Wei, S.; Zhenyu, Z.; Qiwei, P.; Qingtian, G.; Lina, Y.; Changshui, F.; Dong, X.; Hongzhen, W.; Jinzhong, Y. *Macromolecules* **2001**, *34*, 2002-2007.

17. Kuo, W.-J.; Hsiue, G.-H.; Jeng, R.-J. *J. Mater. Chem.* **2002**, *12*, 868-878.

18. Liu, C. *Eur. Phys. J. D* **2002**, *19*, 45-48.

19. Iftime, G.; Labarthet, F.L.; Natansohn, A.; Rochon, P.; Murti, K. *Chem. Mater.* **2002**, *14*, 168-174.

20. Prins, L.J.; Reinhoudt, D.N.; Timmerman, P. *Angew. Chem. Int. Ed.* **2001**, *40*, 2382-2426; p 2385.

21. Atwood, J.L.; Hamada, F.; Robinson, K.D.; Orr, G.W.; Vincent, R.L. *Nature*

1991, *349*, 683-684.

22. Bell, D.A.; Anslyn, E.V. *J. Org. Chem.* **1994**, *59*, 512-514.
23. Schmuck, C.; Wienand, W. *Angew. Chem. Int. Ed.* **2001**, *40*, 4363-4369.
24. Prins, L.J.; Reinhoudt, D.N.; Timmerman, P. *Angew. Chem. Int. Ed.* **2001**, *40*, 2382-2426; pp 2387-2391.
25. Kyogoku, Y.; Lord, R.C.; Rich, A. *Proc. Natl. Acad. Sci. USA* **1967**, *57*, 250-257.
26. Jorgensen, W.L.; Pranata, J. *J. Am. Chem. Soc.* **1990**, *112*, 2008-2010.
27. Pranata, J.; Wierschke, S.G.; Jorgensen, W.L. *J. Am. Chem. Soc.* **1991**, *113*, 2810-2819.
28. Murray, T.J.; Zimmerman, S.C. *J. Am. Chem. Soc.* **1992**, *114*, 4010-4011.
29. Sartorius, J.; Schneider, H.-J. *Chem. Eur. J.* **1996**, *2*, 1446-1452.
30. Nadin, A.; Derrer, S.; McGeary, R.P.; Goodman, J.M.; Raithly, P.R.; Holmes, A.B. *J. Am. Chem. Soc.* **1995**, *117*, 9768-9769.
31. Bisson, A.P.; Hunter, C.A. *Chem. Commun.* **1996**, 1723-1724.
32. Adams, H.; Carver, F.J.; Hunter, C.A.; Morales, J.C.; Seward, E.M. *Angew. Chem. Int. Ed. Engl.* **1996**, *35*, 1542-1544.
33. Gong, B.; Yan, Y.; Zeng, H.; Skrzypczak-Jankunn, E.; Kim, Y.W.; Zhu, J.; Ickes, H. *J. Am. Chem. Soc.* **1999**, *121*, 5607-5608.
34. Zeng, H.; Miller, R.S.; Flowers II, R.A.; Gong, B. *J. Am. Chem. Soc.* **2000**, *122*, 2635-2644.
35. Taylor, R.; Kennard, O.; Versichel, W. *J. Am. Chem. Soc.* **1984**, *106*, 244-248.
36. Ducharme, Y.; Wuest, J.D. *J. Org. Chem.* **1988**, *53*, 5787-5789.
37. Fenlon, E.E.; Murray, T.J.; Baloga, M.H.; Zimmerman, S.C. *J. Org. Chem.*

1993, *58*, 6625-6628.

38. Beijer, F.H.; Kooijman, H.; Spek, A.L.; Sijbesma, R.P.; Meijer, E.W. *Angew. Chem. Int. Ed.* **1998**, *37*, 75-78.

39. Beijer, F.H.; Sijbesma, R.P.; Kooijman, H.; Spek, A.L.; Meijer, E.W. *J. Am. Chem. Soc.* **1998**, *120*, 6761-6769.

40. (a) Zaccaro, J.; Lorut, F.; Ibanez, A. *J. Mater. Chem.* **1999**, *9*, 1091-1095. (b) Ratajczak, H.; Baran, J.; Barycki, J.; Debrus, S.; May, M.; Pietraszko, A.; Ratajczak, H.M.; Tramer, A.; Venturini, J. *J. Mol. Struct.* **2000**, *555*, 149-158. (c) Rai, R.N.; Lan, C.W. *J. Mater. Res.* **2002**, *17*, 1587-1591.

41. Wang, C.; Zhang, C.; Lee, M.S.; Dalton, L.R.; Zhang, H.; Steier, W.H. *Macromolecules* **2001**, *34*, 2359-2363

42. Kato, T.; Mizoshita, N.; Kanie, K. *Macromol. Rapid Commun.* **2001**, *22*, 797-814.

43. For example, (a) Hua, J.; Luo, J.; Qin, J.; Shen, Y.; Zhang, Y.; Lu, Z. *J. Mater. Chem.* **2002**, *12*, 863-867. (b) Altomare, A.; Ciardelli, F.; Gallot, B.; Mader, M.; Solaro, R.; Tirelli, N. *J. Polym. Sci. A: Polym. Chem.* **2001**, *39*, 2957-2977.

44. de Milt, C.; van Zandt, G. *J. Am. Chem. Soc.* **1936**, *58*, 2044-2046.

45. Boudreau, J.A.; Williams, A. *J. Chem. Soc. Perkin Trans. 2* **1977**, 2028-2032.

46. Desos, P.; Schlewer, G.; Wermuth, C.G. *Heterocycles* **1989**, *28*, 1085-1099.

47. Ames, G.R.; Davey, W. *J. Chem. Soc.* **1958**, 1794-1799.

48. Page, G.A.; Tarbell, D.S. *Org. Synt. Coll. Vol. IV* **1963**, 136-140.

49. (a) Ruediger, E.H.; Gandhi, S.S.; Gibson, M.S.; Fărcaşiu, D.; Uncuţa, C. *Can. J. Chem.* **1986**, *64*, 577-579. (b) Migachev, G.I.; Terent'ev, A.M. *Chem.*

Heterocycl. Compd. (Engl. Transl.) **1981**, *17*, 295-298.

50. Godfrey, K.E.; Thrift, R.I. *J. Chem. Soc. C* **1967**, 400-404.
51. Horning, E.C.; Schock, R.U. *J. Am. Chem. Soc.* **1948**, *70*, 2945-2949.
52. Manring, L.E.; Peters, K.S. *J. Am. Chem. Soc.* **1985**, *107*, 6452-6458.
53. Thomas, D.G.; Billman, J.H.; Davis, C.E. *J. Am. Chem. Soc.* **1946**, *68*, 895-896.
54. Bowden, K.; Cook, R.S. *J. Chem. Soc. B* **1968**, 1529-1533.
55. Olah, G.A.; Pavlath, A.E.; Olah, J.A.; Herr, F. *J. Org. Chem.* **1957**, *22*, 879-881.
56. Arenz, C.; Giannis, A. *Eur. J. Org. Chem.* **2001**, 137-140.
57. Bailey, W.F.; Carson, M.W. *J. Org. Chem.* **1998**, *63*, 9960-9967.
58. Hall, D.G.; Tailor, J.; Gravel, M. *Angew. Chem. Int. Ed.* **1999**, *38*, 3064-3067.
59. Nystrom, R.F. *J. Am. Chem. Soc.* **1955**, *77*, 2544-2545.
60. Citterio, A.; Sebastiano, R.; Marion, A. *J. Org. Chem.* **1991**, *56*, 5328-5335.
61. Beugelmans, R.; Singh, G.P.; Bois-Choussy, M.; Chastanet, J.; Zhu, J. *J. Org. Chem.* **1994**, *59*, 5535-5542.
62. Vogel, A.I. *J. Chem. Soc.* **1948**, 624-644.
63. Trnka, T.M.; Grubbs, R.H. *Acc. Chem. Res.* **2001**, *34*, 18-29.
64. Evans, P.E.; Grigg, R.; Monteith, M. *Tetrahedron Lett.* **1999**, *40*, 5247-5250.
65. Lehman, S.E.; Wagener, K.B. *Macromolecules* **2002**, *35*, 48-53.
66. Kuroda, Y.; Lee, H.; Kuwae, A. *J. Phys. Chem.* **1980**, *84*, 3417-3423.
67. Ahn, Y.M.; Yang, K.; Georg, G.I. *Org. Lett.* **2001**, *3*, 1411-1413.
68. Gowda, S.; Gowda, D.C. *Tetrahedron* **2002**, *58*, 2211-2213.
69. Harwood, H.J.; Pyriadi, T.H. *J. Org. Chem.* **1971**, *36*, 821-823.
70. Goswami, S.; Mahapatra, A.K. *Tetrahedron Lett.* **1998**, *39*, 1981-1984.
71. Mathieson, D.W.; Newbery, G. *J. Chem. Soc.* **1949**, 1133-1137.

72. Kornblum, N.; Iffland, D.C. *J. Am. Chem. Soc.* **1949**, *71*, 2137-2143.

73. Bordwell, F.G.; Scamehorn, R.G.; Springer, W.R. *J. Am. Chem. Soc.* **1969**, *91*, 2087-2093.

74. Skinner, W.A.; Schelstraete, M.G.M.; Baker, B.R. *J. Org. Chem.* **1961**, *26*, 1554-1557.

75. Suzuki, M.; Koyano, H.; Noyori, R.; Hashimoto, H.; Negishi, M.; Ichikawa, A.; Ito, S. *Tetrahedron* **1992**, *48*, 2635-2658.

Appendix A – Nuclear Magnetic Resonance Spectra

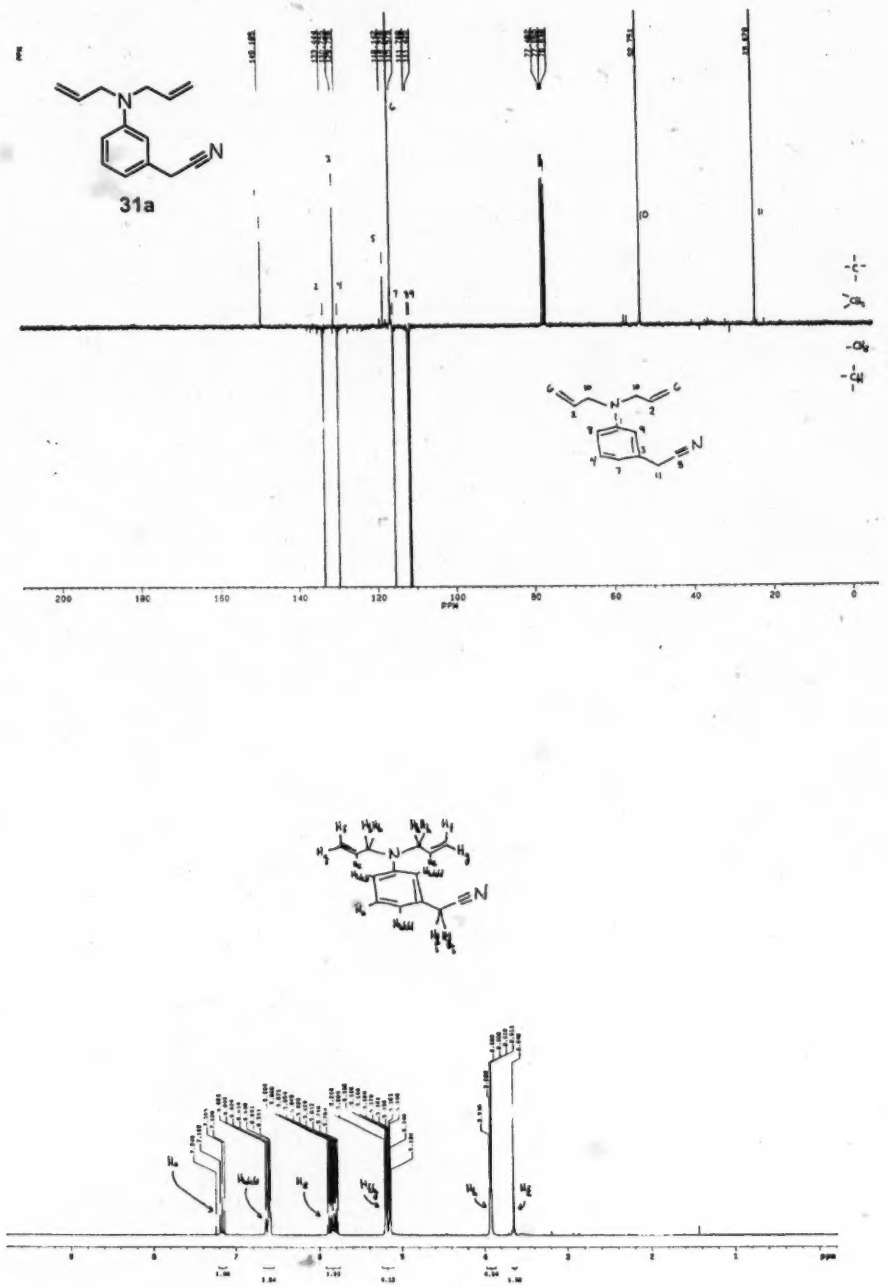

Figure A.1 ^{13}C and ^{1}H NMR spectra of compound **31a**

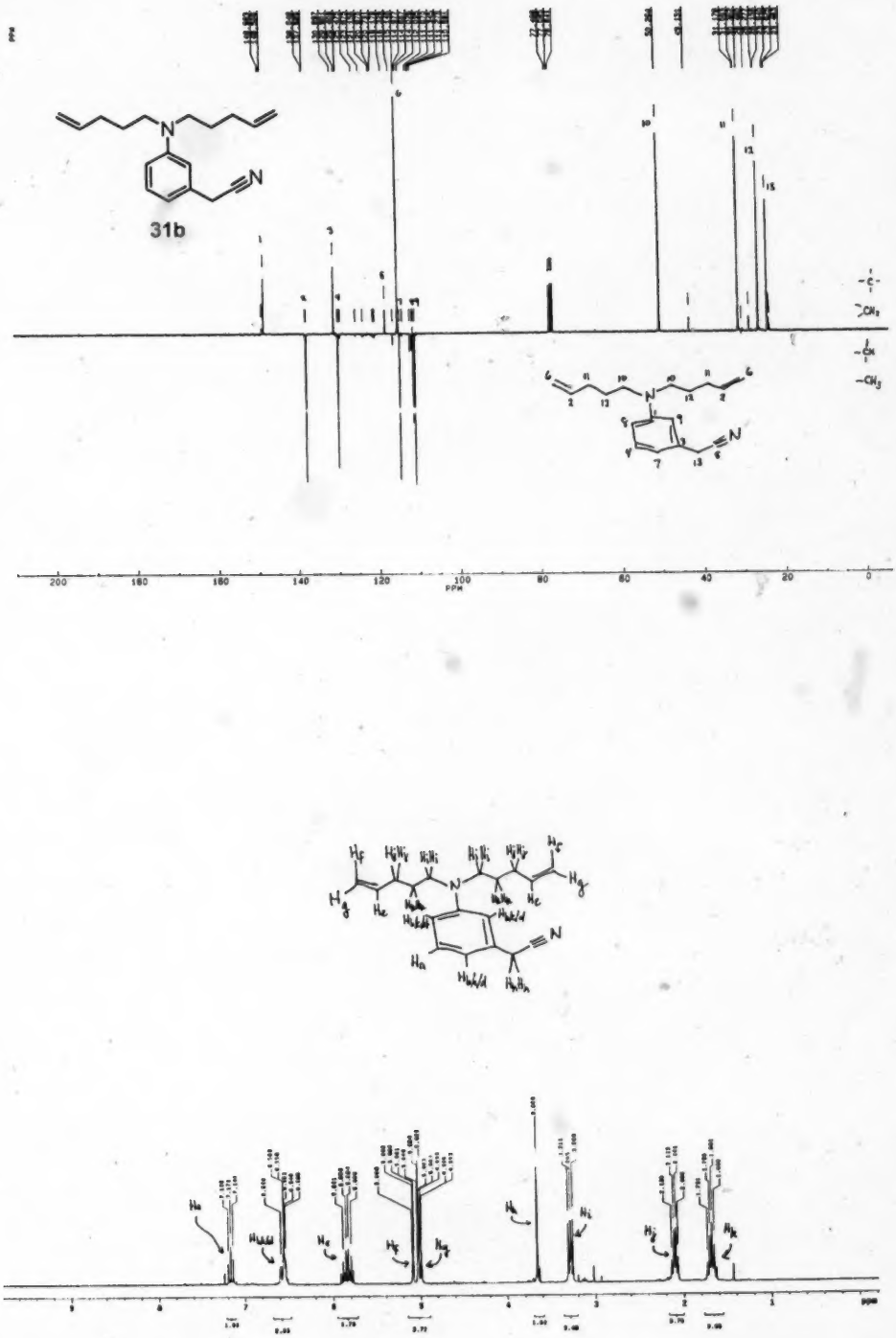

Figure A.2 ^{13}C and ^{1}H NMR spectra of compound **31b**

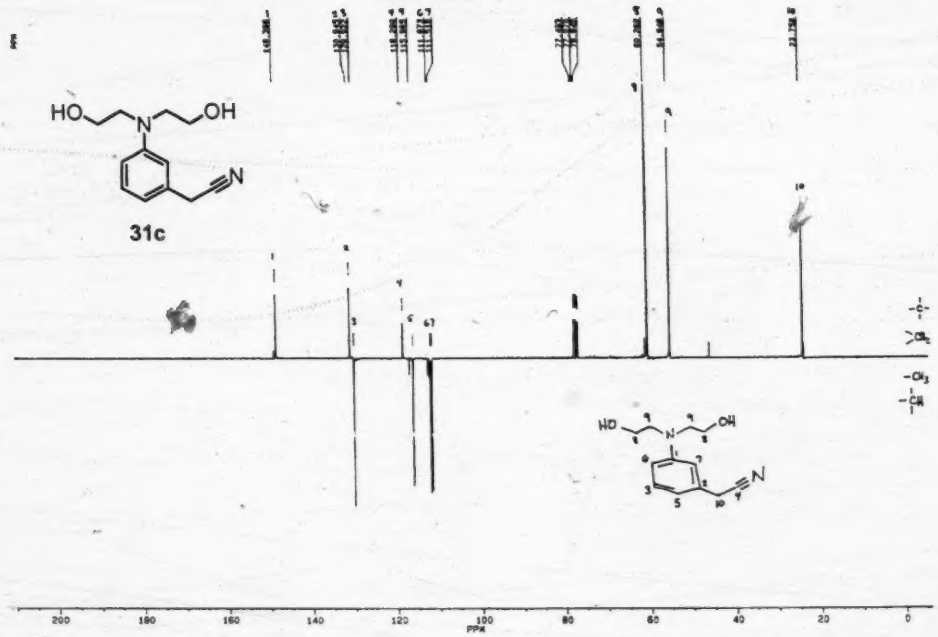

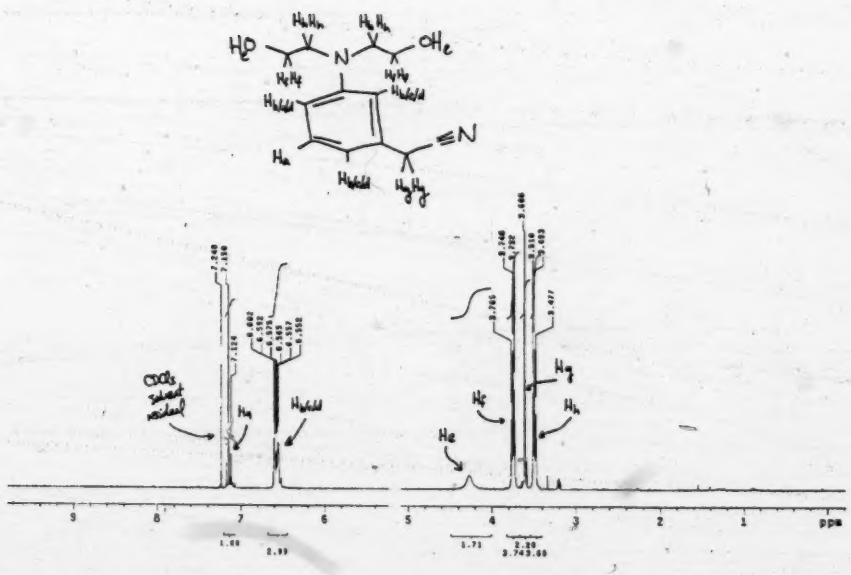

Figure A.3 ^{13}C and ^{1}H NMR spectra of compound **31c**

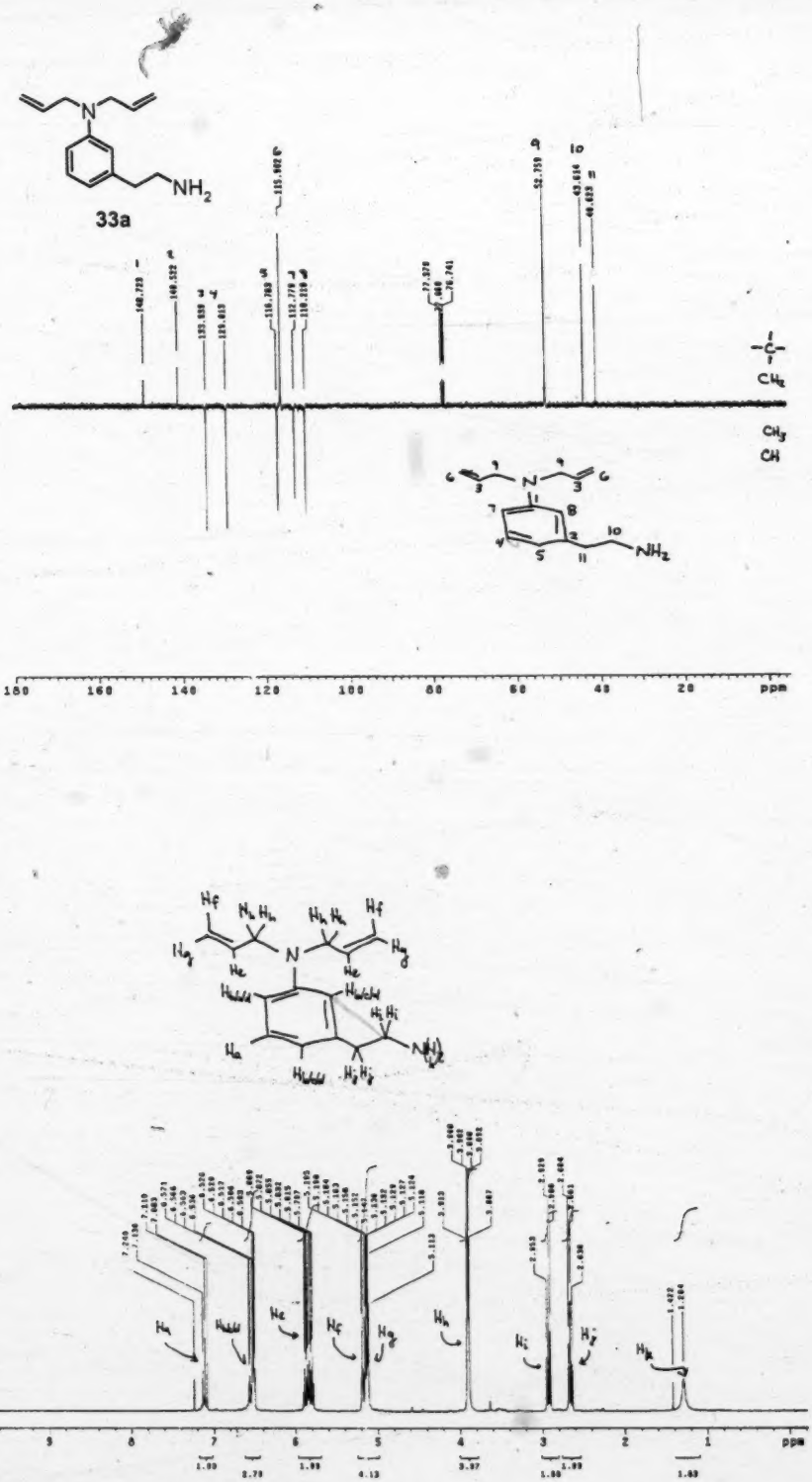

Figure A.4 ^{13}C and ^{1}H NMR spectra of compound **33a**

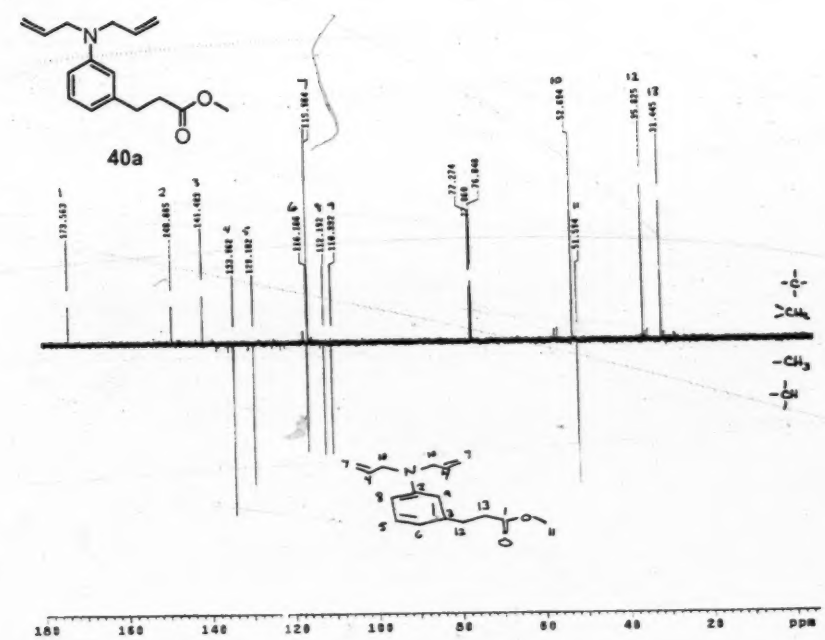

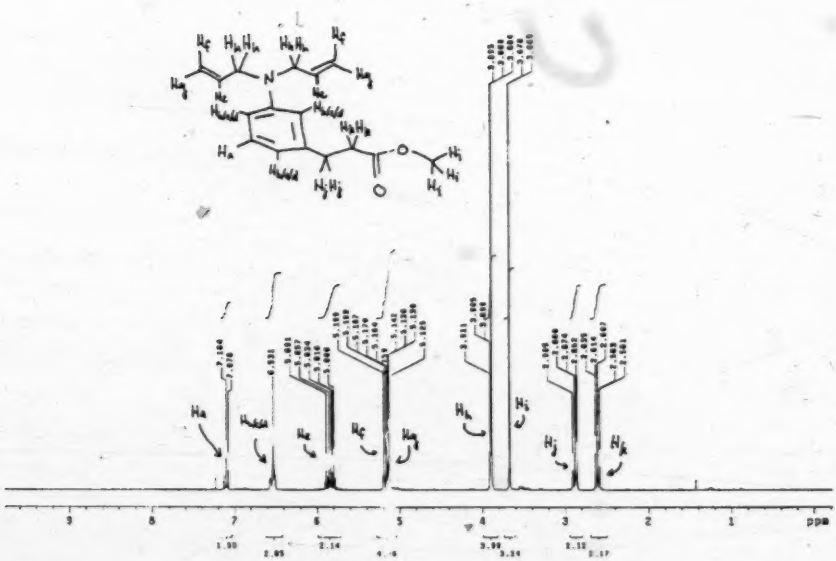

Figure A.5 ^{13}C and ^{1}H NMR spectra of compound **40a**

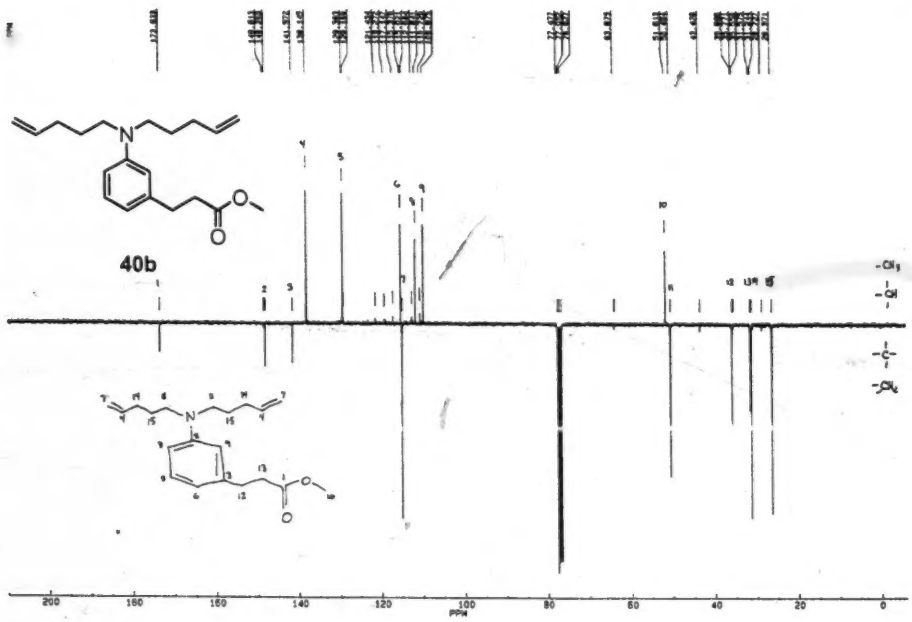

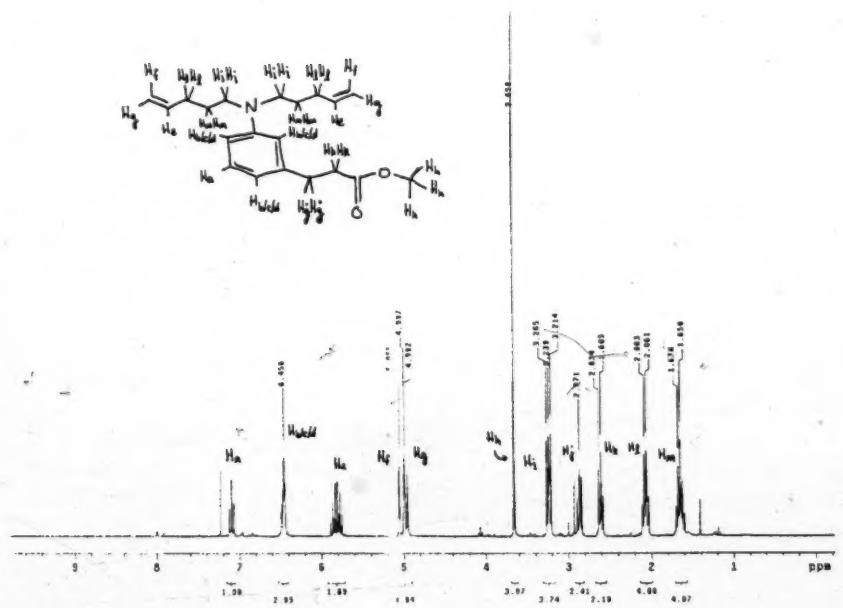

Figure A.6 ^{13}C and ^{1}H NMR spectra of compound **40b**

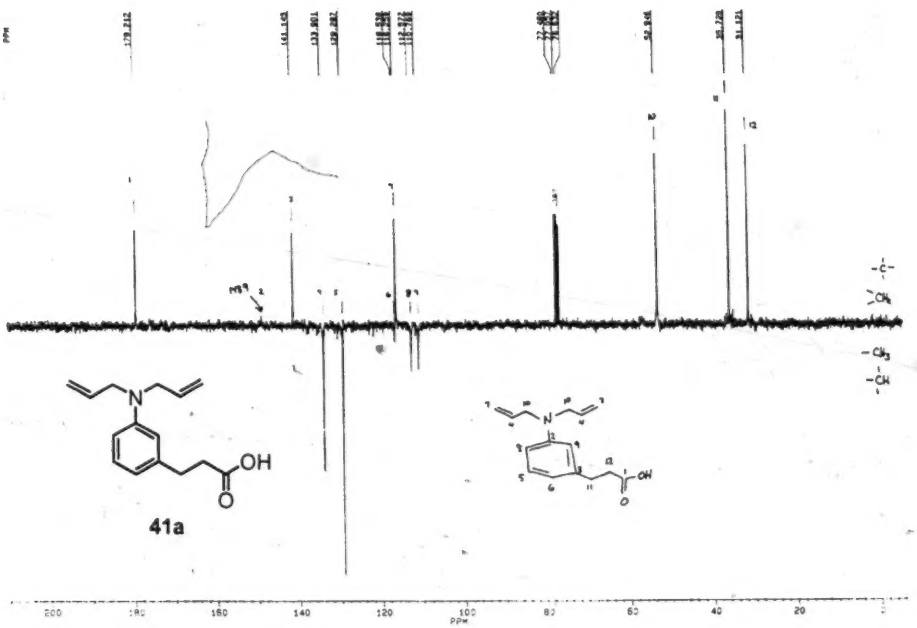

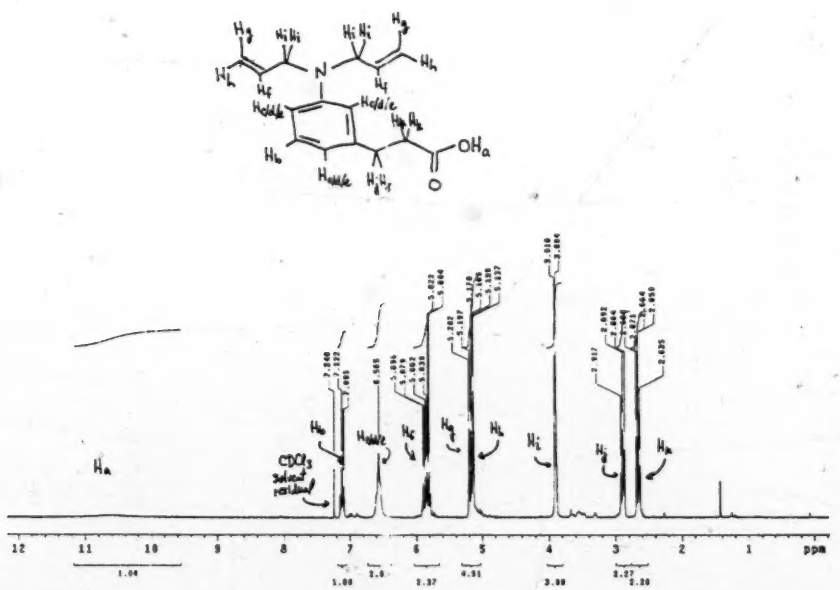

Figure A.7 ^{13}C and ^{1}H NMR spectra of compound **41a**

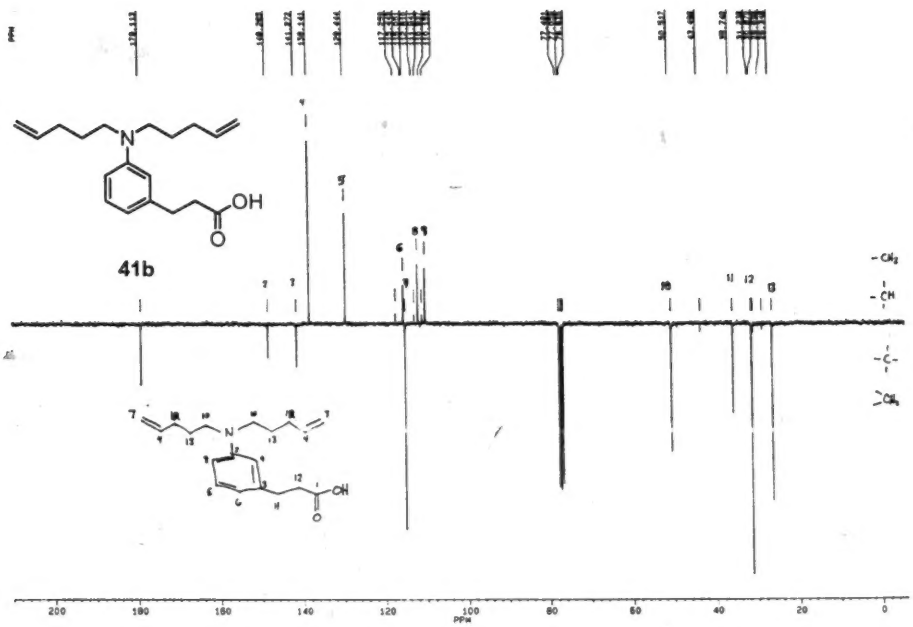

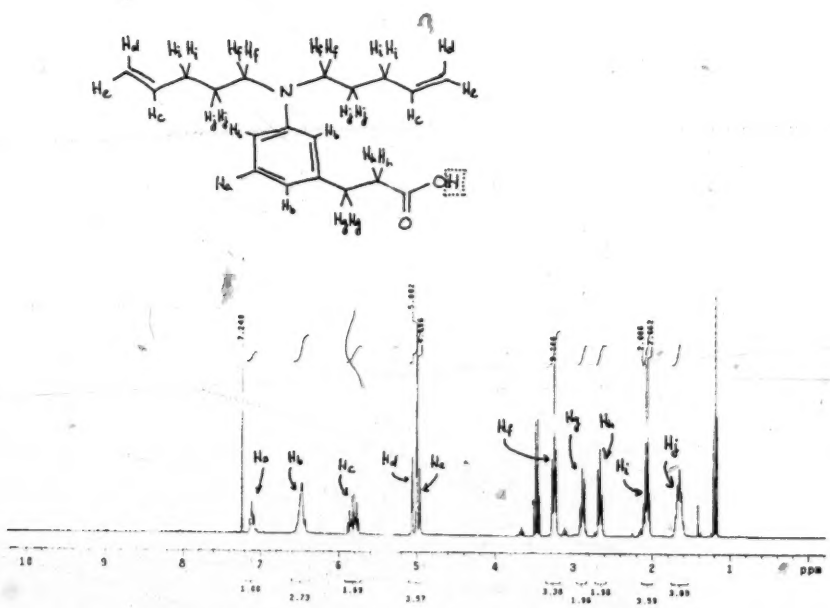

Figure A.8 ^{13}C and ^{1}H NMR spectra of compound **41b**

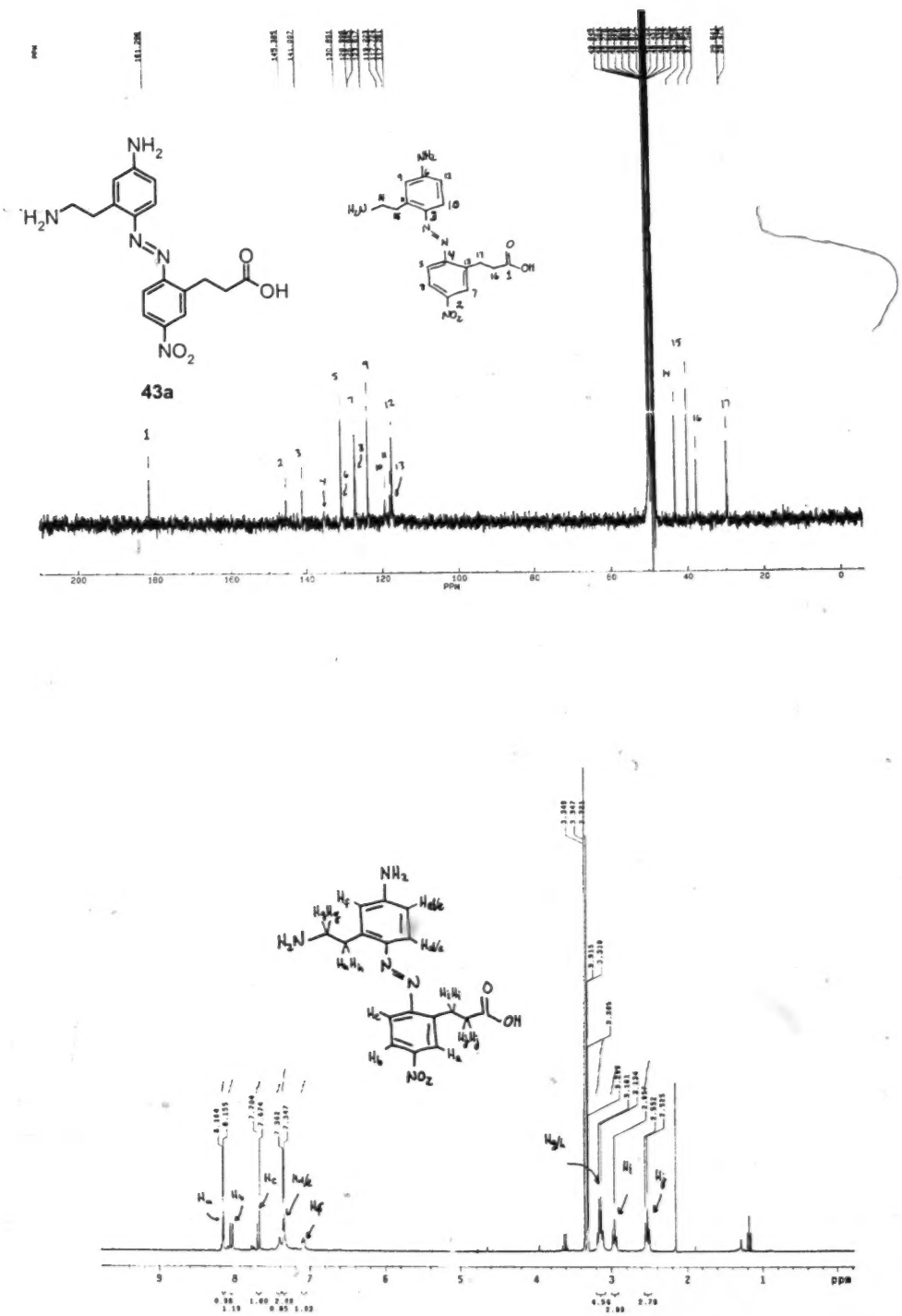

Figure A.9 ^{13}C and ^{1}H NMR spectra of compound **43a**

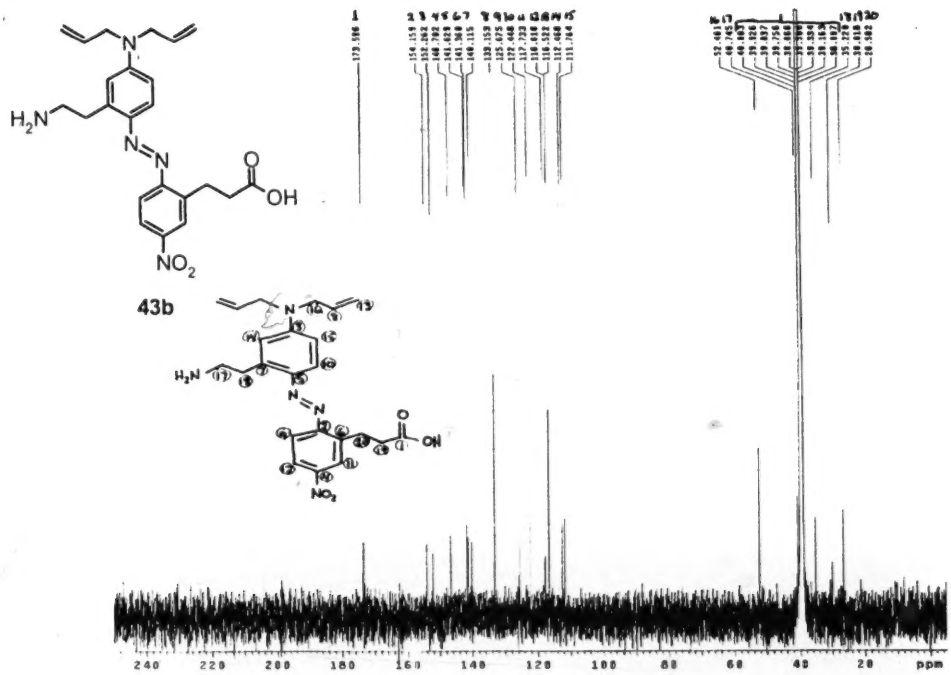

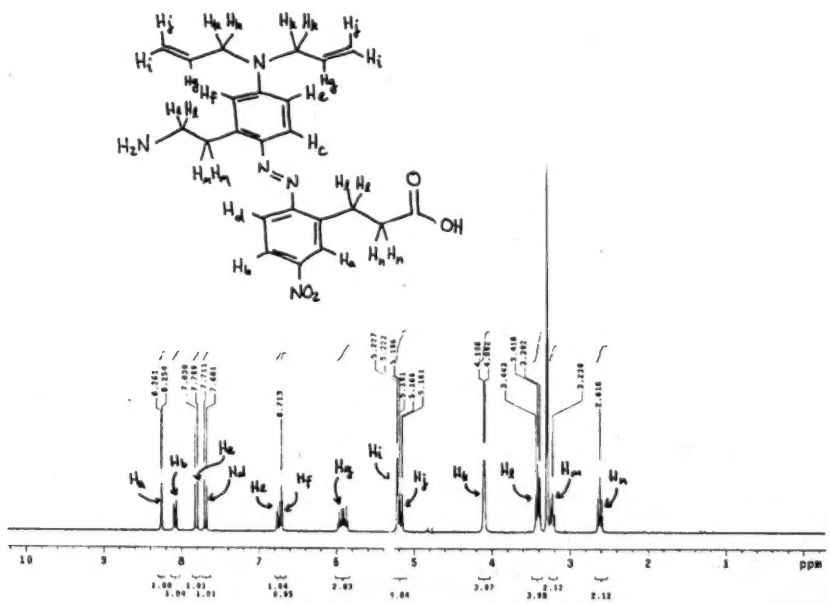

Figure A.10 ^{13}C and ^{1}H NMR spectra of compound **43b**

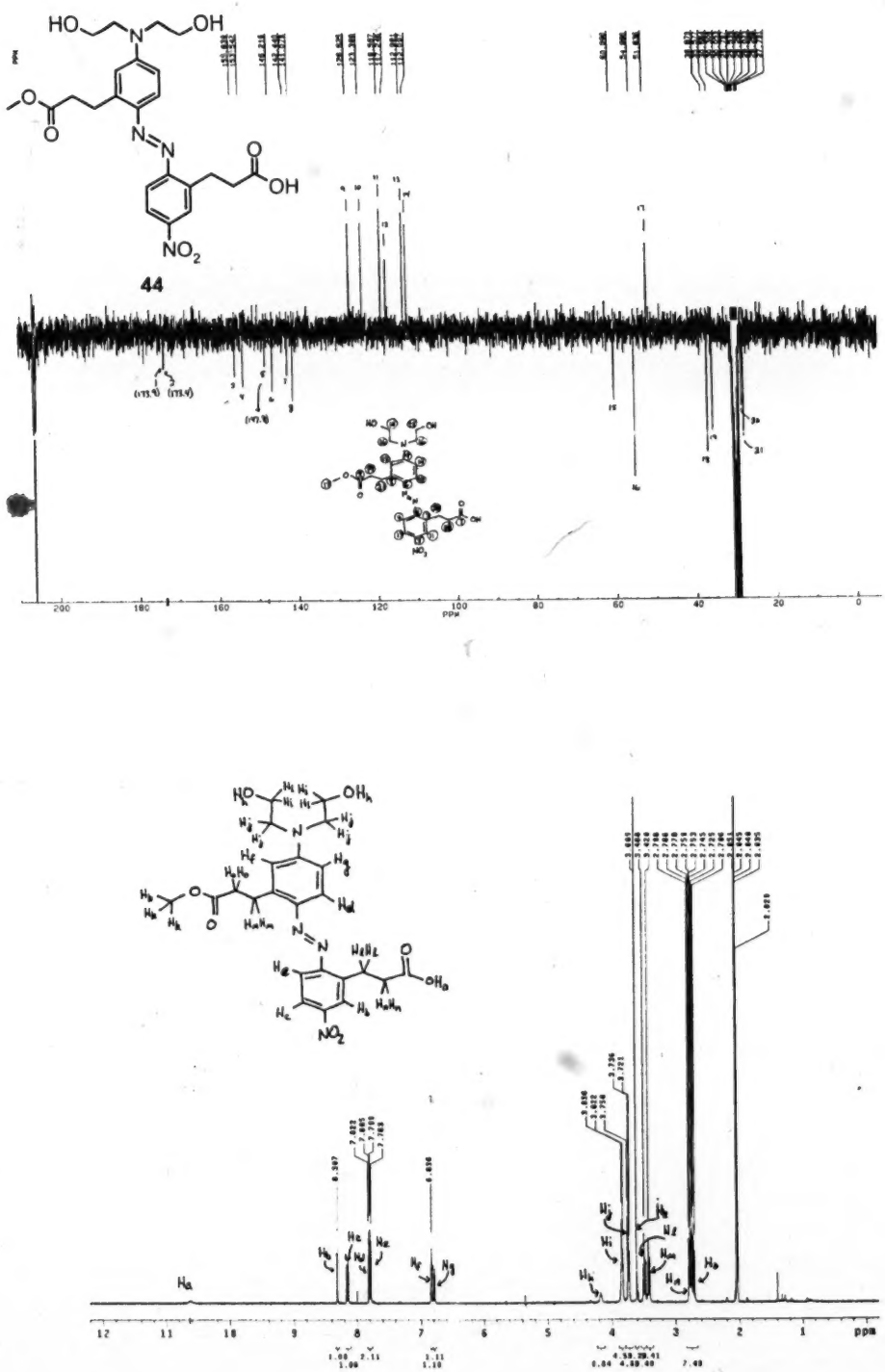

Figure A.11 ^{13}C and ^{1}H NMR spectra of compound **44**

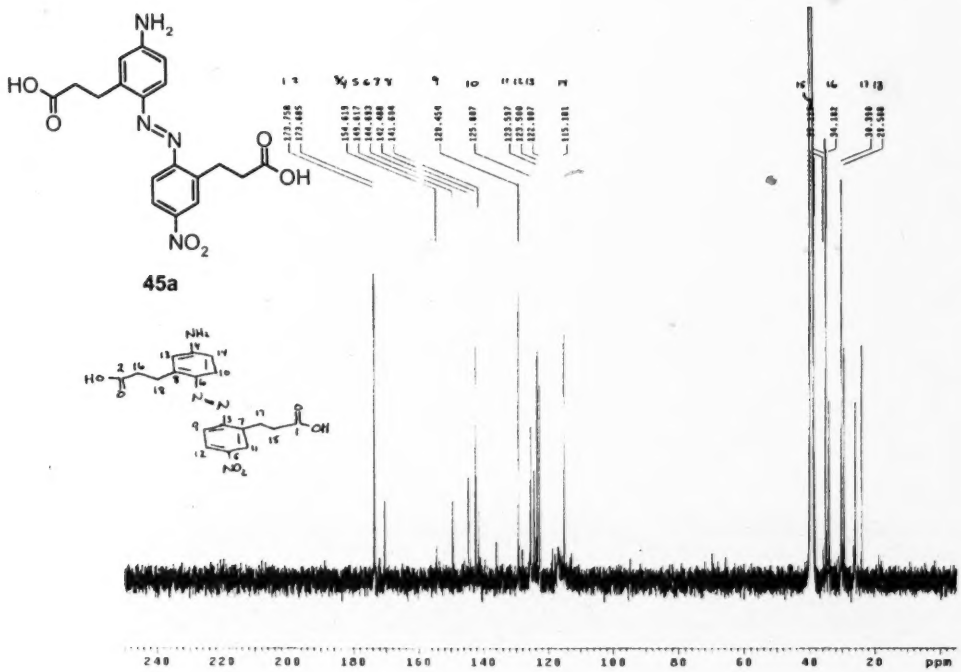

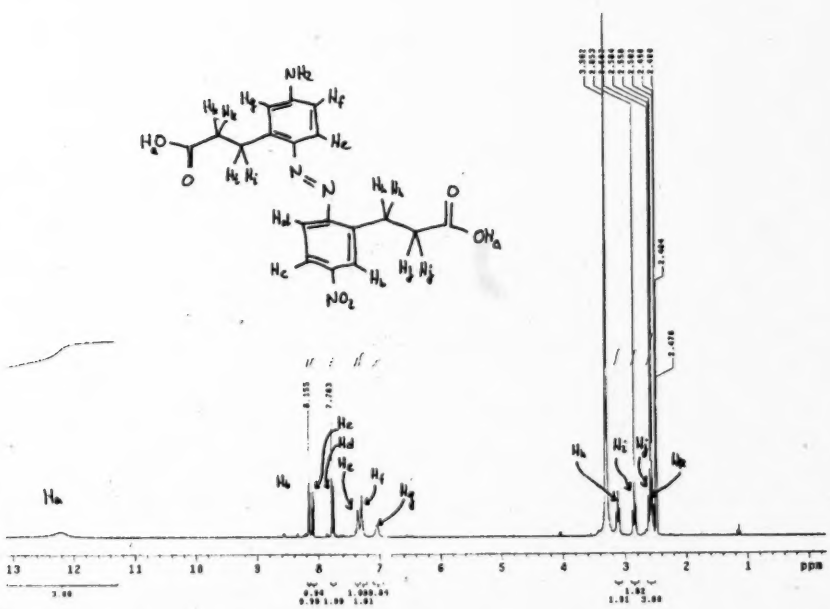

Figure A.12 ^{13}C and ^{1}H NMR spectra of compound **45a**

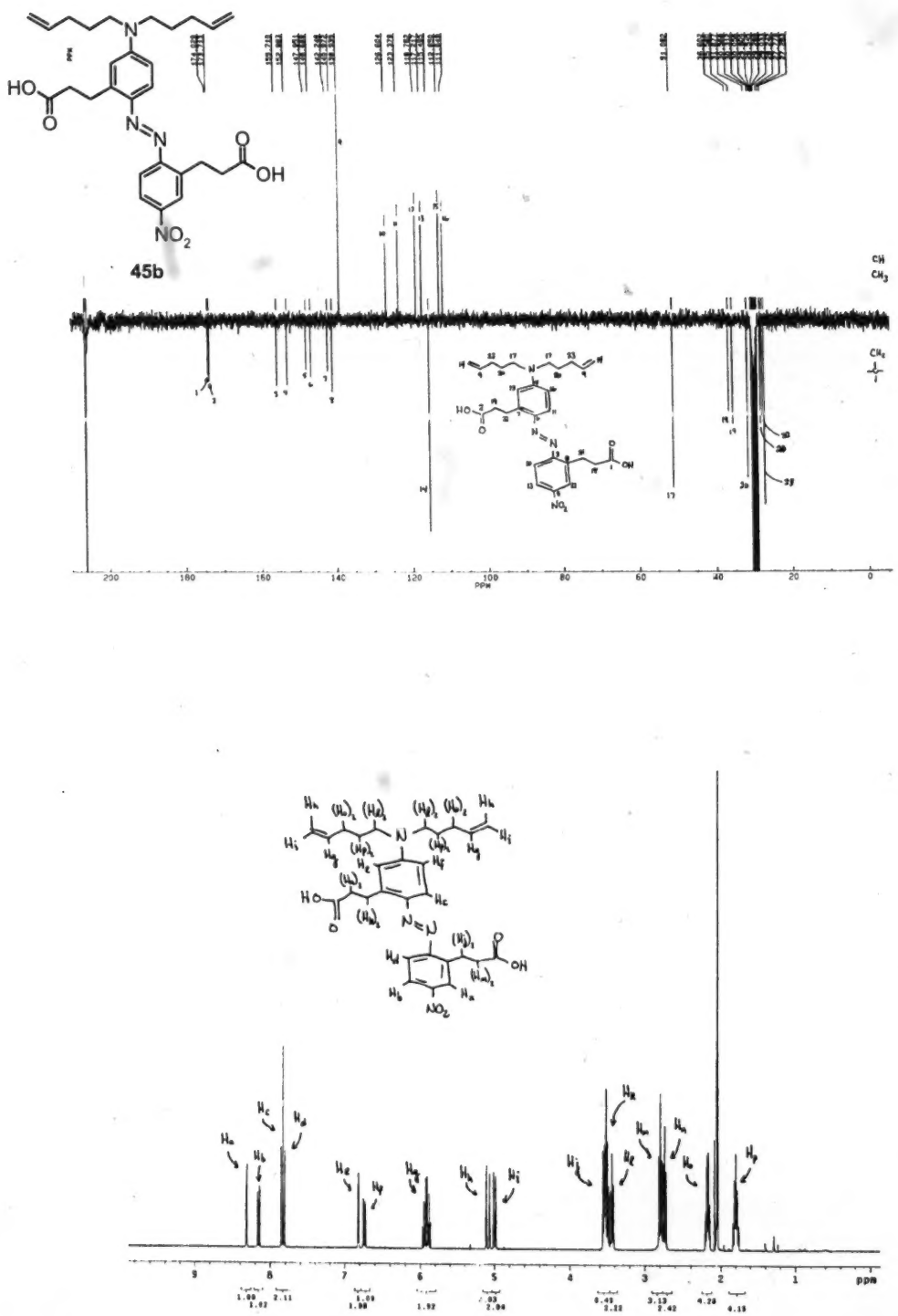

Figure A.13 ^{13}C and ^{1}H NMR spectra of compound **45b**

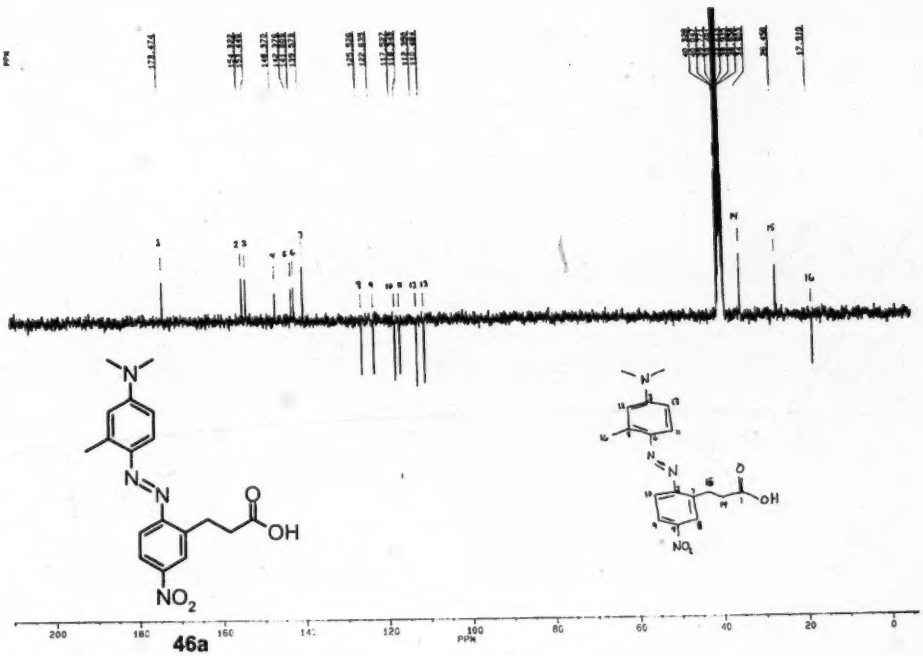

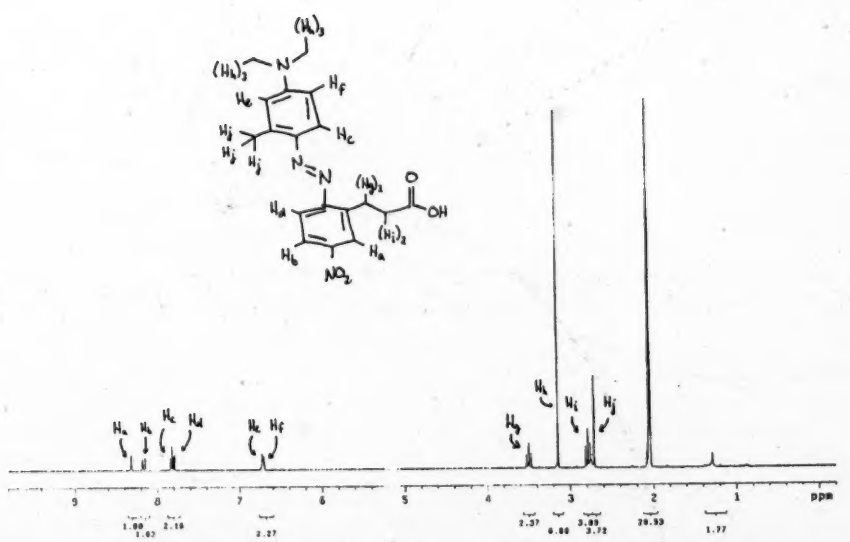

Figure A.14 ^{13}C and ^{1}H NMR spectra of compound **46a**

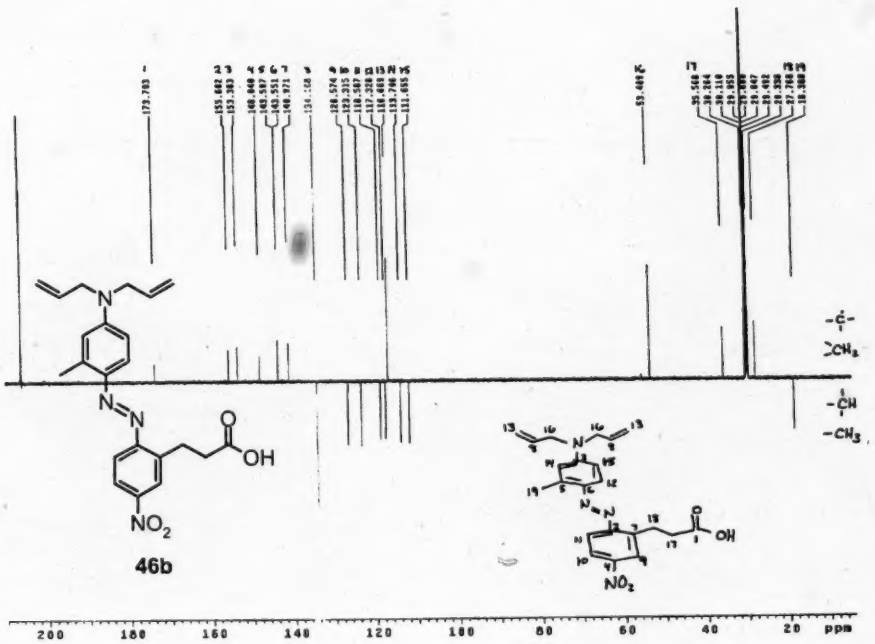

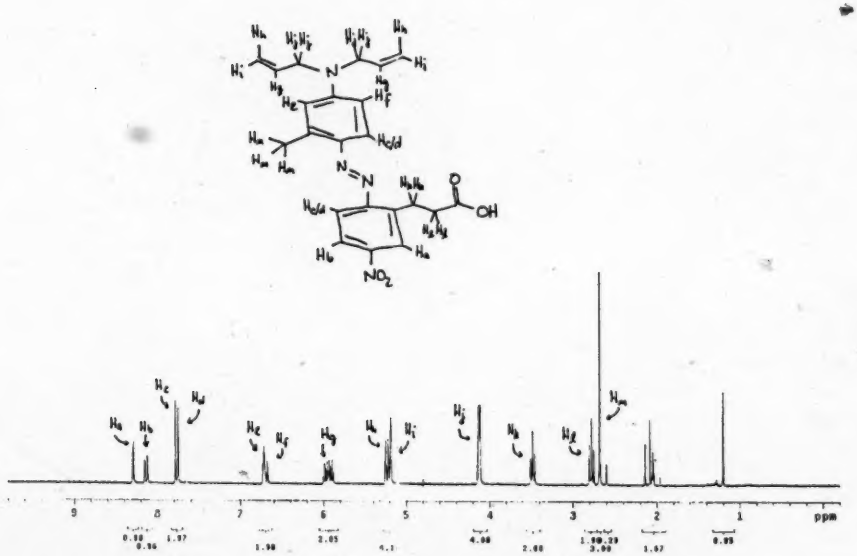

Figure A.15 ^{13}C and ^{1}H NMR spectra of compound **46b**

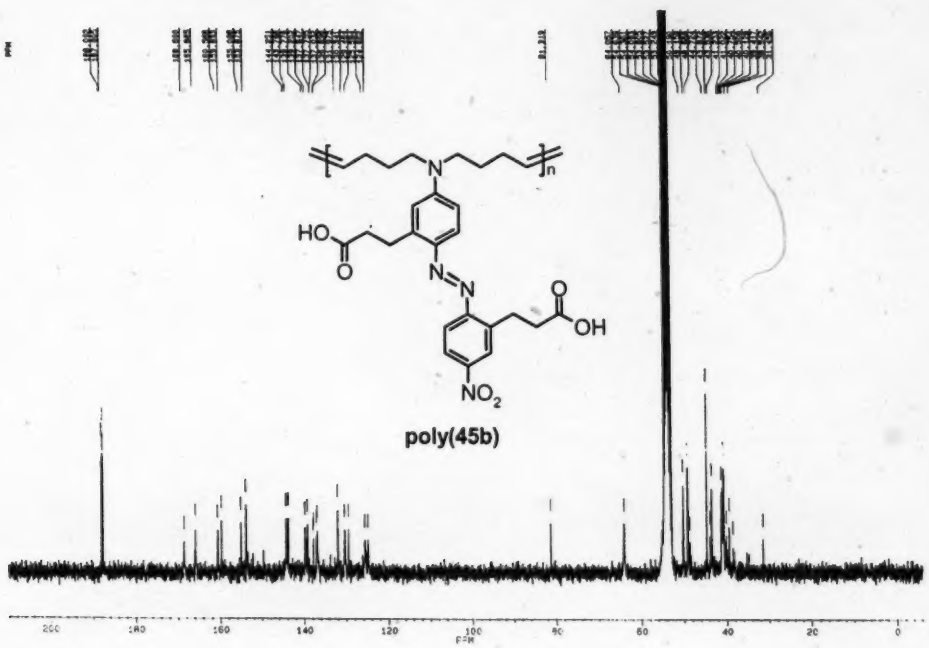

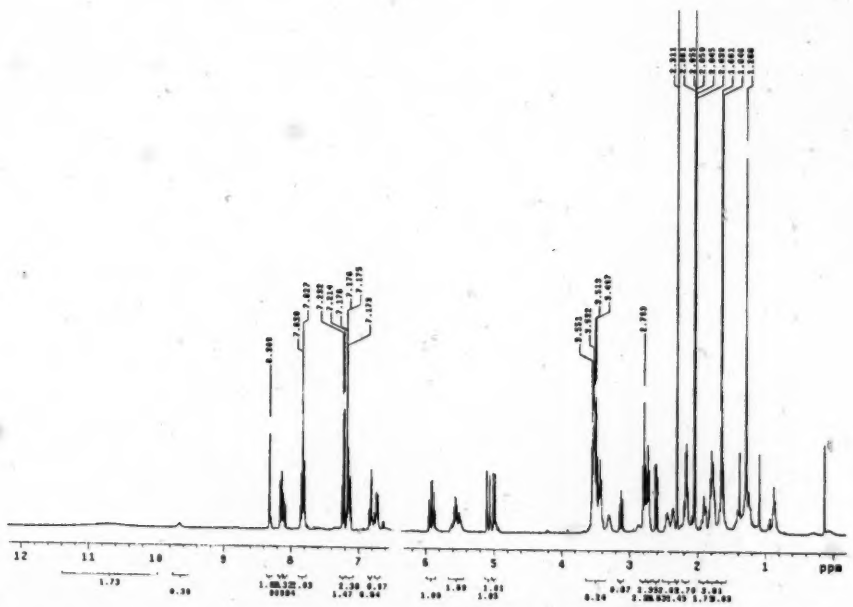

Figure A.16 ^{13}C and ^{1}H NMR spectra of compound **poly(45b)**, the oligomeric material derived from compound **45b**